The comparison of different stress measurements in determining the stress profile of a near-surface low-stress hard-rock mine.

Stjernøya , Norway.

Master Thesis
M.T. Hertogs

Delft University of Technology

TUDelft

SIBELCO

The comparison of different stress measurements in determining the stress profile of a near-surface low-stress hard-rock mine.

Stjernøya , Norway.

by

M.T. Hertogs

Student Name	Student Number
Hertogs	4718909

Supervisor: Dr. A. (Auke) Barnhoorn
Company Advisor: Dr. ir. R.M. (Robrecht) Schmitz
Committee Member: Dr. M. (Masoud) Soleymani Shishvan
Committee Member: Dr. M (Mikael) Rinne
Committee Member: Y. (Yannick) Feldmann, MSc.

Project Duration: February, 2023 - August, 2023
Faculty: Faculty of Civil Engineering and Geosciences
                     Delft

Cover: Nepheline Syenite Mine on Stjernoy Island, Norway (M.T. Hertogs)

TUDelft

Preface

This research on *"The comparison of different stress measurements in determining the stress profile of a near-surface low-stress hard-rock mine"*, conducted by me, M.T. (Max) Hertogs, was done as part of the European Mining Course (EMC/EMMEP) in pursuit of a Master of Science. During the last semester of the two year master programme, I did research at both the Delft University of Technology and on Sibelco's Stjernøya complex to investigate the topic and write this Master's Thesis.

I am extremely grateful to have been given the opportunity to work with and on an active mine-site by Sibelco and, in particular, Robrecht Schmitz. Next to giving me the opportunity to do my thesis at a company, he sparked my interest in pursuing a geotechnical topic within mining and gave plenty of advice during my research. I would also like to thank Jeras Dieleman, who despite my inexperience in doing underground experiments, gave me the confidence and necessary help in doing difficult and heavy testing in a challenging (cold) environment and overall helped me in finishing my master thesis.

I owe gratitude to Auke Barnhoorn for supervising my thesis, challenging my interpretations and overall helping me in the process. Next to that, the staff from the Rock Mechanics laboratory and especially Marc Friebel and Karel Heller aided in preparing samples and setting up the complicated dual test machinery which Debanjan Chandra taught me to operate. I owe a big 'Thank you' to all of them. Also, I would like to thank my committee for giving helpful feedback and for providing me with information (and a very interesting book, Mikael!) to fuel my curiosity and knowledge in mining engineering.

Finally, I would like to express immense gratitude to my family, friends and especially my girlfriend in helping me, guiding me, distracting me and enduring me in the process of writing this thesis.

M.T. Hertogs
Delft, August 2023

Abstract

Measuring rock stress is a difficult process, especially in the Stjernøya Nepheline-Syenite mine in Northern Norway. The complex nature and topography of the shallow deposit makes it difficult to conduct industry standard tests. Therefore, this thesis aims at answering how different stress measurement techniques and their results compare to each other in a shallow low-stress hard-rock mine. To do this, an elaborate laboratory work is done to find a relation between stress (UCS) and acoustic properties and velocities of the nepheline syenite. Using that information, a similar combination of tests is done in the field, namely a flat jack test and acoustic velocity measurements with a hammer and geophones. To give further insight in the gathered field-data, visual classification methods, like RMR are done to verify and aid the tests and the results. The laboratory tests gave more insight in the relation between stress and acoustic velocity. There exists a positive, somewhat logarithmic relation between confining pressure and velocity through the sample, until the end of the elastic domain. Depending on the sample, this becomes more apparent after an initial loading phase between 0 and 10-20 MPa. In this low-stress zone, the wave arrival times could not be accurately observed and tend to give very low results. This problem translated to the field. Despite the flat-jack provided an understandable vertical pressure of 9.8 MPa, the acoustic measurements in the field did not always coincide with this pressure, according to the laboratory relationship, generally giving lower velocities than expected. However, a relation between rock quality and wave-velocity could also be present, as the cracks in the heterogeneous rock could heavily influence acoustic velocity. Therefore, this research concludes that both the flat jack and the acoustic investigative methods have their use in understanding the stress-profile of the shallow deposit. Given the low stresses in the mine, the acoustical investigative method could not be used directly to measure stress, but it can be used as a control for the flat jack tests and have use in monitoring of the rock wall.

Contents

List of Figures

List of Tables

1

Introduction

Due to the ever increasing need of raw materials, the need for mining is now greater then ever. Even though new methods are being developed to extract resources from the earths subsurface, open pit and underground mining are still the most commonly used methods of extraction. For many centuries, engineers have tried to make mining safer. Ever since the analysis of cracking in support timber of mine-roofs, methods of analysing the strength of the walls next to and above the miner have only gotten better and more thorough. This does not mean that we have become specifically better at understanding the rock formations. We are now better in predicting the instability of a rock mass, but this does not mean our methods apply to every rock type and wall. This research focuses on the effective measurement of rock stress in a shallow hard-rock mine in northern Norway, where measuring and understanding the rock mass has been difficult.

1.1. Stjernøya mine

Named after the island that it is located on, the mine of interest is the Stjernøya-mine, that produces nepheline syenite out of the Lillebukt deposit on the south side of the island. The underground part of the mine faces problems with high rock stress phenomena, like spalling (Schmitz and Hack, 2022). Phenomena like these are not uncommon in an underground mine, especially next to excavations, but the apparent low in-situ stress should not be able to break strong and competent rock. The induction of stress in a rock cannot be prevented, but it could be measured and predicted, and that is where the Sibelco team finds trouble. To define how much information is necessary per location, the Sibelco team uses categories defined in Eurocode 7 STANDARD (2004) as is stated in (Schmitz, 2018).

1.2. Eurocode 7

In the Eurocode 7 it is stated that depending on the importance of and risks associated with the engineering project, a category is assigned to that project. The lowest category, Category 1, requires little knowledge of the country-rock, resulting in an 'empirical' design based on a few rock-parameters with negligible risks. For the highest category, Category 3, a detailed engineering plan will be made, based on as much rock-stress knowledge as possible, to mitigate risks. It can thus be said that depending on the category, different types of information is necessary. To gather that data, a range of methods are available to the team in Stjernøya. These methods vary from optical or empirical measurements like rock mass classifications to pure stress measurements like flat-jack measurements, overcoring or hydraulic fracking and also acoustic methods like seismic imaging or P-wave velocity measurements.

1.3. Questions

Because Sibelco's Stjernøya site has a lot of different areas and projects, a decision needs to be made on what Category should be assigned to a certain project in a certain area. Following this, a decision needs to be made on what measurement technique should be used to generate the data necessary for that Category. A difficult environment like the shallow-lying Stjernøya site requires a good understanding of both the measurement methods and the implications of the surrounding petrology. If

you would be able to measure efficiently and correctly at multiple area's of the mine, depending on the Eurocode-category, there can be less risk of rock mechanical failure. Next to that, economical and planning benefits can be achieved by more efficient application of stress measurements. Consequently, this report aims at answering the following sub questions:

- How efficient and accurate are hand-held stress measurement tools?
- How do mechanical and acoustic tests in the field compare to acoustical and mechanical stress tests in the lab?
- What is the influence of a low in-situ stress on the accuracy of stress tests in the field?
- What is the use of visual or empirical rock mass classification in stress measurements?

Combined, they raise the following research question:
How do you measure stress efficiently and precisely to understand high-stress phenomena in a hard rock mine with low in-situ stress?

1.4. Research
The research aims to measure, analyse and compare the stress-state of the Lillebukt deposit in various ways and use the compared and adjusted data to create a method of predicting the stress at various locations in the mine. There are multiple tools, like ultrasonic acoustic transducers and flatjacks, at hand in the mine to determine the in-situ stress vectors and these will be used to measure on site. The main location of interest will be the corner that connects the old access tunnel (Ort i Felt) with the new access route towards the stopes. This has stress measurement results dating back to the 1970s (Myrvang, 1973) available, which can be used for comparison, as the corner is far away from the active mining and the surrounding area has not changed since the measurement from Myrvang. Core samples gathered in that area, as well as other already available samples from previous research are consequently also analysed in the TU Delft Rock Mechanics laboratory to get a comprehensive overview of the rock and its endured stresses. Engineering interpretation of the rock mass will also be done to help the analytical process and truly understand the macro-scale properties of the subject of measurement.

1.5. Hypothesis
It can be hypothesized that the most effective and fast way to gather data from a large rock mass is through acoustics or micro-seismics. The travelling Pressure (P) and Shear (S) waves generated by a hammer blow, for instance, can be recorded at a certain distance from the source. The speeds of these waves can be compared to lab results, relating it to stresses. If the stresses from the acoustic measurements then coincide with flat-jack results and further engineering analysis, the acoustics can be confirmed and the correlated stresses interpreted as true stresses in the subsurface model of the mine.

1.6. Build-up
To reach this level of understanding, the topic will be subdivided in the following chapters. Chapter 2 will cover some geological background of the mine and properties of Nepheline Syenite. A literature review on (relevant) rock mechanical testing will be done in Chapter 3, along with an elaborate methodological and analytical explanation per tests. In a Chapter 4 the results of the different tests will be given. Chapter 5 shows a comparison between the results and literature and also a division of results based on the Eurocode 7. Finally, Chapters 6 and 7 will discuss results, conclude the research and also include recommendations for future research or measurements.

2

Nepheline Syenite

As specified before, the underground complex that is researched in this thesis is Sibelco's Stjernøya mine. In this mine, nepheline syenite is extracted from the Lillebukt alkaline complex for use in, among others, ceramics and the glass industry. The underground mine and quarry are located on the island of Stjernøya (Figure 2.1) and has steadily developed from a small underground sublevel stoping mine towards an open pit mine that uses the older stopes for backfill and as drawpoints for the mined out material in the open-pit producing months (June - December).
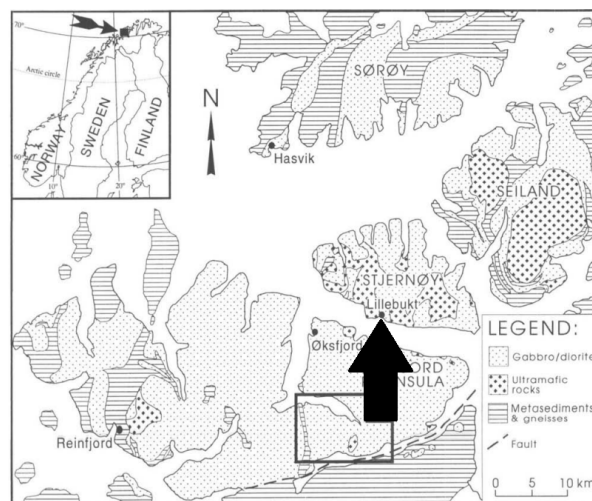
Figure 2.1: Location of Stjernøya and Lillebukt alkaline complex at the arrow (Reginiussen et al., 1995).

2.1. Geology

The geology of the island has been described by Heier (1961), Bryhni (1962), Robins and Gardner (1975), Ramsay and Sturt (1970) and Geis (1979) in the 1960's and 1970's. Later, company reports from first Norsk Nefelin, then North Cape Minerals and later Sibelco Nordic, focusing more on the geotechnical (Dahle, 2007) and geochemical (Gautneb et al., 2009) properties of the alkaline complex followed.

Heier (1961) was the first to publicly report about the geology of the southern part of the island Stjernøya in the Seiland-region. He reported on multiple economic purpuses of the *'Layered Gabbro, Hornbledite, Carbonatite and nepheline syenite on Stjernøy, North Norway.'*. The island of Stjernøya lies in line with the Norwegian Caledonides, a sequence of nappes that were created during the Caledonian orogeny. Even though the island of Stjernøya appears to be part of the Kalak-Nappe complex, the origin of the rocks apparent on Stjernøya are non-orogenic. The mafic and ultra-mafic rocks on Stjernøya must

thus be part of an intrusion that happened during the orogenic period Sturt et al. (1975). The syenites and carbonatites are also part of this mafic intrusion, that is unique for this area in Norway. The age of these plutons has been estimated by Pedersen et al. (1989) using U-Pb dating. It was then confirmed that the mafic intrusions happened during the Middle- late Cambrian boundary (531 +- 2 Ma and 523 +-2 Ma). The exact localities of the different rock types in the Lillebukt complex as mentioned by Heier (1961) can be seen in the geological map in appendix C and was sketched up by Bruland (1980).

Geis (1979) studied the origin of the nepheline syenite more precisely. The unknown property of the nepheline syenite was its feldspar. The feldspar shows clear lineation, whereas the nepheline syenite does not. Geis concluded that the nepheline syenite must thus be of metosomatic origin, associated with high grade metamorphism. The nepheline syenite is then a direct result of nephelinization of the syenitic intrusion during the caledonian orogeny. This would explain the differences in mineralization of the feldspar and the nepheline.

After its deposition, the nepheline syenite was intruded by several veins, most apparent are the thick black diabase veins or dykes which were already observed by Heier (1961). Later research by Geis (1979) and Ramsay and Sturt (1970) determined that these dykes must have originated from fissures flowing into cracks opened up by folding to which the nepheline syenite was subjected shortly after its deposition. No apparent major geological processes have later enacted upon the nepheline syenite, making it a very capable rock without major weakness zones due to secondary faulting or folding present. This is backed up by rock mechanical research on the mine (Schmitz and Hack, 2022), (Dahle, 2007), (Johansson, 2001) and (A. Argilaga, 2017).

2.2. Rock Mechanical Properties

Below, accepted rock mechanical and chemical properties of the nepheline syenite are shown. They are taken from researches done by the company itself about the nepheline syenite and the deposit

Chemical composition: (Heier, 1961), (Oostman, 2023)

- $\pm$ 50% K-Feldspar $KAlSi_3O_8$
- $\pm$ 35% Nepheline $(Na, K)AlSiO_4$
- Traces of: Calcite, Clinopyrox. Hornblende, Biotite, Rutile (in Feldspar), Titanite, Apatite, Opaques, Zeolites, Muscovite
- Low in Rare Earth Elements

Rock Mechanical Properties: (Dahle, 2007), (Schmitz and Hack, 2022), (Myrvang, 2007), (A. Argilaga, 2017)

- Youngs Modulus: 26 GPa
- Poissons Ratio: 0.24
- Density: 2600 kg/m^3
- Average Principal Horizontal stress (σ_1): 3 MPa + Depth[m] x 0.0020 MPa
- Average Secondary Horizontal stress (σ_3): 1 MPa + Depth[m] x 0.0015 MPa
- Average Principal Vertical stress (σ_2): Depth[m] x Density (kg/m^3) x 9.81 (m/s)

It is remarkable to see that the primary stress tensor (σ_1) is the horizontal component of the stress. A large horizontal stress component is most likely the result of left-over forces generated during the thrusting of the Caledonian Orogeny or the result of cooling patterns. Research about this, like the one from Sheorey (1994) also stated that it can be approximated but it is heavily dependant on the horizontal Young's Modulus E_h. Thickness of crust also influences the horizontal stress level, with a thicker crust leading to a larger horizontal stress. The lack of an apparent large vertical stress tensor (σ_2), as mentioned before, is due to the mine being in a mountain above sea level and not deep-lying in the subsurface, thus not giving a very high vertical stress.

2.3. Past Research

A lot of geological research on Stjernøya has been done over the years, as seen by the previous paragraphs. Recent studies on the island either focus on the potential of apatite and phosphorus leaching (Gautneb et al., 2009) or technical reports on problems in the mine (Schmitz and Hack, 2022), (Oostman, 2023), (A. Argilaga, 2017). One of the most apparent problems is the apparition of spalling on several places in the mine. Spalling is a failure mode of rock masses that are either severely fractured or under reasonably high stress, like very deep deposits (Figure 3.2)(Kaiser et al., 2000).

Because of the spalling occuring in such a low-stress underground complex, Sibelco launched several researches into its origin. It is a rock mechanical ground rule that spalling occurs at stresses that approximate half of the uniaxial compressive strength of the rock. This condition is, according to almost all the previous measurements done in the mine, never met.

Stress could not be mechanically measured at the vehemently spalled regions due to the impossibility of drilling a large borehole or sawing a slot. Next to that, it is generally accepted within the mine that high stresses are rare. To start an investigation on non-mechanical, non-invasive deeper monitoring methods in the Stjernøya mine, Mulder (2019) investigated the Kaiser-effect on the rock in the laboratory. Despite interesting findings in the lab, the application of acoustical investigative method did not emerge as the solution to monitoring the spalled areas. Therefore, new research focused more on the mineralogy of the nepheline syenite and less on the stress enacting upon the rock mass. Recent mineralogical investigations by Oostman (2023) and van Tooren (2022) propose a solution. Apparent amphibole lineation occurs at several spots within the underground complex, usually at areas that are subject to spalling. It is possible that the lineation made the host rock weaker and more susceptible to spalling. Figure 2.2 shows the lineation of amphibole at an area subject to spalling. Sibelco geotechnical engineers applied orange paint to see which part of the wall falls of and thus causes the removal of the orange paint. After multiple visits to the mine and conversations with staff, it must be said that spalling does seem to occur where this lineation is present. However, not every area with lineation has spalling and not every spalled rock mass has this striking mineralogical feature.

To come to a more thorough conclusion, effective, non-invasive deeper stress measurement are necessary. If stresses are measured to be low in a lot of spalled areas in the mine, it can be concluded that the spalling cannot be the result of just rock mechanical stress but it is rather a result of geological processes, as described by Ramsay and Sturt (1970), that have enacted upon the rock mass. The possibility of spalling being the result of a combination of stress and mineralogically weaker rock should also be investigated. Next to that, rock mass stress measurements are also important as input for the stress model of the mine, either as true input values or for calibration. Would a quick and effective stress measurement coincide with the expectation of the model, more trust can be put in both the model and the stress measurement. For the transition of the Stjernøya mine into a mature mine, a good stress model is very important, given the difficulties created by the mining method, topography and geology.

Figure 2.2: Lineation of amphiboles in the nepheline syenite at an area subject to spalling (Oostman, 2023).

3

Measuring Rock Strength and Stress

The following chapter aims at explaining the principles, physics and mechanics behind the stress within rock and the measurement of that property. The understanding of these is very important for giving any analytical review of the rock stress measurements. First, rock strength and stress is explained. Then, individual attention is given to the tests performed in this research, explaining the methodology and principles of analysis.

3.1. Rock Strength, Stress and its Parameters

The strength of rock is upheld by the bonds between its components: the minerals it consists of. During the process of formation of the rock, minerals are being put together and held together. This is either via interlocking of the minerals during its formation, because of immense pressure and temperature, or by cementation of a secondary, finer, mineral that (partially) fills the cavities between the minerals. These processes can happen multiple times, fuelled by geological and chemical processes that occur within or around the rock.

Even though the past shapes the rock and thus also its strength, it does not leave behind visual markers that indicate the levels of stress the rock has endured or is enduring. For this, tests need to be conducted. There are different lab-tests for different rock strength parameters. Listed in Table 3.1, the three most important mechanical parameters regarding rocks can be found.

Table 3.1: Rock Mechanical Parameters

Parameter	Sign	Unit	Description
Stress	σ	Pa or N/m2	Force Per Area
Traction	T	- Pa or N/m2	Negative Stress
Strain	ε	%/m/m2/m3	Deformation (compression is positive, dilation is negative)

The in situ stress parameters in Table 3.1 originate from the model by Augustin Louis Cauchy (1827). He stated that stress inside and on a body, with infinite small stress tensors acting on it from 3D-planes, can be found by knowing just three stresses in the perpendicular direction in the three dimensional plane. In this report, these stresses shall be further referred to as sigma 1, sigma 2 and sigma 3, called the principal stresses. How they enact upon an opening within a rock mass can be seen in Figure 3.1.

These parameters (sigma 1, 2 and 3) do not indicate the actual stress or strain enacted upon a rock with one hundred percent precision. As with most tests or research within the field of Geosciences, they rather give approximations of this value, given a (sometimes rather large) uncertainty.

However, a multitude of rock mechanical testing to find the sigma's, combined with a (finite-element)
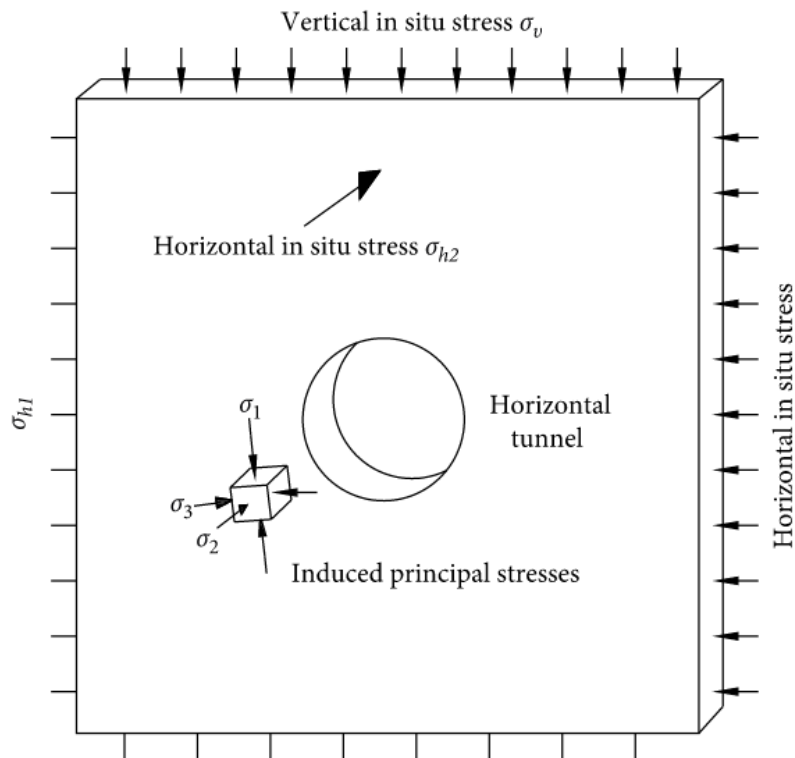
Figure 3.1: Sigma 1, 2 and 3 acting upon an underground opening (Hoek, 2000).

model can provide useful information about the overall stress state of a body, like a subsurface terrain of a mining area. The knowledge of the stress state of such a body allows a planner or engineer to make key decisions about the lay-out of the mine and above all, safety. This is especially important where the rock mass fails, or is expected to be failing in the (near) future. This can happen for a multitude of reasons and is generally a result of either brittle rock or high stresses, or a combination of both. Figure 3.2 depicts these failure modes. It is to prevent these that most rock mechanical testing and acquisition of knowledge about the stress is necessary in the mine.

The previously mentioned Eurocode 7 (STANDARD, 2004) also uses the possible failure modes in the choice of Category. Stille and Palmström (2018) reviewed the classes as specified in the Eurocode 7 and applied geotechnical risk, uncertainty and consequence classes to it (Figure 3.3). This created a similar diagram as the one in Figure 3.2. Now, however, the geotechnical input is comprised into three classes and the other one is an interprative risk scale based on the size and use of the underground opening. Using this figure, geotechnical projects in the Stjernøya mine are interpreted and measurements are done accordingly.

	Massive $(RMR > 75)$	Moderately Fractured $(50 > RMR < 75)$	Highly Fractured $(RMR < 50)$
Low In-Situ Stress $(\sigma_1 / \sigma_c < 0.15)$	Linear elastic response.	Falling or sliding of blocks and wedges.	Unravelling of blocks from the excavation surface.
Intermediate In-Situ Stress $(0.15 > \sigma_1 / \sigma_c < 0.4)$	Brittle failure adjacent to excavation boundary.	Localized brittle failure of intact rock and movement of blocks.	Localized brittle failure of intact rock and unravelling along discontinuities.
High In-Situ Stress $(\sigma_1 / \sigma_c > 0.4)$	Brittle failure around the excavation.	Brittle failure of intact rock around the excavation and movement of blocks.	Squeezing and swelling rocks. Elastic/plastic continuum.
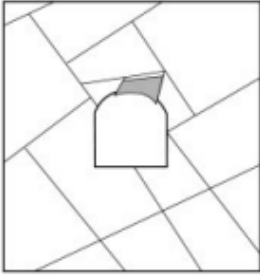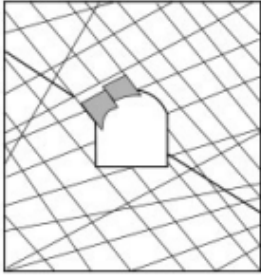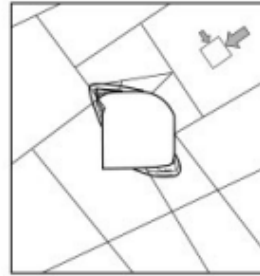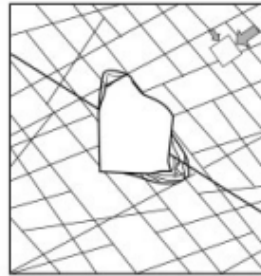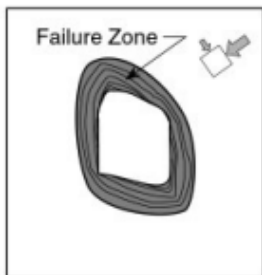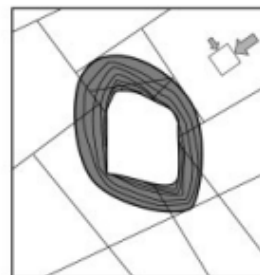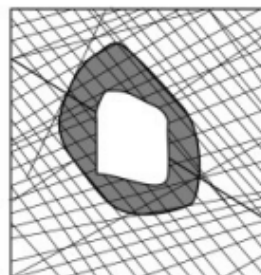
Figure 3.2: Failure modes on an underground opening (Kaiser et al., 2000).

BEFORE EXCAVATION for planning		Geotechnical Category		
Consequences class (CC)	Examples. Typical rock constructions	Ground Uncertainty		
		low	medium	High
CC1 Low	- Simple foundations on rock - Low – moderately high rock cuttings - Tunnels of small size (< 4 m span)	GC1	GC1 / GC 2	GC2
CC2 Medium	- Complicated foundations on rock - High to very high rock cuttings - Large tunnels (4 to 15 m span) - Environmental requirements	GC1 / GC2	GC2	GC2 / GC3
CC3 High	- Undersea tunnels, all sizes - Unlined pressure tunnels, all sizes - Strict environmental requirements - Large caverns or very large tunnels (span > 15m) - Tunnels with limited rock overburden	GC2	GC2 / GC3	GC3

Consequences classes (in accordance with EN 1990):
CC1: **Low** consequences for loss of human life, or economic; social or environmental consequences are **small or negligible**
CC2: **Medium** consequences for loss of human life; or economic; social or environmental consequences are **considerable**
CC3: **High** consequences for loss of human life, or economic; social or environmental consequences are **very high**

Classes of Geological and Ground Uncertainty (before excavation):
Low: Clear and simple geology and ground conditions. Ground parameters can be easily found. Experience from construction in similar ground conditions.
Medium: Clear geology and ground conditions. Methods exist both to assess ground conditions and for dimensioning. Experience from construction in similar ground conditions can be documented.
High: Unclear geology and/or ground conditions with potential for problematic tunnel excavation. There are limited possibilities to assess the ground conditions before excavation starts

Figure 3.3: Eurocode 7 categories and risks (Stille and Palmström, 2018).

3.2. Rock Mechanical Laboratory Tests

Before one can make a stress model or make a decision on what information is necessary, they need to understand testing on rock. During the determination on what tests to conduct on a rock mass or sample, it is essential to know what you want to measure and what you do not want or cannot measure. Full reviews on measurement techniques can be found in literature. Zang and Stephannson (2009) provided a list in their book in which most variants of any relevant rock mechanical stress test are presented.

As this research aims at a particular hard rock mine, certain tests may be more suitable to conduct because of availability of machinery and sensors. Also in the laboratory, a selection needs to be made, based on the characteristics of the rock and the availability of test apparatus and samples .

On the mine site, the strain relief flat jack method is used to measure and approximate in-situ stresses, to be used in modelling software. Additionally, tomographic low-frequency P-wave acoustics are used to find the velocity of the rock. The velocity of the wave can then be compared with the CHILE (Continuous Homogeneous Isotropic Linear Elastic) behaviour of the rock, to find parts where it does not behave according to CHILE, and it thus found discontinuities in the rock. Also, Rock Mass Ratings and Q-values can be used to aid engineering analysis and to find properties of the rock mass and its visual discontinuities.

In the lab, to make just comparisons with the in-situ testing, a suitable replacement for the flat jack test needs to be found. Because of the lack of a large enough rock mass within the lab, strain relief testing is difficult. Instead, a strain induced method is chosen. Acoustic P- and S-Wave transducers will be used in combination with uniaxial compressive strength (UCS) tests. The next paragraphs will be aimed at explaining the tests used and research on the applicability and accuracy of them.

The research focuses on two sites in the mine. The first and prime location is on the intersection of the old access tunnel (Ort i Felt, Figure 3.4) with the new access ramp towards the top of the mine.

This location will be reffered to in this research by Hoek van Myrvang (HvM) or Corner of Myrvang. This is where Myrvang (1973) conducted stress measurements, which were added to the World Stress Map by Stephansson (1987).

Figure 3.4: The sign indicating the start of the Ort i Felt tunnel.

The secondary is location is the location of which samples where retrieved from the Stjernoya site during previous research in the TU Delft (Mulder, 2019). This is an accessible wall between stope 1 of mine 2 and the larger stope of mine 1. The locations of both measurement areas are highlighted in figure 3.5.

3.2.1. Unconfined Compressive Strength testing
The laboratory is a controlled environment in which rather uncontrollable and unknown factors that are present in the field can be removed to create 'true' measurements on a rock sample. Even though the main focus of rock mechanical monitoring in a mine is aimed at the uncontrollable and unknown factors of a rock mass, laboratory testing is necessary to find reference parameters of your rock sample. Unconfined compressive strength (UCS) testing is widely used and documented as one of the prime methods of testing the true strength of a rock as it is relatively easy to set up, but not without its complications, as stated by Goodman (1991).

UCS testing is the way of finding the unconfined compressive strength of a rock via the application of a uniform and increasing stress tensor on the vertical axis of a cylindrical-cut rock sample. Additionally, a radial strain chain can be applied to find the strain in another direction than the regular axial strain. A laboratory set-up for a standard UCS test can be seen in Figure 3.6, and regulations for UCS testing can be found in the ASTM D7012-14e1 (2017) document regarding the test.

The sample fitted into the machine is defined by its rock type and its dimensions (diameter and length). Çelik (2017) states that here have been many experiments done on the what should be the correct ratio between diameter and length of a sample. The general consensus and standards like the one from ASTM (2017) (1 to 2-2.5) and ISRM (2007) (1 to 2.5-3) is that a sample should be at least twice as

Figure 3.5: Lay-out of Stjernøya mine.
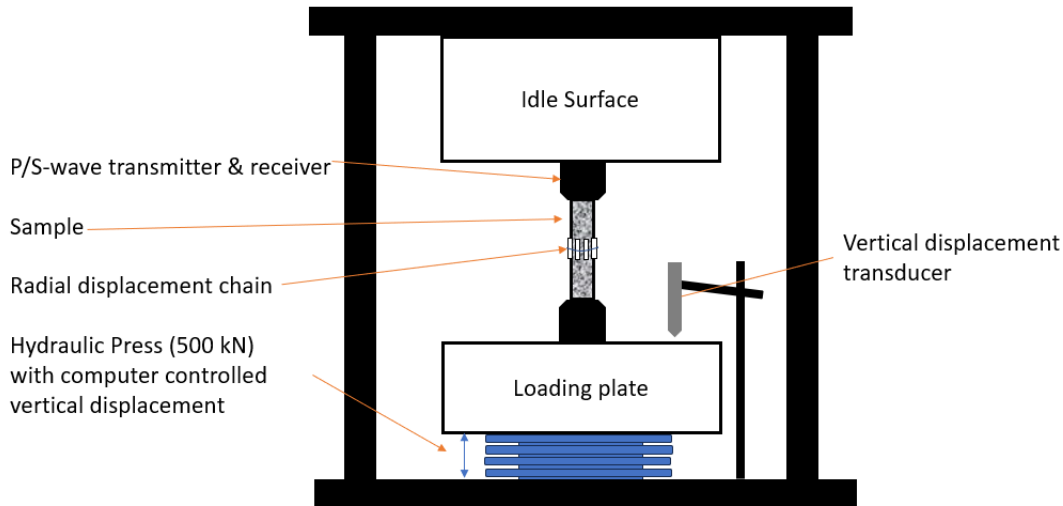
Figure 3.6: Typical set-up used for a UCS-test, as used in this research.

long as its diameter, but no more than thrice as long. ASTM also mentions that a sample should have a diameter of at least 47 millimeters. As this is usually not the case for mining-related tests (and also in this report), the ASTM states that this is acceptable, as long as a remark is placed at the result-section of the tested sample (ASTM D7012-14e1, 2017).

Measuring a cylindrical rock sample will provide information of a rock sample on its uniaxial compressive strength. Next to that, it will give a representation of the elastic-plastic behaviour of the rock sample, by measuring the strain the sample induces because of the stress applied to it. From the continuous measuring of both strain and stress, the elastic constants of the rock sample can be determined.

There are two main elastic constants directly found from the data generated by the UCS test. These are the Young's Modulus (or Elastic Modulus) (Young, 1845) and the Poisson's Ratio. To find the Young's Modulus, one must find the difference in strain after the application of a change in load or stress, as seen by Formula 3.1. Only a CHILE material has a static Elastic modulus. During loading, rock can feature multiple elastic stages with different elastic moduli. Therefore, an often used term is the dynamic elastic modulus or E_d, this is more useful for describing a rock and also for later analysis and correlation. Poisson's ratio (Formula 3.2) is found by relating axial strain with radial strain, to see how a sample covers a change in axial strain with a change in radial strain. Figure 3.7 showcases a typical stress-strain curve, from which Youngs Modulus and Poissons ratio can be found. The zones specified there are continuous per increasing stress and are as follows;

   I. Crack closure. (Increase in P-wave speed)
  II. Elastic domain. (E and ν are retrieved from this zone)
 III. Crack Initiation. (Start decrease P-wave speed)
 IV. Increasing crack density. (UCS at end of this zone)
  V. Macro-cracking. (Destruction of the core, low P-wave speed)
 VI. Residual. (Broken core)

$$E = \frac{\sigma}{\varepsilon} \tag{3.1}$$

$$\nu = -\frac{d\varepsilon_{\text{radial}}}{d\varepsilon_{\text{axial}}} = \frac{d\varepsilon_{\text{x}}}{d\varepsilon_{\text{z}}} \tag{3.2}$$

Loading in an active underground environment is rarely performed in the same way as a UCS-test. To better understand the effect of the dynamic application of load on the samples, that is for instance generated by drift creation, drilling and blasting or refill practices, cyclic loading can be applied. Rocks
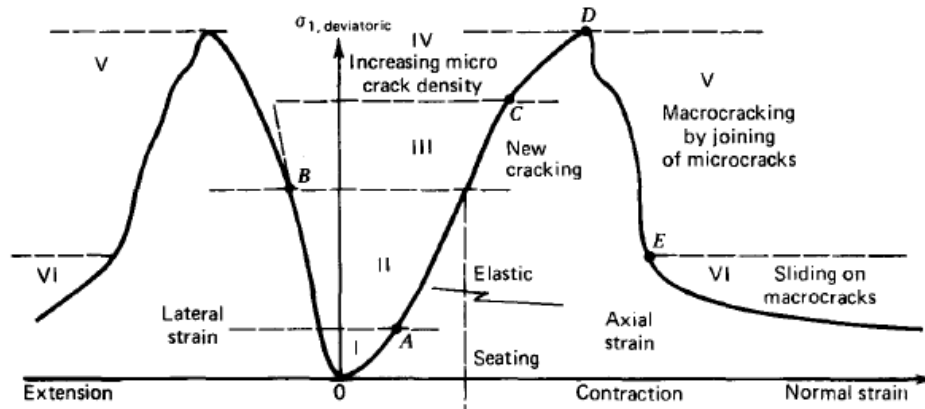
Figure 3.7: Strain zones of a rock specimen under loading (Goodman, 1991).

can either strengthen or weaken as a result of the cycles of stress applied to them. As a result of this, a common term to describe the effect of long term varying load on a rock sample is fatigue. As explained by Momeni et al. (2015), who tested granitic samples, cyclic loading can be used to find more dynamic values for Youngs Moduli. Moreover, it shows that the continuous opening and closing of cracks has an influence on the final strength of the samples and the strain that it endures. The research also found that cyclic loading gives an indication of fatigue levels of the samples. Granitic rock as used in Momeni et al. (2015) exhibited a decrease in fatigue stress (or fatigue UCS) with an increase in fatigue life (more cycles of loading) according to a negative power law.

Methodology
The laboratory tests of this research are all conducted within the TU Delft's own rock mechanical laboratory. Using the support of the laboratory technicians, this laboratory has produced results for more than a hundred years. The machinery adheres to the standards of the ASTM, like the ASTM D7012-14e1 (2017) for Uniaxial Compressive Testing. As a starting reference, an older (2019) block of nepheline syenite, as used in the research by Mulder (2019), was cut in cylindrical samples, using a diamond drill (Figure 3.8). The block is from a known location in the mine where a flat-jack test has been conducted (Measurement location stope 2) in the past and acoustic measurements will be done on in this thesis. These 2 cylindrical cuts were later made into five $30mm$(diameter) - 70 mm (length) samples using a diamond cutter.

A choice was made for the $30mm$ diameter and 70 mm length to match the apparent strength of the nepheline syenite and the capabilities of the load cell (maximum 500 kN of load). It is important that the sample can be broken, thus a relatively high (2.3) ratio between length and diameter was preferred over the TU Delft standard 30x60 configuration. Also, material properties allowed for a cut of 5 even 30x70 samples. In case a sample showed brittle behaviour at the sides, a choice could be made to remove 10 millimeters from the length of all samples, something that would not be possible when using 30-60 millimeter samples from the start. Later, the samples from Hoek van Myrvang were drilled in the mine using a diamond drill (3.9) of $40mm$. Therefore, a choice was made to make those samples >80 mm of length, to match the guidelines as specified in the ASTM D7012-14e1 (2017).

Figure 3.8: The author of this report drilling the samples from a nepheline syenite block.

Figure 3.9: The location of the sampling drillholes compared to the old drillhole by Myrvang in 1973.

The samples were then dried and put into the set up of the UCS-machine. A schematic of the set-up is visible in Figure 3.6 in the previous paragraphs and an actual image of a sample between the several plates is visible in Figure 3.10.

Figure 3.10: A (broken) nepheline syenite sample in the set-up as described before.

To start the test, a begin and end point are specified in the loading software of the load cell. Two displacement transducers are set to minimum amount of displacement and coupled to each other to calculate average axial strain during the application of load. Furthermore, a chain is put around the sample to actively measure the radial strain by the sample.

Once the safety barriers are put into place, loading can begin using a strain-controlled mode. This implies that every second, the load cell tries to achieve a certain amount ($0.001 \ mm$) of strain. It is important that the acoustic and stress-strain measurement start at the exact same time for further reference and comparison in analysis. During the test, until loading, strain measurements, both axial and radial are taken. Once a sample breaks and no longer has any strength left, the test is stopped and the data analysed. A summary of the samples with notes can be seen in Table 3.2. Furthermore, some of the samples will be loaded cyclically, to achieve fatigue values and to see the possible change in UCS, strain and thus elasticity. This will be achieved by loading the first sample in the sample group towards its maximum UCS. Using this UCS, the next samples can be loaded towards roughly 10% of that UCS, and consequently unloaded. The next loading cycle on that same sample will be increasingly powerful

towards 30% of the UCS of its predecessor, and consequently unloaded. Cycles then follow to 50 and 70 % of the UCS value. The final loading cycle will go on until the breaking of the sample is achieved.

Table 3.2: Samples used in the UCS-test

Sample ID:	Diameter (mm)	Length (mm)	Note
ALU1	30	70	Dummy sample
NSLM1	29.82	70.13	Had a crack in it (visible before loading)
NSLM2	29.79	70.09	
NSLM3	29.85	70.17	Errattic loading, no data gathered
NSLM4	29.91	70.15	
NSLM5	29.78	70.04	
ALU2	40	80	Dummy sample for new set-up
HvMCore1	39.91	80.54	
HvMCore2	41.10	80.53	Does not adhere to ASTM D4729-19 (2019)
HvMCore3	39.65	80.42	Visibly cracked sample
HvMCore4	39.70	80.41	
HvMCore5	39.60	80.25	
HvMCore6	39.61	80.09	Cracks visible
HvMCore7	39.80	79.91	

Analysis

By applying the formula's mentioned in Chapter 3 and then in particular formula's 3.2 and 3.1 on the elastic (straight) part of the stress strain curve (Figure 3.7) one can obtain the elastic parameters. The UCS of the samples is the peak load or the highest stress the sample could sustain without breaking. The problem with the set up is the usage of the pistons and metal plates between the loading plates and the sample. This does not influence the UCS but it does influence the measured axial elastic parameters.

To allow for removal of the 'error' generated by the usage of different material as the sample, the set up is fitted with an aluminium sample (with a known Young's Modulus of 70 GPa) and consequently measured. The found stress-strain curve can then be rid of the elasticity induced by the aluminium sample, which generates a curve that fits the strain of the set up. For evaluation purposes, the Young's Modulus of this strain is consequently found and using this Young's modulus, future tests on samples can be adjusted accordingly.

The data that is found after adjusting for the set up is compared with the values of the other samples and ones found in literature to see if they can be interpreted as correct measurements. Following this check, the Young's Modulus (E) and Poisson's ratio (ν) can be used to calculate the Bulk Modulus (Formula 3.3), Shear Modulus (Formula 3.4), Lamé's first Parameter (Formula 3.5) and the P-wave Modulus (Formula 3.6). These can then be used to interpret the data more thoroughly and for comparison with other tests.

$$K = \frac{E}{3(1-2\nu)} \qquad \text{Bulk Modulus (GPa)} \qquad (3.3)$$

$$G = \frac{E}{2(1+\nu)} \qquad \text{Shear Modulus (GPa)} \qquad (3.4)$$

$$\lambda = \frac{E\nu}{(1+\nu)(1-2\nu)} \qquad \text{Lamé's First Parameter (GPa)} \qquad (3.5)$$

$$M = \frac{E(1-\nu)}{(1+\nu)(1-2\nu)} \qquad \text{P-wave Modulus (GPa)} \qquad (3.6)$$

3.2.2. High Frequency Acoustic P/S-wave measurements

The way the UCS test is performed makes it possible to also put acoustic (also known as seismic), ultrasonic P and S waves through the sample. The P wave, short for primary wave or pressure wave,

is an elastic wave that propagates through a medium, generated by a source. This source can be as large as an earthquake or as small as an piezo-electric transduction, as used in the laboratory. The S-wave, short for secondary wave or shear wave, is also an elastic wave that propagates through a medium.

The difference between the two is in the names they have been given. P waves come before S waves, hence the primary and secondary. Next to that, P waves are waves in the form of pressure (compression and dilation), thus only moving the medium in one direction, parallel to the propagation of the P wave. S waves, on the other hand, are shearing through the medium, meaning they move the medium perpendicular to the wave propagation, thus needing more energy and losing speed. Because of the higher energy of the S-wave, the S-wave is more powerful than the P-wave. This difference is also seen in earthquakes, where the quicker P-wave is used as an indicator for the more destructive, but slower, S-wave and Rayleigh waves. Figure 3.11 depicts the difference between P-wave and S-wave.
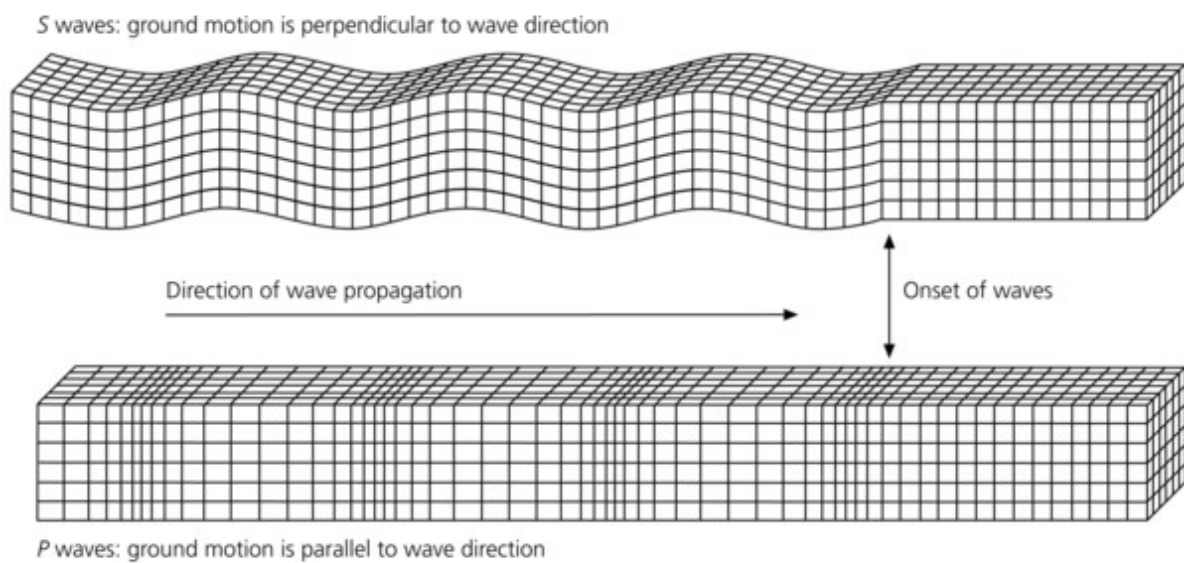
Figure 3.11: Difference between P-wave and S-wave (Newman, 2018)

"Listening" to a P- or S-wave will give information about the wave form and arrival time of both waves. The relevance of this information has been studied a lot over the years. Bieniawski (1978) called it 'petite seismic' and correlated the frequency of the seismic S-waves, generated by a hammer, with the in-situ Young's Modulus. He found an empirical relation, Equation 3.7, between the two properties.

$$E_{\text{M}}(GPa) = 0.054f - 9.2, \qquad \text{with } f \text{ in } Hz \qquad (3.7)$$

More recently, with the ever evolving methods of generating and measuring P-waves, Zhang et al. (2021) described the relation between stress and P-wave speed in sandstone samples, concluding that in the elastic zone, speed and stress correlate strongly. P-wave speed evolves non-linearly with increasing and decreasing stress. When the loads exceed the elastic capacity of the sample, the P-wave speed starts to decrease. This usually happens after 70 % of the peak strength or UCS.

The strong correlation between rock characteristics and P-wave speed is also confirmed by Rahman and Sarkar (2021), who through the application of a neural network, (un-)supervised learning and a large lithological dataset, found that per lithological group there exists a correlation between P-wave velocity (Vp) in granites, and UCS, Equation 3.8.

$$UCS = 5.095Vp^{1.8671} \qquad (3.8)$$

A similar study, conducted by Yesiloglu-Gultekin et al. (2013) also found a correlation (Formula 3.9) between UCS and P-wave velocity in granitic rocks which gives similar results to that of Rahman and Sarkar (2021).

$$UCS = 0.027Vp - 19.759 \tag{3.9}$$

Barton (2006) covers the correlation of seismic or acoustic velocity of a rock with multiple properties of the rock mass, like rock quality (RQD), attenuation and anisotropy, this will be used later in this research. Also, this book shows that laboratory results from the seismic velocity are essential to correctly interpret the field data gathered.

Using the dynamic properties of the P-wave and S-wave, it is also possible to calculate a dynamic elastic modulus. This is done by using formulae 3.10, 3.11, 3.12, 3.13 with ρ being the density of the medium (kg/m^3). It uses the elastic properties of rock and the dynamic Poissons ratio to find this modulus. As the resultant value of that calculation is usually estimated higher than the static Youngs Modulus found via the stress-strain relation, various studies have been done on finding a way to correlate both values.

$$M = \rho V_\mathsf{p}{}^2, \qquad \text{P} - \text{wave Modulus (GPa)} \tag{3.10}$$

$$G = \rho V_\mathsf{s}{}^2, \qquad \text{S} - \text{wave Modulus (GPa)} \tag{3.11}$$

$$\nu_\mathsf{d} = \frac{V_\mathsf{p}{}^2 - 2V_\mathsf{s}{}^2}{2(V_\mathsf{p}{}^2 - V_\mathsf{s}{}^2)}, \qquad \text{Dynamic Poisson's Ratio} \tag{3.12}$$

$$E_\mathsf{d} = M * \left[\frac{(1 + \nu_\mathsf{d})(1 - 2\nu_\mathsf{d})}{(1 - \nu_\mathsf{d})}\right], \qquad \text{Dynamic Young's Modulus (GPa)} \tag{3.13}$$

Li et al. (2006) studied these dynamic properties of rock and found a strong correlation between the two, but also stated that elastic moduli are stress dependent and should thus be treated as such. They also gave three correlation formulae (3.14, 3.15, 3.16), retrieved from literature, to transform dynamic elastic moduli in the more used, but static Youngs Modulus.

$$E_\mathsf{s} = 1.263E_\mathsf{d} - 29.5, \qquad \text{(King, 1983)} \tag{3.14}$$

$$E_\mathsf{s} = 0.74E_\mathsf{d} - 0.82, \qquad \text{(Eissa and Kazi, 1988)} \tag{3.15}$$

$$\log_{10}(E_\mathsf{s}) = 0.02 + 0.7\log_{10}(\rho E_\mathsf{d}), \qquad \text{(Eissa and Kazi, 1988)} \tag{3.16}$$

It can thus be observed from literature that there is a clear significance in measuring P and S-wave speeds in a sample, for multiple purposes. The combination with uniaxial loading makes it also suitable to measure and monitor the dynamic moduli in a rock, which might give insightful data for comparison between measuring velocities in the mine and measuring velocities in the lab. Chen et al. (2020) also studied the effect of the dynamic properties of rock samples using cyclic loading and found similar results to the correlation formulae (3.14, 3.15, 3.16). Interestingly, they found the velocities at low stress to be decreasing after multiple loading cycles. They attributed this phenomenon to the initiation of cracks in the higher stress domain. The peak stress in the research by Chen et al. (2020) increased gradually after every cycle and with it the P-wave velocity.

By applying cyclic loading on the samples, it can be interesting to see whether the Kaiser effect, as explained by Mulder (2019), is also observable using active acoustics. It has mostly been used to observe the 'stress-memory' of rock samples using acoustic emissions, which according to the Kaiser Effect should be dominantly observed after the increasing stress surpassed the previous stress-state of the rock sample.

Methodology
During a UCS-test (Figure 3.6), the nepheline syenite is held in its place by two aligned transducers (see Figure 3.10) to prevent measuring a different S-wave phase. The ceramic piezo-electric transducers are fed by an amplifier which amplifies the signal from an oscilloscope. While testing, the top transducers sends a signal through a conducting lubricant, stainless-steel piston, the sample, conducting lubricant,
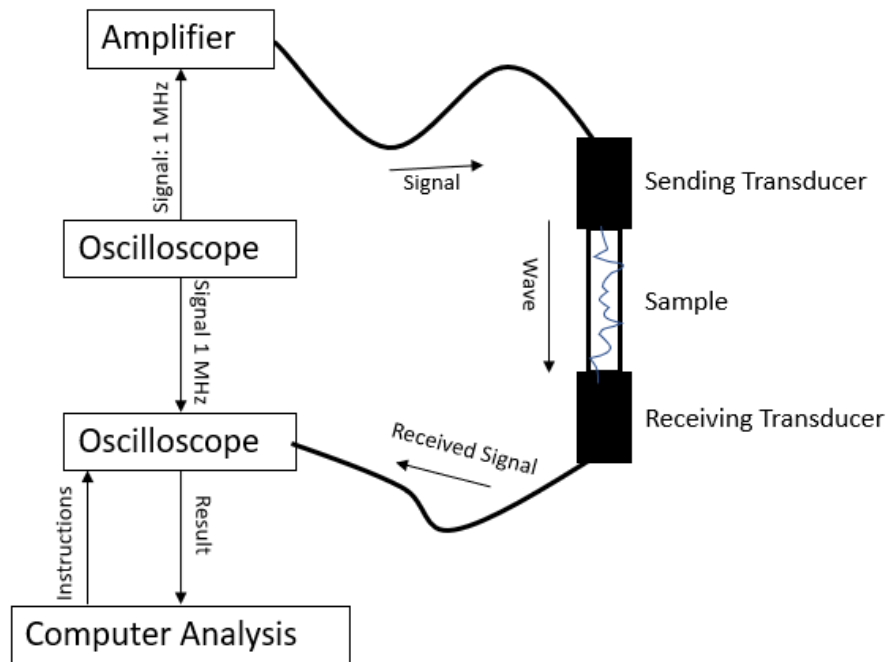
Figure 3.12: Schematic of the Active Acoustic signals and data during measurement.

stainless-steel piston towards the receiving transducer. This signal is then received in a processing oscilloscope, next to the original wave-form, produced by the producing oscilloscope. Via filtering and measuring over a time of 5 seconds, one can obtain a standing wave related to the stress the sample is enduring around that time. A schematic of the data gathering and processing using Active Acoustics is visible in Figure 3.12

To remove unwanted data one would have to remove the time it takes the wave to travel through the pistons. By measuring a known (aluminium) sample, traveltime adjustments can be made for the media that are not the sample. Noticeable on Figure 3.10 are the tapes around the stainless steel pistons. These tapes hold a rubber cylinder in place, which can harmlessly apply uniform pressure at the transducers to achieve a good transmission of the signal. Once applying stress using the hydraulic pump, the starting position of the measurement is the moment when a solid waveform can be measured using the pistons.

During the UCS test, active measurements are taken over a 5 second period. Because of the calculating capabilities of the oscilloscopes, the period it takes to do the averaging takes around 10 seconds. This means that a half of the acoustic data is not measured. Nonetheless, the representation of the waves should still be sufficient for the purpose of the research.

After a sample breaks and the load-cell is stopped, it is important to immediately also stop the acoustic measurement, to ensure comparison for results. Then data is then stored and analysed.

Analysis
The acoustic measurement results in the acquisition of a wave profile over time (amplitude against time) per time step, where each time step correlates with 1 wave profile generated. A general UCS test generates between 65 and 100 time steps of 10 seconds in which the average wave-data of that time step is stored. As this data is created as binary data, the first step for analysis is the conversion of the data into normal integers. The code for this conversion is provided by the laboratory staff. The second step is to take a rolling average of the data over a certain period of time (μs), using a simple convolution.

The averaged data is now ready to be interpreted on travel time. The travel time is the time it takes for the wave to go from its source to its receiver. As the transducers used in this research are capable of generating both a P-wave and a S-wave, every measurement will require two readings of travel time. As waves are undulating and sometimes tricky to read without bias, this research created a code that aims at approximating the onset of the wave-arrival as good as possible.

The found travel time now needs to be adjusted for the time it takes to travel through the pistons before the wave transfers to the sample. For this adjustment, the aluminium dummy test comes in useful. By subtracting the time it takes to travel through the known aluminium sample (length as specified and P-wave-speed of 6420 m/s, S-wave-speed of 3040 m/s), the residual travel time can be found. This is now the time that will be subtracted from any found travel times and ensures a most accurate result as possible. The travel time, in combination with the length of the sample can further be converted into a wave-speed. Following the explanation in Chapter 3 and formulae 3.10,3.11,3.12 and 3.13, the travel times can be turned into elastic properties for comparison with the values found in the chapter above.

Also interesting for the analysis is the comparison with results found in the acoustic velocity measurements. Although the tests are not conducted in exactly the same way, the medium should behave in a similar manner and have the same wave speeds. This holds as long as the laboratory tested rock has the same properties as the rock that is acoustically measured in the field.

3.3. Rock Mechanical Field Tests

Because the tests had to be performed in an area without an active power supply, all the power was supplied by either batteries or the engine of a large tractor at the site. The cold environment ($\pm 3^{o}C$) of the mine also influenced the durability of the testing equipment and the power of the batteries. Nonetheless, with some handywork, tests could be conducted to the highest precision possible. The testing was done during the downtime of the mine, to prevent vibrations and other nuisances by the active mining operations. The absence of mining operations also ensured safety during the tests, as the location is next to the access road.

3.3.1. Flat Jack Test

The technique of flat jack testing has been introduced by Tincelin (1953) in France in 1952 as the first scientific way to measure stress in-situ in a rock mass. Since then, it has been further developed and used and is a well-known method in both mining and construction stress determination (Dodds, 1969), Alexander (1960), Panek and Stock (1964) and Schmitz and Bertges (2020). Flat jack testing is based on, as its name suggests, the application of a flat jack into a slot in a wall. The flat jack is in fact nothing more than two steel plates filled with hydraulic fluid, welded together in a shape of choice (usually rectangular or semi-rectangular/semi-circular). Two nozzles are welded on it to connect to an hydraulic pump. Despite its apparent ease to perform, ASTM has withdrawn the standard for the performance of the flat jack method to determine in-situ stresses and deformation moduli (ASTM D4729-08, 2017). Nonetheless, this research tried to keep the standard in mind whilst performing the flat jack test.

This slot is cut in whatever direction is wanted. He and Hatzor (2015) suggest that, in order to find the exact three dimensional stress profile in an ideal round tunnel of CHILE rock, a combination of six flat jack tests, at three different angles against the tunnel direction and at three different angles against the tunnel radius, would give the exact in-situ stress tensors. This is, however, not always necessary, depending on the result you are after. Goodman (1991),for instance, suggest at least 2 measurements, in the roof and in the wall. A single stress measurement, in combination with other methods like acoustics, can also give a full impression of the absolute in-situ stress state, given a proper correlation between acoustic measurements and stress (Leeman, 1964). This knowledge might already be good enough for engineering purposes (STANDARD, 2004).

A flat jack test, as seen in Figure 3.13, is set up in the following way. In a desirable location, the slot is cut using a cutting method, like a blade-saw or a diamond-saw. It is necessary to create an opening large enough that it will fit the desired flat jack. This flat jack cannot be outside the slot, for sound measurement and safety. Upon opening the slot, the rock mass will deform because of the
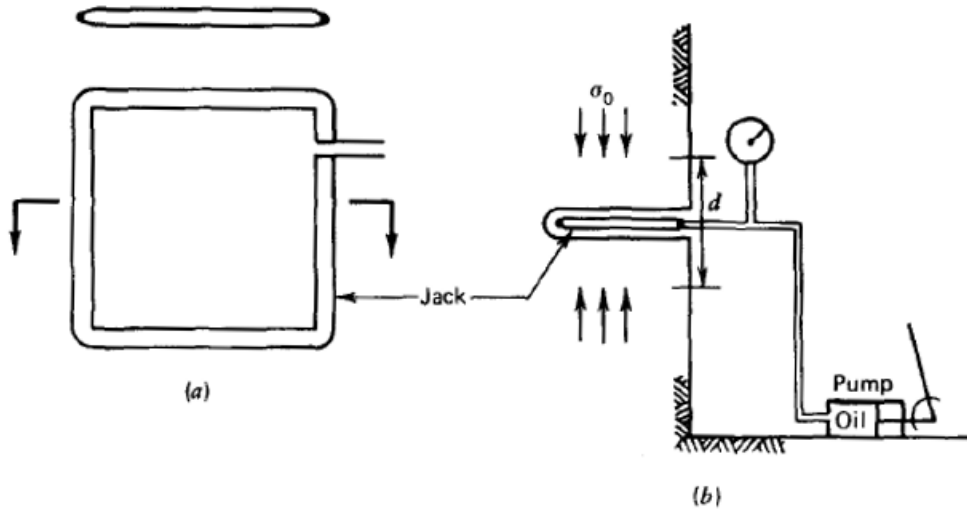
Figure 3.13: Flat jack (a) and Flat jack set-up (b) from Goodman (1991).

in-situ stress (σ_0 in Figure 3.13) or traction. Therefore, strain measurements (d in Figure 3.13) need to be taken to measure the deformation of the host rock. This can be done with strain gauges or with lasers. It is important to keep the measurement of deformation close to the slot over a length that is approximately one-third to a half of the length of the flat jack (Tincelin, 1953) (Goodman, 1991).

Upon the completion of the cut-out of the slot, one waits for the stabilization of the strain relief. Then, the flat jack can be inserted. The flat jack is pressurized (via the oil and pump in Figure 3.13) with relatively small increments, to actively measure the stress (with a manometer in Figure 3.13) and strain acting upon the rock. Once the strain has returned to its initial value, the stable value at the start of pressurization, the final pressure in the flat jack can be called the cancellation pressure. Schmitz and Bertges (2020) reported on a new method of flat jack testing, using a laser, this will also be the method used in this report whilst ASTM D4729-19 (2019) standards will still be adhered to for this test.

The direct results of the tests are then the cancellation pressure, along with a plot of the strain against the applied pressure. Various methods can consequently be used to determine the principle stress perpendicular to the flat jack. As indicated before, this is dependent on the location of the flat jack, the size of the flat jack and the size of the slot. The calculations mentioned in the ASTM document are based on workouts by Dodds (1969), Alexander (1960) and Panek and Stock (1964) and have since the 1960s been accepted and used for doing flat jack tests and calculating elastic response of rock masses. They are based on the elastic theory principle proposed by Tincelin (1953) that a flat jack is a elliptical opening in an infinite stressed sheet, where W is the displacement of the opening. This displacement is built up by three individual displacements, namely (ASTM D4729-08, 2017):

- W_0 = The displacement on one side of the slot during cutting of an infinitely thin slot
- W_1 = The displacement on one side of the slot due to finite slot width
- W_2 = The displacement on one side of the slot due to biaxial stress (σ_2)

Realizing that $W = W_0 + W_1 + W_2$, it becomes clear that the application of stress to cancel this displacement using the flat jack (W_{fj}) also cancels out all these individual displacements or:

$$W_{fj} = W = W_0 + W_1 + W_2 \tag{3.17}$$

Via elastic theory and trigonometry, formulas (not mentioned in this report) for W_0, W_1 and W_2 were derived. Using 3.17, a formula for W_{fj} could also follow:

$$W_{fj} = \frac{PC_0}{E} * \left\{ (1-\mu) \left[\sqrt{1 + \frac{Y^2}{C_0^2}} - \frac{Y}{C_0} \right] + (1+\mu) / \sqrt{1 + \frac{Y^2}{C_0^2}} \right\} \tag{3.18}$$
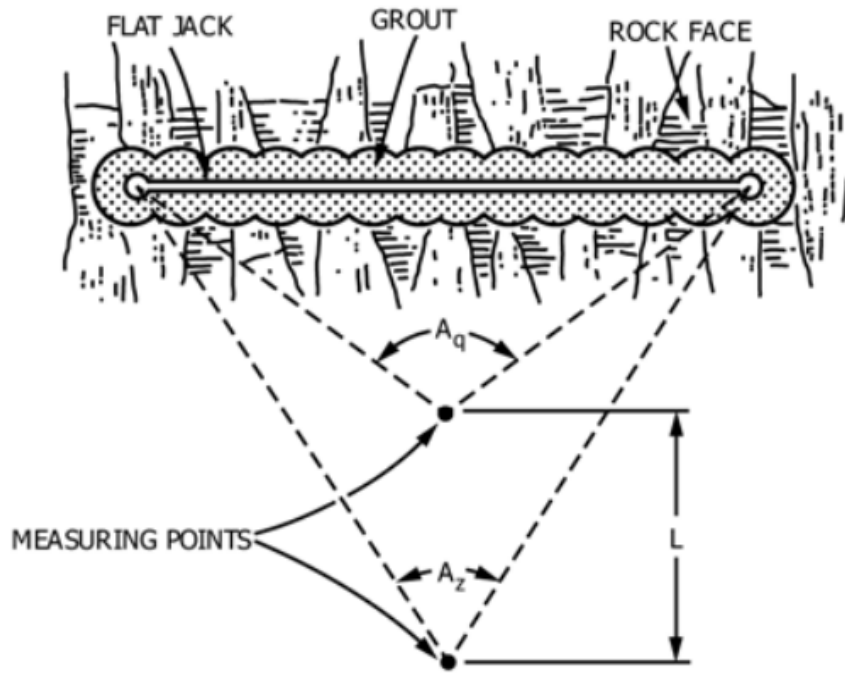
Figure 3.14: Geometric description for elastic calculations (ASTM D4729-08, 2017).

where:

- P = Cancellation Pressure (MPa)
- C_0 = Half length of the flat-jack (mm)
- E = Youngs Modulus (MPa)
- μ = Poissons ratio
- Y = distance of deformation measurement point to center of flat jack. (mm)

This displacement at the flat jack should always be greater than the measurement made above or $W_{fj} > \Delta d$ and as such can act as a control measure of the flat jack method. Further analysis can be done on the induced strain in the rock mass, to find the elastic modulus, given that measurements are done in two points that lie a distance L from each other in a line perpendicular to the flat jack (Figure 3.14). To then calculate the elastic modulus, the following formula applies:

$$E = \frac{PLR}{2\pi\Delta d} \tag{3.19}$$

Here:

- E = Youngs Modulus (MPa)
- P = Cancellation Pressure (MPa)
- L = Distance between measuring points (mm)
- R = The stress distribution factor
- Δd = deformation measurements between points. (mm)

The stress distribution factor R can be formulated using the geometry visible in Figure 3.14, the Poisson's ratio μ and the angles from the measuring points to the ends of the flat jack, A_q and A_z:

$$R = A_q + \sin A_q - \mu(A_q - \sin A_q) + A_z + \sin A_z - \mu(A_z - \sin A_z) \tag{3.20}$$

Finally, the cancellation pressure P needs to be adjusted to find the actual stresses acting on the rock mass of interest. The method used in ASTM D4729-08 (2017) states the following formula but no clear adjustment constants:

$$\sigma = P * a + Q * b \tag{3.21}$$

Where Q is the stress parallel to the flat jack and a and b are the adjustment constants governed by the geology and geometry of the flat jack and the slot. In industry reports, such as Schmitz and Bertges (2020), the adjustment is done with a method known as the tributary area method. Being derived from room and pillar mining (Figure 3.15), this method takes into account the overhang that is cut away by the diamond-saw, but not supported by the flat jack. To get an as good as possible result from the comparison of the pressure imposed by the flat jack with the actual acting stresses, the overhang should be taken into account. The workflow for the tributary area method is as follows:

First one compares the total slot area with the area of the flat jack, to determine which area of the 'roof' is supported by the flat jack and which area is supported by the wall. Using that information, the extraction ratio r (Hauquin et al., 2016) can be found and formula 3.22 can be used to retrieve the real stress (σ_{real}) from the pressure in the flat jack (σ_{measured}). This is an adaptation of Formula 3.21, and assumes the stresses acting on the plate to be only perpendicular.

$$\sigma_{\text{real}} = \sigma_{\text{measured}}(1 - r) \tag{3.22}$$
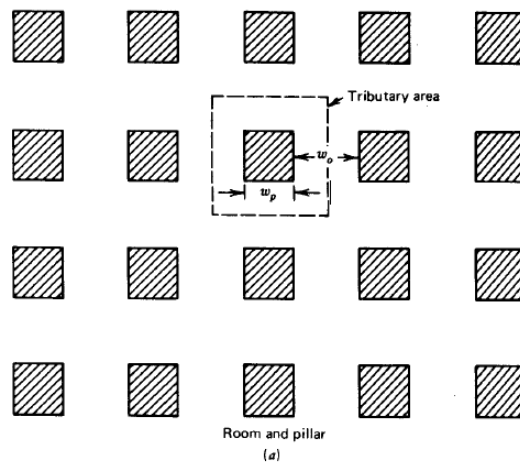
Figure 3.15: Tributary area in room and pillar mining to calculate pressures in the pillar induced by the additional overhang (Goodman, 1991).

If multiple flat jacks are done in 2 stress directions, it could be useful to utilize the Kirsch-equations, as specified by Kirsch (1898) for openings in a rock-mass. However, this method assumes a CHILE rock mass. Khodabin and Hosseinitoudeshki (2014) tried to figure out a way to interpret the Kirsch parameters for non-homogeneous rock, but only did this for tunnels and larger openings. It is thus questionable whether this also applies to smaller openings, like a flat jack. Now some formula's will follow to explain the The modified Kirsch equation, as specified by Goodman (1991) is shown in equations 3.23, 3.24, 3.25.

$$\sigma_{\text{r}} = \frac{P1 + P2}{2}\left(1 - \frac{a^2}{r^2}\right) + \frac{P1 - P2}{2}\left(1 - \frac{4a^2}{r^2} + \frac{3a^4}{r^4}\right)\cos(2\theta) \tag{3.23}$$

$$\sigma_{\theta} = \frac{P1 + P2}{2}\left(1 - \frac{a^2}{r^2}\right) - \frac{P1 - P2}{2}\left(1 + \frac{3a^4}{r^4}\right)\cos(2\theta) \tag{3.24}$$

$$\tau_{\text{r}\theta} = -\frac{P1 - P2}{2}\left(1 + \frac{2a^2}{r^2} - \frac{3a^4}{r^4}\right)\sin(2\theta) \tag{3.25}$$

In the equations above, σ_{r} is the stress resulting from the opening at a distance r in the wall, σ_{θ} is the stress at angle θ from that opening, $\tau_{\theta r}$ is the traction at the point with coordinates (r,τ) resulting from the opening. Inputs are $P1$ (σ_1), $P2$ (σ_2) and a is the radius of the opening.

Figure 3.16: The laser measuring deformation with respect to the plate attached to the wall.

Methodology

The flat jack is set up in the following way, as specified by Schmitz and Bertges (2020). First, a location needs to be determined. This is preferably done at a accessible part of the rock mass, to make the handling of the preparatory work easier. It is also important that the area is relatively flat and is suitable for the type of stress you want to measure. It is thus chosen to take a flat area at the height of one's hip, some 3 metres from the stress measurement in the World Stress Map.

At this location, a bar of around 3 metres in length is connected to the rock mass via rock-bolts. The bar is leveled as much as possible. Then, in the middle of the bar, a bolt is connected at 13.5 cm, which is around 1/3 of the length of the flat jack (35 cm). It is from this bolt that the strain measurement will be taken, with respect to the bar (Figure 3.16). This bolt is consequently fitted with a plate that is also leveled. Finally, a saw-stabiliser is attached to the wall. It is important to make sure this attachment is in the exact right position, as the horizontal and vertical dip of this attachment will determine the angle in which the flat jack fits in the wall.

Finally, a laser is attached to the bar, pointing towards the plate attached to the rock-bolt. Using this laser, continuous measurements are taken of the strain endured by the rock mass. Once the laser is set up, an initial measurement can be taken. This is the zero-deformation measurement and will be the reference point for the loading cycle as it indicates the cancellation pressure. With this important distance noted, the diamond saw can be attached to the stabiliser and using hydraulic power a 4 mm slot can be cut into the wall. This is a tedious process ($\pm$ 12 hours) as the rock is very hard and it cannot be automated due to the ever changing rock conditions. The sawing thus had to be made comfortable (Figure 3.17). During the sawing, measurements are taken to reconstruct the test as precisely as possible after its completion.

Also the sawing process is measured to see how much more sawing is required to fit a flat jack and for reference in the tributary area method. To measure the stress perfectly, a slot of exactly the shape of the flat jack would be ideal. To prevent the flat jack from bursting during the loading cycle, a certain distance between the jack and the pointy saw-pattern is required. The final set up of the flat jack in the

wall and the attachments on the wall can be seen in Figure 3.18.

Figure 3.17: The sawing of the slot of the flatjack (by Jeras Dieleman).

Figure 3.18: The set up of the flatjack.

After the insertion of the flat jack, the hydraulic hose is attached to one end of the jack and the other to a manometer. This manometer is then connected to a manually operated hydraulic pump, for precision pumping. Once everything is connected and tested (e.g. pressurization is possible) and no air is left in the hose or the flat jack, the flat jack measurement could commence. It is, however, chosen to take a break before loading the rock again, to let the deformation stabilize. The first reading on the laser (Figure 3.16) is then maximum deformation. The pressure in the flat jack is consequently and increased with steps of 1 MPa per pumping increment. Every time, the pressure as well as the deformation is noted down in a spreadsheet and a handbook, along with the time. This is continued until the zero deformation criterium is met. After that, the unloading of the jack can begin in slightly larger steps of 5
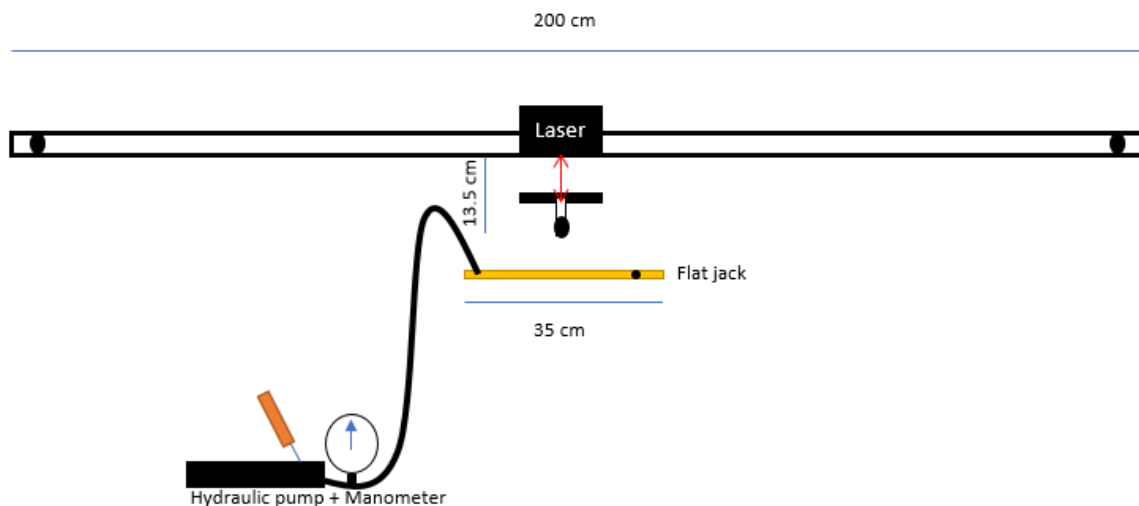
Figure 3.19: A schematic of the set up of the flatjack.

MPa. Once the flat jack is no longer under pressure a second cycle can begin and after that, a third. This whole process takes no longer than 2 hours. For reference and understanding, a schematic of the flat jack can be seen in Figure 3.19.

Next to the flatjack measurement, precise measurements of the location and the set up are taken using a laser-theodolite. It does so by measuring laser travel time and angle between the theodolite and two known and visible reference points in the mine and connecting that knowledge with the same technique applied to a point on the wall. Using the data collected by the theodolite, levelling of the flat jack can be corrected for by using Elastic Theory. Also, by knowing the exact location of the measurement, the stress value found can later be implemented in the stress model of the mine.

Analysis
By applying the methodology, the flat jack yields a pressure-strain graph and an adjusted stress value. The Youngs Modulus can be retrieved from the stress-strain curve or by using the ASTM-mentioned method. Analysis should be done carefully, as this Youngs Modulus is very dependent on the local rock mass quality and the stress-level. It might be better to compare it with the Modulus found using the RMR or Q-rating system instead of comparing it with the Youngs Modulus found in the UCS-test or Acoustic tests. That being said, the rock in the rock mass is still the same as measured in the laboratory and using the other tests, thus yielding the same rock mechanical parameters, only differing because of macro-scale differences (cracks, shear zones).

3.3.2. Acoustic Velocity Measurements
Acoustic Velocity Measurements works according to the same principles as the high frequency P and S-wave measurements in the lab. The low-frequency waves are generated and measured at one end of the medium and then propagate through the medium to the receiver, which stores the data stored in the wave in a computer. Tomography is the act using waves to describe sections of a body, and thus generating a two dimensional or three dimensional image.

The implementation of acoustic tomography is being researched since the 1980s. Thill et al. (1989) argued that the technique could have important use in the mining industry for multiple uses. The report compared the application of techniques used in borehole-logging of the oil and gas industry with applicability in mining. It identified the following 7 potential and promising uses of acoustics or seismics in mines:

  1. Elastic and Deformational Properties

2. Anisotropy
3. Porosity
4. Rock Quality
5. Geological Anomalies
6. Water Content
7. Stress state

Friedel et al. (1995) used extensive Acoustic or Seismic Tomography in a deep silver mine to find highly stressed zones. Even though it was hard to construct a full three dimensional image using only seismic tomography, their research did manage to easily find highly stressed zones using the tomographic sections. They also concluded that tomographic imaging or measurements should be done during maintenance or shift changes, as the slightest noise can drastically offset the data. Also, the research by Friedel et al. (1995) found that it was hard to determine the exact path of the waves, due to backfill and other non-host rock material. Waves would merely go around these low-velocity zones and thus any results could not be interpreted correctly.

More recently Dong et al. (2022) also used acoustic tomography to find anomalies in heterogeneous subsurface rock masses. Even though a full recreation of the anomaly was not achieved due to the complexity of acoustic tomography, it was possible to conclude a good understanding of the subjected rock mass. As a concluding statement, they stated that sensor placement and reduction of background noise if very important for this technique.

Methodology
On the same rock mass in which the flat jack measurement was done, also acoustic measurements could be taken. The location is ideal for this as it features two semi-parallel walls in it, one at the access tunnel and one at the indent in which the transformer block is located. As this is not the case in all parts of the mine as it is not a room and pillar mine, measurements along the wall that has the flat jack in it were also conducted.

On both sides of the pillar, five rock bolts were drilled into their respective walls (approximately 10 cm into the rock), giving 10 locations of measurements. Also on the walls along the underground opening bolts were places (WSP and WNP). On the bolts, a geophone is places using the thread of the rock bolt (Figure 3.21) to assure firm attachment and thus transmission of the acoustic wave.

The mine only had 3 available geophones (developed by Sibelco and Dr. Bertges Vermessungstechnik, type AANDOS, 2017) so for ease of measurement it was chosen to only use two, one sender and one receiver. The sender is less sensitive as the receiver, as the sender is close to the source and thus needs more dampening for a clear signal representation. After testing and calibrating the geophones, testing could commence. This was done from the locations as seen in Figure 3.20.
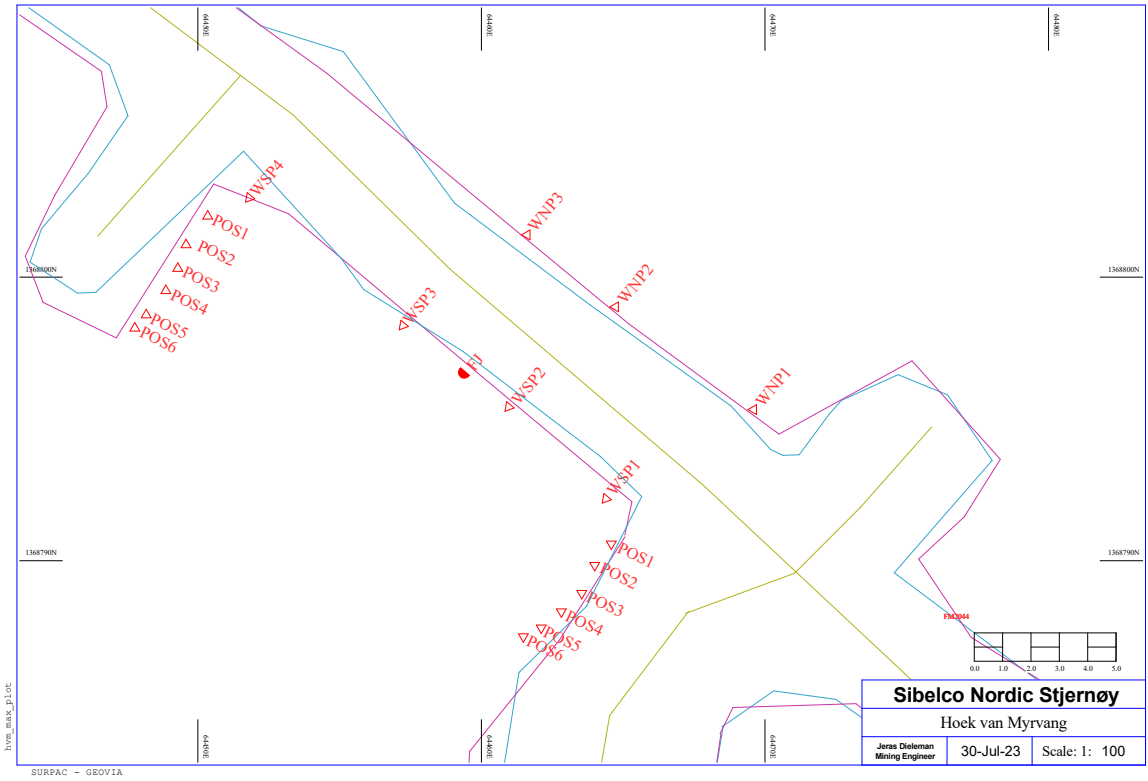
Figure 3.20: Locations of geophones with respect to flat-jack.

Figure 3.21: AaNDoS geophone connected to a rock bolt.

As by Figure 3.22, two geophones, a sender and a receiver, are connected to the rock bolts in the wall. After this, a hammer blow is applied to the wall to create a wave (seismic/acoustic, low frequency P-wave). This wave propagates through the rock mass to the very close sender and the opposite receiver. The geophones record the wave signal and send it to the computer. The hammer strikes three times for comparison. Then, the data is saved on the computer and the geophones are switched from position 1 to position 2 on both sides of the rock mass. The same action is repeated and the geophones are replaced again and again till position 6 is reached. To ensure stability of the data and to create a clearer image for the tomography, the sender and receiver are switched from tunnel to transformer and vice versa. Following this, the whole process is done again. After testing, the recorded data is analysed.
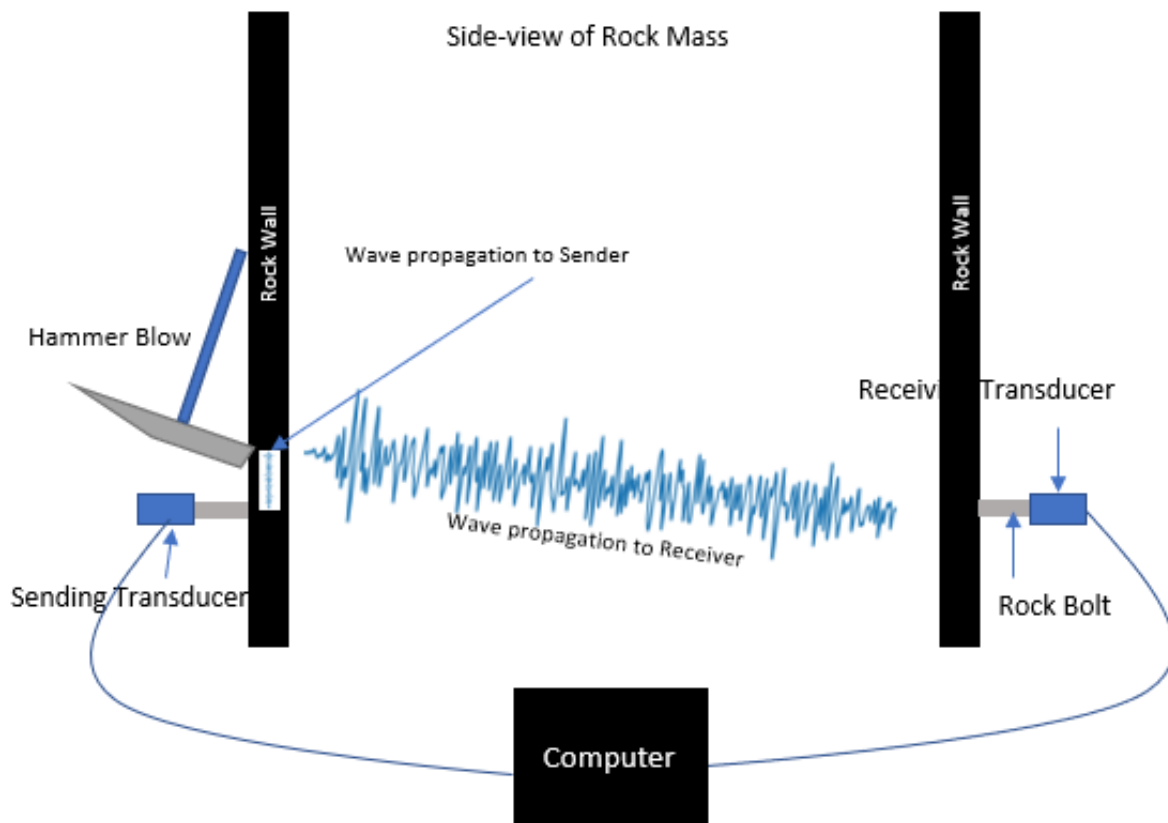
Figure 3.22: A schematic of the set up of the acoustic test in the mine from tunnel (left) to transformer (right).

After the test through the pillar, a sonic velocity test through the wall of the where the flat jack was (named WSP) situated is conducted. This will be done from locations spaced roughly 4.5 metres from eachother. From each location measurements will be done to all the other locations on that wall and vice versa, creating 12 separate measurements along the wall. The test and installation procedure is the same as the test through the pillar. Figure 3.20 shows the bolt locations (WSP) on the respective wall with respect to the flat jack. A similar test was done on the opposing wall (WNP). There, only three measurement points were added, as a massive weakness zone intersected the wall outcrop. Figure 3.20 shows the locations of measurements on that side of the wall.

Thirdly, a test lined out similar to the WSP measurement was done on the wall in stope 1 of underground mine 2. Interestingly, during geotechnical work by Schmitz (Aug. 2018), the flat jack of that measurement showed extension and no compression during the cutting of the slot. No traction-value could be found but perhaps the measurement of acoustic velocities will provide the answer.

Analysis
Once again, the in-field acoustic measurements should be handled the same way as the laboratory measurements. The measurements produce a binary file that was converted by the provider of the equipment and then stored in a text file denoting time and amplitude. As two measurements are taken and the source wave is produced by a hammer blow and thus not exactly known, analysis is done on the difference between the two waves, as well as on the wave-form of a single wave. As for now, only velocity analysis is done, due to the difficulty of reading the data files properly and the amount of noise on the data. The velocity analysis itself is rather simple and compares the arrival time of the wave at the sender (the first receiver) with the arrival time at the second receiver and divides this by the distance between the two points. The found velocity, which is a P-wave velocity, can then be compared with values found in the lab to correlate a stress based on velocity with it.

3.3.3. RMR and Q-value rating

The most challenging part of underground rock monitoring is the identification and understanding of weaker parts of the rock mass. With the aforementioned methods it is possible to measure stresses at certain locations, but identifying locations that are prone to failure because of bad rock quality is still difficult. It is too time-consuming to utilize either of those methods on every part of the mine. Numerical models can predict stresses in the mine, but this is not always also an indication of the quality of the rock. This problem was already identified long ago by Barton et al. (1974) and Bieniawski (1978) who built upon the Rock Quality Designation (Deere, 1964) to develop their respective RMR (Rock Mass Rating) (Bieniawski, 1989) (Developed between 1960 and 1973) and Q (rock mass Quality)-value (Barton et al., 1974) rating systems. The rating sheets can be found in the Appendix A (RMR) and Appendix B (Q-value rating).

These methods rely on visual interpretation of the rock mass, visible in underground openings. In the respective work of Barton and Bieniawski it becomes apparent that, because of the change of scale, different interpretations can be made on the strength of a rock mass. The ratings are based on the occurrence and state of joints (small scale recurring discontinuities) in the rock, along with other macroscale properties of the area of interest. Nonetheless, it still relies on information from the lab, like UCS, and information from core logging (RQD).

Barton (2006), who is the creator of the Q-system, did extensive research into the applicability of the Q and RMR rating systems into scientific methods that are less prone to interpretation bias, but more prone to measurement errors, like stress and velocity measurements. The extensive work covers the relations between velocity, attenuation and stress. A highlighted case-study in the book shows remarkable resemblance to this research, as also there, velocity, stress and a rating system were used to qualify a rock mass in the shallow subsurface of Norway. In this research (Barton et al., 1994), the subsurface was thoroughly measured on rock quality (RQD) via cores. Also cross-borehole acoustics were done, of which the results are visible in Figure 3.23.

Notable from this research was that although the velocity increased with increasing depth (Barton assumed increasing depth also meant increasing stress), the RQD (which is also used in the RMR and Q-rating systems, based on joints in the rock) from the cores stayed roughly the same with increasing depth. This is of interest in the mine because this means that velocity is not completely dependant on the joints in the rock and that perhaps confining pressure (the in-situ rock stress) closes the joints in the rock mass, leading to a higher velocity.
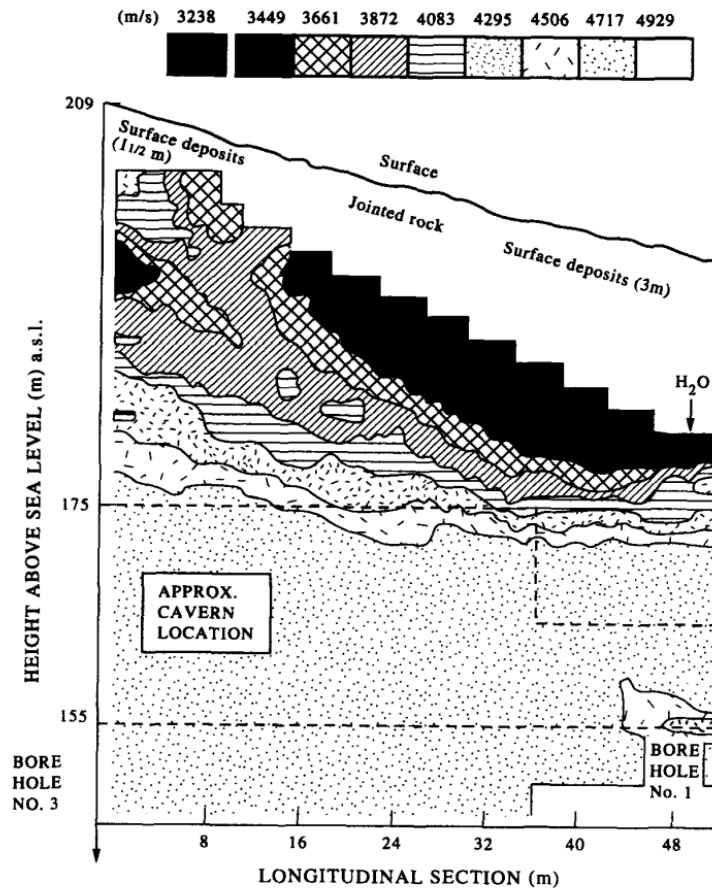
Figure 3.23: Velocity profile of Gjøvik cavern site (Barton et al., 1994).

Rock quality rating systems are mostly used to determine the need for additional support of walls and roofs in underground openings. That being said, it can, in combination with additional geotechnical monitoring methods, also be used as a monitoring method and correlates reasonably well with other properties of the rock, like the acoustic velocities (mainly P-wave) measured during the tomography or by cross-borehole measurements. This has been done and confirmed in multiple case studies, like Hemmati Nourani et al. (2017), Barton (2002), Barton et al. (1974) and Liu et al. (2021), although it was noted that correlating should not be taken as exact science and correlation at every case can be different.

Methodology
The RMR and Q-value rating in the underground mine was only done on the walls WSP and WNP following the ASTM D5878-19 (2019) standard. The forms as visible in the Appendices B and C are filled out and orientations of joint sets are measured using a geological compass. For further analysis, the found values of the RMR and Q can be compared using the known relating formulas with other rating systems, acoustics, stress and elasticity values. Additionally, acoustic velocities and UCS-values can be used as input into a RMR conversion system to find the Mohr-Coulomb parameters (friction angle, cohesion) of the rock mass. Next to that, joint set stereonets using the orientations found at both walls are created. Especially for engineering purposes this can be interesting.

Analysis
The RMR and Q-rating system are analysed by retrieving all necessary parameters from the rock mass and the tests (acoustics and mechanical). Together, these produce a final value, taking into account the SRF or stress reduction factor. This factor is similar to the Eurocode 7 risk-categories as seen in

Figure 3.3. Therefore, it is difficult to analyse the RMR and Q-rating systems on a pure scientific note. Nonetheless, the rating systems can be analysed on robustness (high and low estimates), similarity (do they compare to each other) and the advice that follows from the final results of the systems. Next to that, calculations using the input parameters of the rating systems can give useful rock parameters like the friction angle and cohesion, but also an estimate on seismic velocity. This can then be compared with the actually measured seismic velocity. Overall, the rating systems are not suitable as a sole analysis method, but rather a method to support and further analyse acoustic and mechanical monitoring methods.

3.4. Different Tests

Of course the aforementioned selection of tests are not the only possible tests at the Stjernøya site. It would be possible to, for instance, use a contractor to perform a different stress test. To be able to give a proper comparison between tests, two other tests are included in this review also. Because no actual tests are performed with them, only a brief summary of the implications and forthcoming of both the overcoring method and the hydraulic fracturing method.

3.4.1. Overcoring

The overcoring method is a method developed by the US Bureau of Mines to be able to measure rock stress in a three-dimensional way (Goodman, 1991). It is performed by first coring a borehole and putting a six-arm deformation measurement cylinder in it. Then, a larger (more than 2x diameter) borehole is cored over the initial measurement borehole. As this new coring cancels out the in-situ stresses that might have enacted upon the rock, the whole core is set to expand (or in theory, it could also compress). The measurement of this expansion via the deformation gauges inside the drilled core gives a three-dimensional strain. Using the assumed to be known elasticity of the rock, a set of equations can be set up to retrieve three-dimensional stress formulae from the strain. As these stresses are dependable on each other, at least one stress-tensor (out of σ_1, σ_2 or σ_3) should be known or assumed to solve the resulting equations, otherwise, only an elastic relation between the stresses is found.

3.4.2. Hydraulic fracturing

Hydraulic fracturing is also described by (Goodman, 1991) as a method to achieve stress information in boreholes at considerable depths (deeper than <800 metres), at places where no rock face is available to measure stress and preferrably the vertical stress is known. The method works by pressurizing a volume between two packers inside a borehole with water. This increasing pressure will at some point cancel out the compressional rock stress around the edges of the volume. The induction of tensile forces creates a crack, called a hydrofrac. This fracture will propagate and fill with the pressurized fluid until the pressure inside the volume falls to the so-called shut-in pressure, at which the pressure in the volume is steady. Using the Kirsch equations and the knowledge of the direction of crack-propagation a lot of useful information about the principal stresses and directions is generated.

This method is used extensively by the oil and gas industry to measure stress in deep boreholes, (Zang et al., 2017), however, combined hydraulic fracturing in a 410 metres deep hard rock mine in Sweden with measuring acoustic emissions, measured in a 20-30 metre borehole from an underground opening. The results from just the hydraulic fracturing gave horizontal stress, based on a known vertical stress because of overburden. The counting of acoustic emissions in and around the borehole gave useful information on rock mass strength and hydrofrac propagation. Also, Zang et al. (2017) researched the influence of different hydraulic loading conditions on the crack propagation and acoustic emissions creation. Despite the generation of useful information using two measurement techniques together, it was stated that more research on the topic was necessary.

3.4.3. Logistics and Costs

Finally, it must be stated that both techniques are not available in the remote Stjernøya and must be done by a contractor from somewhere else in Norway. These logistical constraints will add significant amount of extra time to the time it takes to drill boreholes in a confined underground opening, and perform the tests. This adds to significant extra costs of hiring a non-company contractor when performing

a hydraulic fracturing tests. Also, it must be stated that is difficult to perform the hydraulic fracturing method near the surface of the wall as it is a very invasive method that literally aims to break the rock, which might already be broken near the wall surface. Technically, the most important downside of both techniques is the requirement for a 'known' (vertical) stress tensor. In the fjord-like structure of the Lille-bukt complex, the vertical stress is very spatially variable, making it almost impossible to apply these methods.

4

Results

In this chapter, the results of the aforementioned tests will be reported. As this thesis aims to compare the conducted tests, this chapter will also elaborate on the similarities and differences between tests and the resultant data from them. To start, a quick overview of previous data can be seen in Table 4.1. Next to the data from the Ort i Felt location (HvM), also results from the Stope 1 at mine 2 (NSLM) will be shown, both lab and in-field results.

Table 4.1: The data of the overcoring test at the Ort i Felt location from the World Stress Map (Heidbach et al., 2016) as reported by Stephansson (1987) and measured by Myrvang (1973)

Characteristics	σ_1 (MPa)	σ_2 (MPa)	σ_3 (MPa)	E (GPa)	Poissons Ratio
Overcoring (38cm)	17.3	9.7	7.3	58	0.2

4.1. Laboratory Tests

4.1.1. Unconfined Compressive Strength Test

The UCS-tests produce stress-strain curves. One of them is visible in Figure 4.1, the rest of the stress-strain curves can be seen in the appendix. Samples all showed similar reactions to loading, following the classical elastic-plastic response of rock towards pressure. A rather long period was necessary for some samples to get through the initial loading phase (I). The elastic domain(II) persevered quite long until about 75-85% of the final UCS. The final phases (III and IV) happened rather quickly for most samples, generating a very large increase in radial strain before bursting vehemently (Figure 4.2). The results of all the tests can be seen in Table 4.2. Good to note is the length-diameter ratio of the samples. The NSLM samples have a diameter:length ratio of 30:70 mm, whereas the HvM samples have a diameter:length ratio of 40:80 mm. Despite this fact, results did not differ greatly regarding UCS and Elasticity.
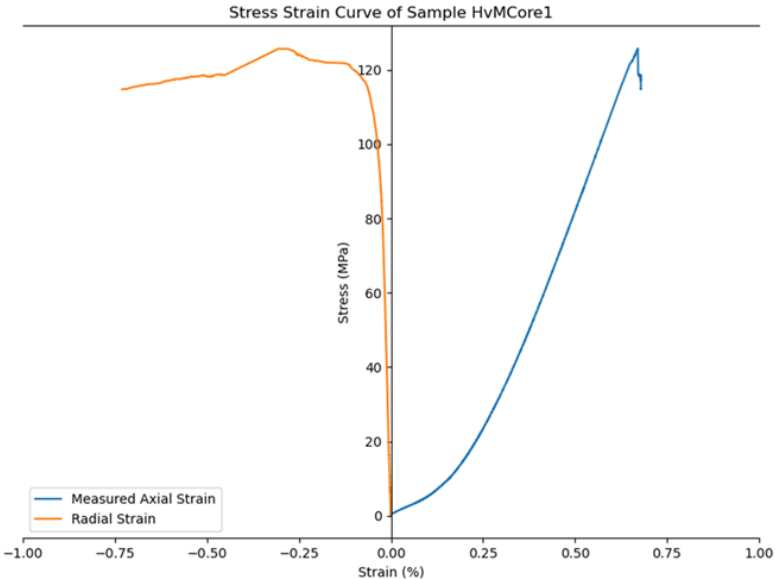
Figure 4.1: Stress-strain curve from nepheline-syenite sample HvMCore1.

Figure 4.2: The bursting of nepheline-syenite sample HvMCore1 after reaching its UCS.

The stress-strain curves are plotted without the elasticity of the set up in them. The Young's Modulus of the set up was found using the benchmark (with the Aluminium sample) and found to be 77.64 GPa for

the NSLM-samples and 44.19 GPa for the HvM-samples, because they needed a different set-up due to height increase of the samples. This was consequently multiplied with the induced stress to be able to remove the strain taken by the set up. What is remarkable about the stress-strain curve of sample NSLM2 and NSLM4 and possibly also NSLM1 is that the samples all show a similar jump in strain, both radial and axial, at around 1/2 the UCS. This phenomenon (see Figure D.3 in the Appendix) was also visible during testing. As the samples behaved differently after the event, but still had a lot of strength left in them, it is chosen to report two differing elastic moduli and two different Poisson's ratios. They can be seen in Table 4.2 as First Stage and Second Stage.

The trigger of this change in elasticity could be a spalling event, which is known to occur at around 1/2 the UCS-value of a rock sample. The HvMCore1 sample, however, was used as a benchmark for the cyclic loading tests and did not show the 'spalling-event'. The samples HvMCore2,HvMCore3 and HvMCore7 did show a sudden increase in radial strain at approximately 50% of the final UCS.

In general, the results of the cyclic loading, as visible in Figures 4.3 and 4.4 , show that the rock in the lower stress domain (10-70 MPa) behaves elastic. It was noteworthy during testing that the loading time for the cycle, the second time of loading the same stress range, is lower than the first time the sample went through loading of the same stress-range. No apparent change in UCS or Elasticity is visible from the cyclic loading in comparison to non-cylic loaded samples. A difference in Young's Modulus is visible between the NSLM and HvM Samples. The HvM samples have a higher Young's Modulus in the 60-80 MPa domain. A difference in sample length might be the reasons for this.

The height of the UCS correlates quite well with visible indicators of core quality, pre-noted before testing, and visible in Table 4.2. Other than that, the results of the tests show great similarity. Only the difference in Poisson's ratio stands out. Some samples show a large sudden increase in radial strain during the spalling event. This greatly influences the radial strain, giving a very different Poisson's Ratio in the higher stressed domain. Overall, the nepheline syenite of the sampled locations tends to show stress response in the direction parallel to the loading direction. If it cannot endure anymore pressure, it relieves stress with large increases in radial strain, not necessarily meaning the complete destruction of the core.
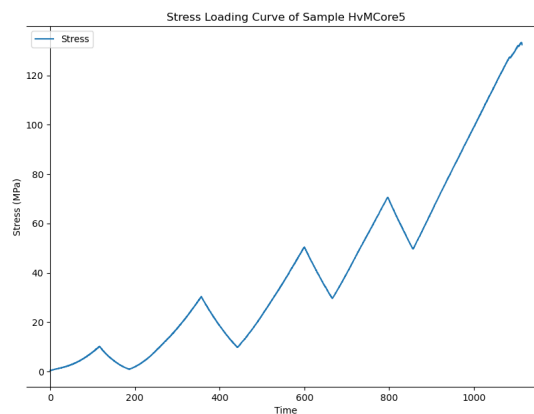
Figure 4.3: Stress-time(s) curve from nepheline-syenite sample HvMCore5.
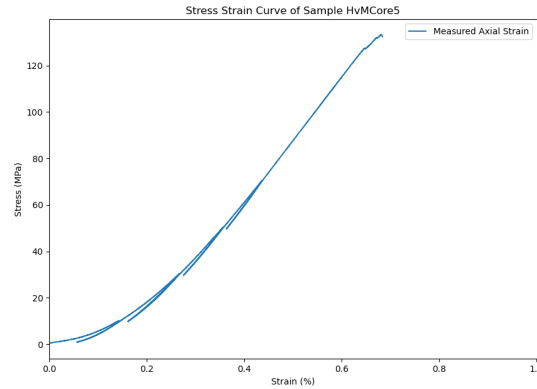
Figure 4.4: Stress-strain curve from nepheline-syenite sample HvMCore5.

Table 4.2: Results from stress-strain tests.

Sample ID:	UCS (MPa)	Youngs Modulus E (GPa)		Poisson's Ratio ν		Note
		First stage [20-40 MPa]	Second stage [60-80 MPa]	First stage [40 MPa]	Second stage [80 MPa]	
ALU1	*not reached*	70.00	-	0.10	-	Benchmark
NSLM1	74.91	39.81	-	0.002	-	Cracks Visible
NSLM2	122.41	33.04	47.68	0.35	0.0117	
NSLM4	115.76	30.94	46.21	0.29	0.0139	
Average NSLM	119.085	31.99	46.945	0.32	0.0128	Leaving out NSLM1
ALU2	*not reached*	70.00	-	0.10	-	Benchmark
HvMCore1	125.65	33.50	55.02	0.29	0.21	
HvMCore2	119.43	28.09	58.75	0.35	0.024	Cyclic
HvMCore3	138.66	36.85	66.99	0.51	0.28	Cyclic
HvMCore4	106.53	30.96	62.11	0.516	0.259	Cyclic, Visibly broken
HvMCore5	133.32	41.98	65.64	0.31	0.0243	Cyclic
HvMCore6	150.86	44.52	67.80	0.33	0.204	Cyclic
HvMCore7	113.13	40.42	64.73	0.26	0.0202	Cyclic, Cracks Visible
Average HvM	126.80	36.62	63.01	0.37	0.15	
Average Total	125.08	35.59	59.44	0.36	0.12	

4.1.2. High Frequency Acoustic P/S-wave measurements

Wave evolution

During the continuous loading of the NSLM samples in the UCS-test, the acoustic amplitude changes. The visible wave-form evolved from a very small amplitude, to a maximum of 0.65 mV at around 70% of the UCS-value after which it returned to a very small amplitude after breaking. During cyclic loading, this growth of wave amplitude is even more apparent. Figure 4.9 shows the growing amplitude over time, along with the applied stress. As the figure shows, the amplitude closely follows the stress until this maximum point is reached at about 70 or 75 % of the UCS. For visualisation purposes, the evolving of the wave form can be seen in Figure 4.5, where a averaged wave over 250 datapoints (1 datapoint represent $1.6 * 10^{-9}$ seconds) is visible. The averaging is done to remove noise from the data.

The visible wave in that figure is the full wave. Therefore, the S-wave, which is significantly more powerful than the P-wave, is dominant in those representations. The P-wave, however, follows a similar evolution, as seen in Figure 4.6. Amplitude growth is also visible in Figures 4.7 and 4.8, where it also becomes clear that the wave becomes weaker after about two-thirds of the maximum load. This might indicate that the material is already deforming and cracking long (70-80% UCS) before the maximal load is achieved. It should be noted that these waveforms are averaged, enlargening the problems in especially the low stress domain. Difficulty in picking the wave was primarlily encountered due to noise undulation, offset and unclear P-wave onset.

(a) Acoustic Representation at Timestep 1

(b) Acoustic Representation at Timestep 30

(c) Acoustic Representation at Timestep 60

(d) Acoustic Representation at Timestep 90
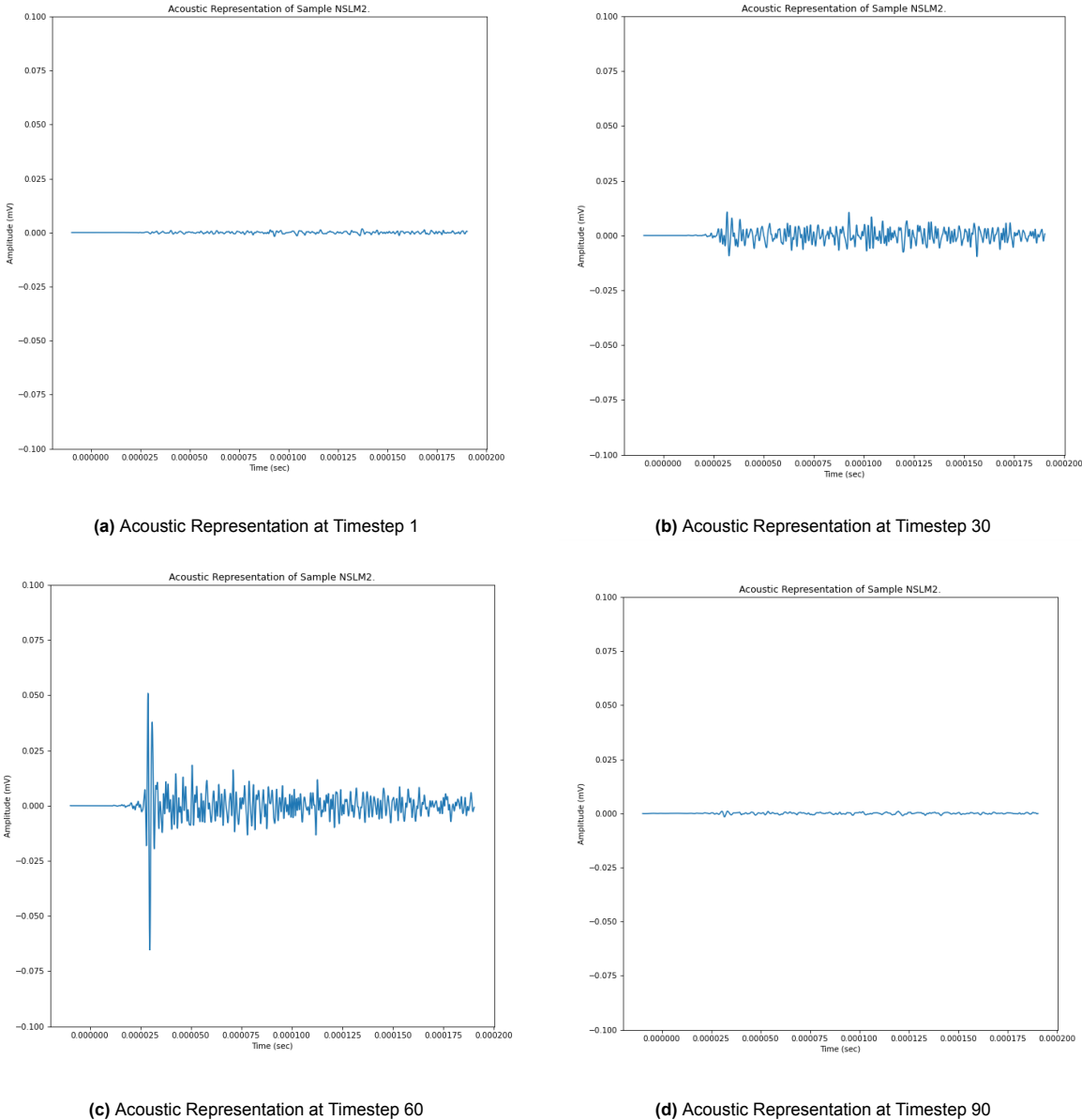
Figure 4.5: Waveform evolution during increasing stress on sample NSLM2.
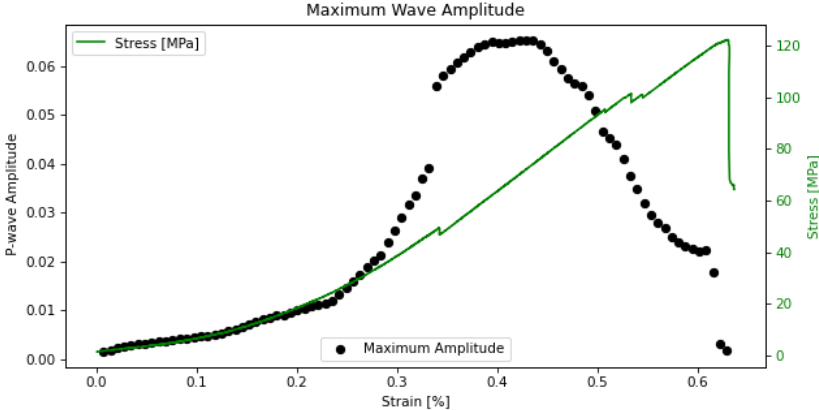
Figure 4.7: Maximum P-wave amplitude of sample NSLM2 against the applied stress.

(a) P-wave Representation at Timestep 1

(b) P-wave Representation at Timestep 30

(c) P-wave Representation at Timestep 60

(d) P-wave Representation at Timestep 90
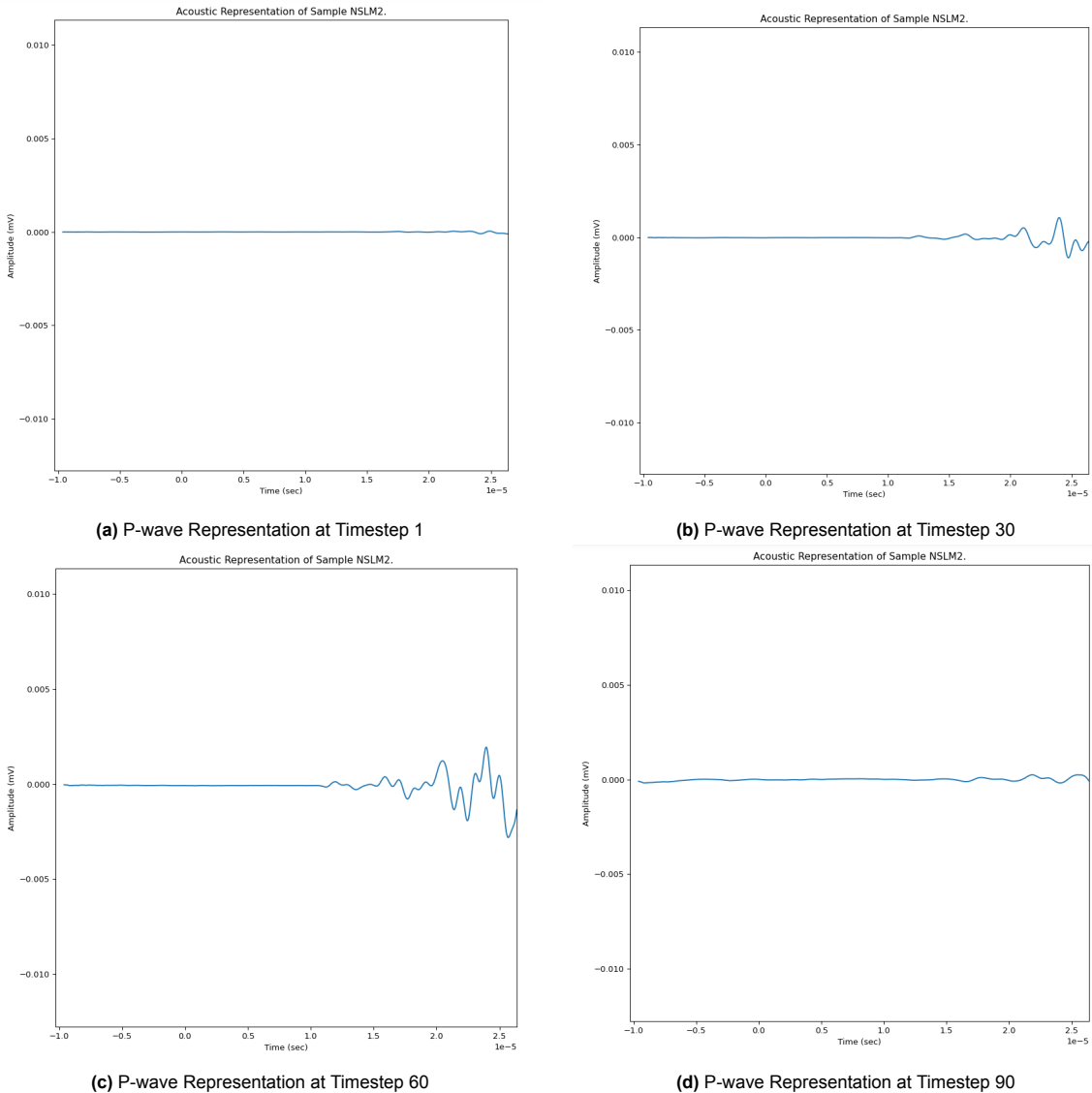
Figure 4.6: P-wave evolution during increasing stress on sample NSLM2.
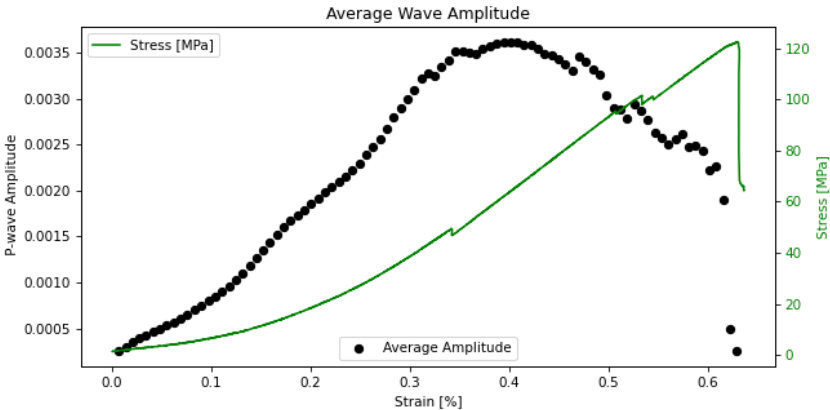
Figure 4.8: Average P-wave amplitude of sample NSLM2 against the applied stress.

(a) Hand-picked and Code-picked P-wave Arrival times of sample NSLM2.

(b) Correlation between Hand picked and Code picked arrival times of sample NSLM2. R = 0.88

(c) Hand-picked and Code-picked P-wave Arrival times of sample HvMCore1.

(d) Correlation between Hand picked and Code picked arrival times of sample HvMCore1. R = 0.93
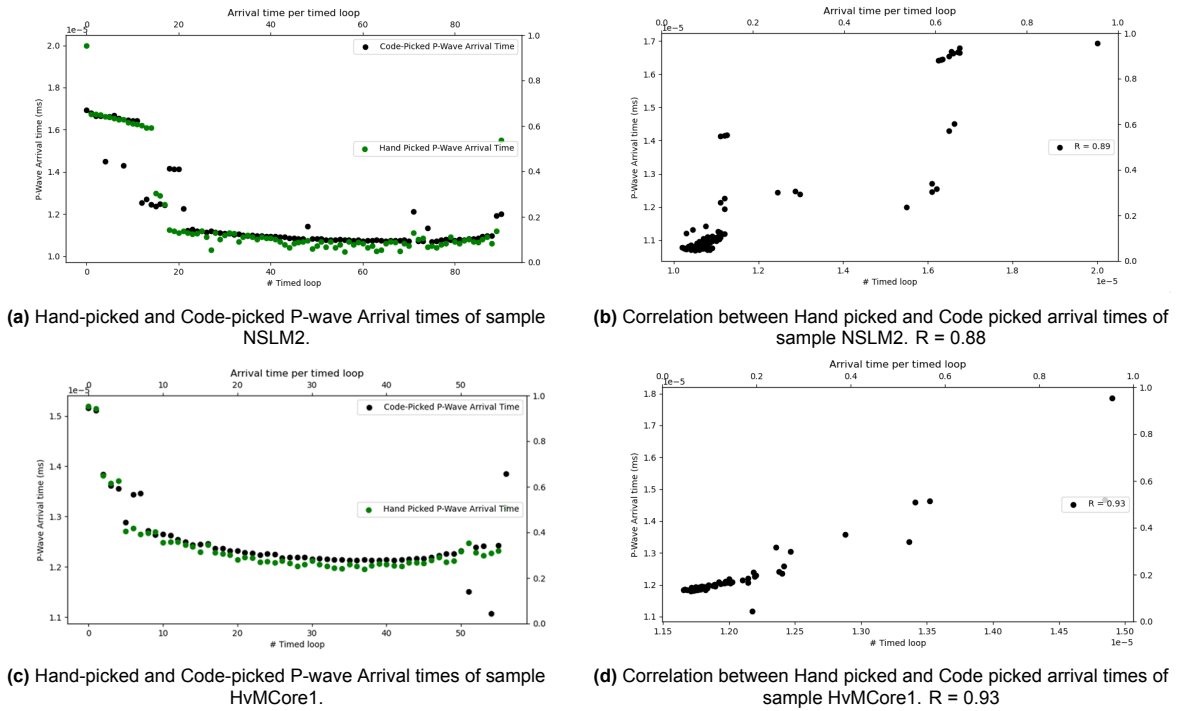
Figure 4.10: Correlations of hand picked arrival times with code picked arrival times.
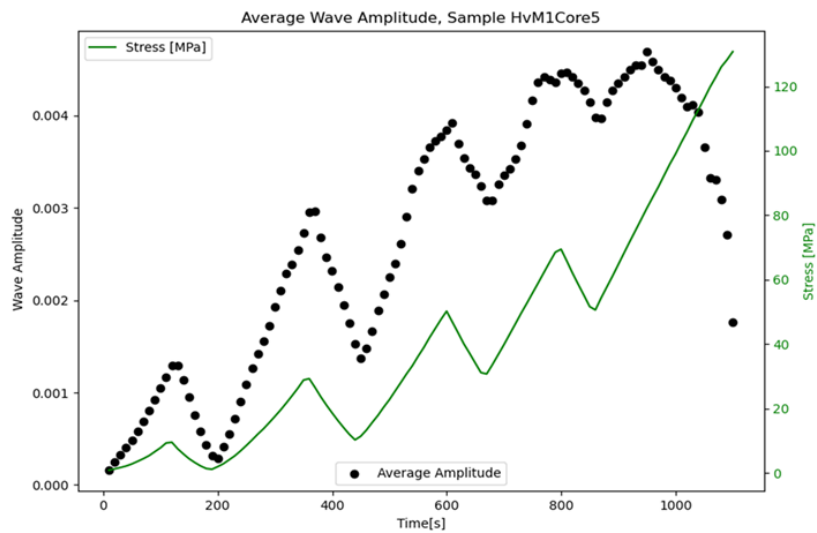
Figure 4.9: Average P-wave amplitude of sample HvMCore5 against the applied stress.

Wave Interpretation and Picking

After analysing the wave-form visually, the wave forms can also be analysed on arrival times, for both P-wave and S-wave. This can be done manually, which is a tedious process, or via a computer script that 'picks' the wave. The script denotes the time where the wave surpasses a certain threshold and the looks back for the starting point of the wave. Both P-wave arrival times next to each other can be seen in Figure 4.10a and 4.10c. The hand picked method and the code picked method correlate well, as visible in Figure 4.10b and 4.10d. It can even be said that the code is less biased for fluctuations of the wave-offset, as it produces values that jump around less.

The found arrival time can consequently be combined into a wave speed by using the length of the

sample. This wave speed is calculated and plotted against the strain or time of measured during test, as these parameters are the controlled parameters during the loading. This also made it possible to fit a formula to the speeds, relating it to the Stress on the sample. In order to check whether this method of fitting stress against code-picked P-wave speed worked, elastic dummy samples, an aluminium and a sandstone core, have been used. From these fits it can be concluded that the method should work correctly. After removing severe outliers at the begin and end due to irregular starting times of the press and acoustic measurements, both the aluminium (Figure 4.11) and the sandstone (Figure 4.12) core produce a smooth curve in which the P-wave speed grows with increasing stress. The formula of the aluminium core further confirms this, as the 'zero-point' of the power function is the sonic speed in aluminium, 6420 m/s. It is not strange that this is the result of the test, as this speed was used to calibrate the acoustic measurements.
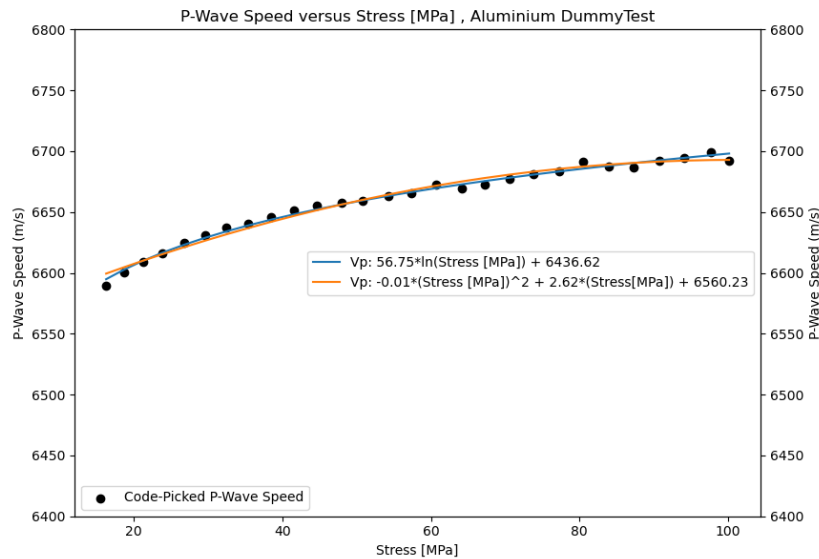
Figure 4.11: P-wave speed versus stress on an aluminium sample.
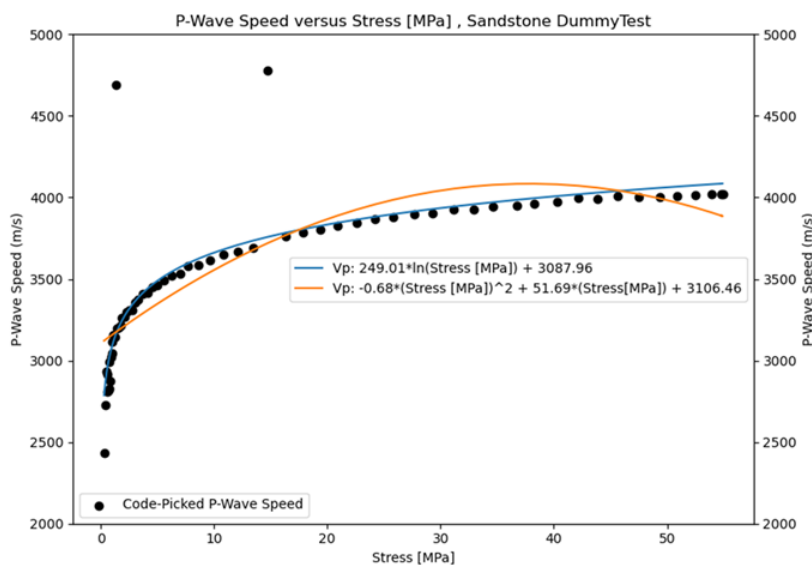
Figure 4.12: P-wave speed versus stress on a sandstone sample.

Sonic Speeds
Resulting from the finetuning process of the Wave-picking are the following Stress-Speed plots:

Figure 4.13 shows the P-wave speeds in non-cyclically loaded sample HvMCore1, including a fit of a power curve to the data. This sample was used as a benchmark and depicts the overall response of the P-wave speeds of the samples really well. Next to that, the clear step-wise increase during the crack-closure phase in the low-stress domain is visible, next to the gradual lowering of the P-wave speed after approximately 75% [80 MPa] of the UCS.
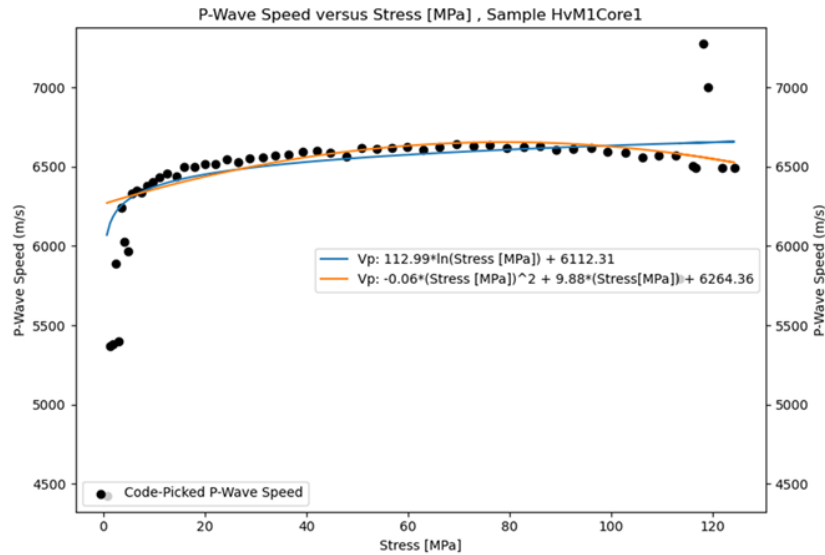
Figure 4.13: P-wave speeds of sample HvMCore1 under increasing stress.

Figure 4.14 shows a similar curve to HvMCore1. The only difference is the multitude of speeds in the low-stress domain. This is due to the multitude of cyclic loading in that domain and might be a proof for the cracks reopening during unloading in the lower stress domain after closing during loading. Once the lower stress domain is passed, also this sample shows a clear increase of speed until about 75% of UCS is reached. It could be that this is the starting point of the crack intitiation phase, as this point is also the point where the amplitude of the waves begins to lower again for all the samples, indicating that the transmission of waves through the samples is worsening.
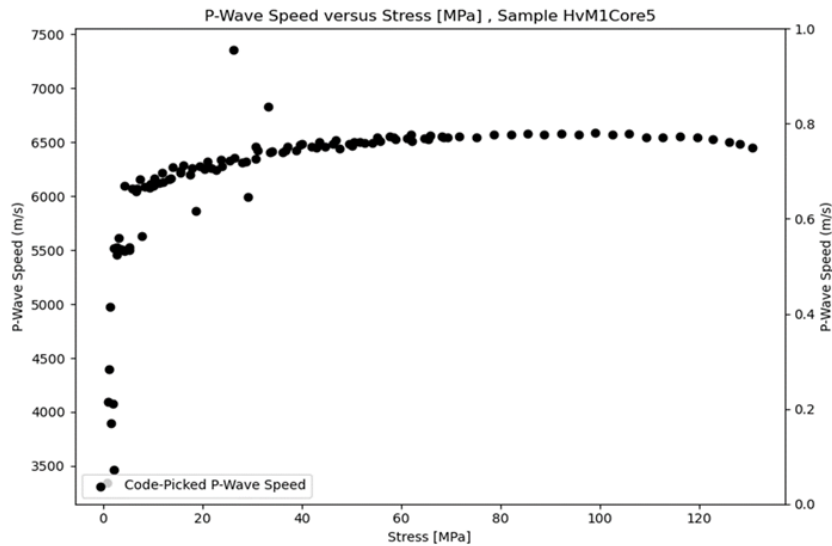
Figure 4.14: P-wave speeds of sample HvMCore5 under increasing stress.

Also, it is interesting to see the P-wave arrival time and stress against time. Figure 4.15 clearly shows the decrease of arrival time during loading and increase of arrival time during unloading. This is further proof for cracks being reopened during unloading and also influencing P-wave velocity in samples.
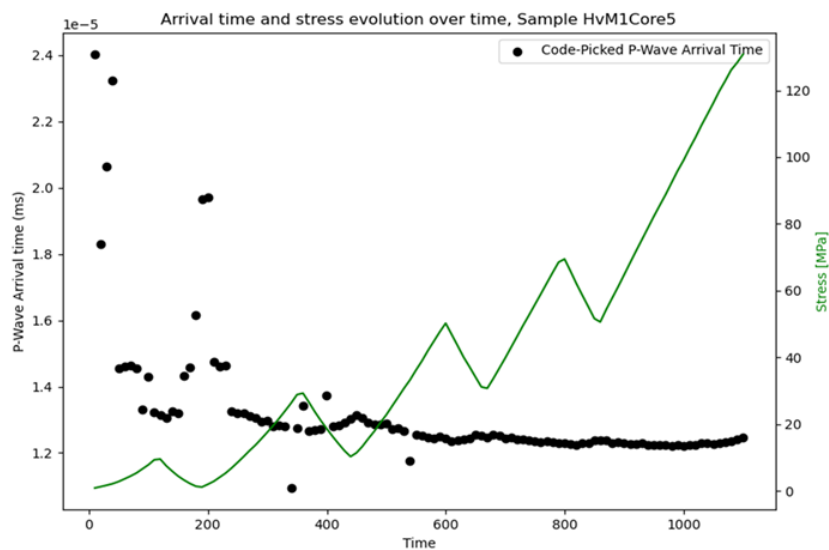
Figure 4.15: P-wave arrival times of sample HvMCore5 under increasing stress.

The S-wave speeds are less important for this research, as they not being produced in the field measurements and thus irrelevant for comparison, but still measured for elastic calculations and better understanding of the rock properties. For sample HvMCore1 the typical S-wave evolution is visible, showing a distinct straight line after the crack closure phase has completed. This is logical as the S-wave cannot protrude through very elastic media, like the air in the cracks. After this stage, the S-wave is well picked up by the code due to the large amplitude of the S-wave. The results of S-wave arrival time can be seen in Figures 4.16. Notable is the jump in speed close to the breaking of the sample. Perhaps the automatic wave picking produces an erratic arrival time. Another reason might be the interference of audible breaking sounds during the final period of testing, disrupting the signal. Similar

problems arise in the P-wave picking, but less obvious than with the S-wave picking. A plot of the S-wave speeds against stress, along with a power-fit is visible in Figure 4.17
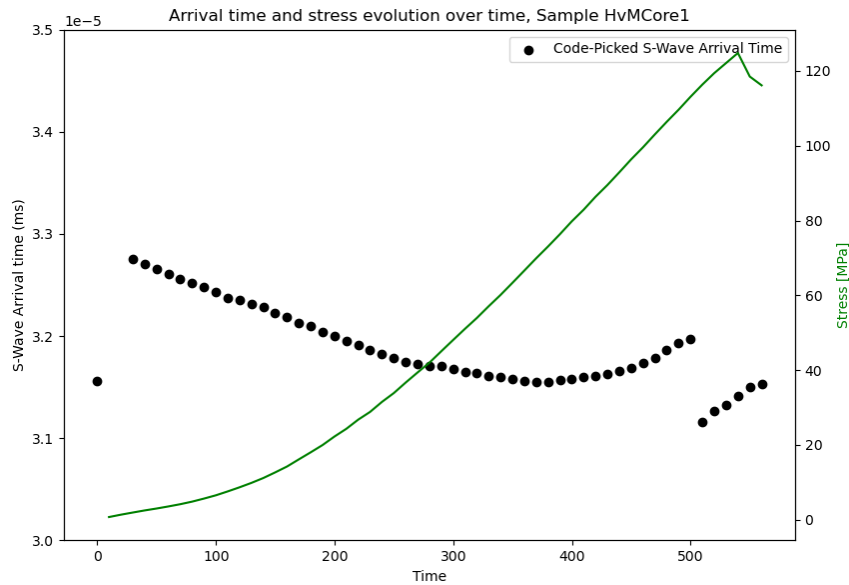
Figure 4.16: S-wave Arrival times of under increasing stress of sample HvMCore1.
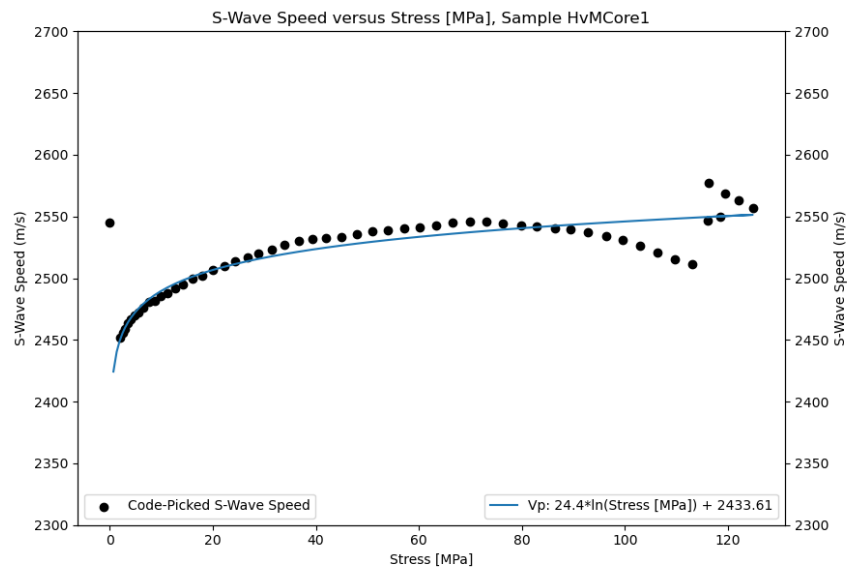
Figure 4.17: S-wave speed under increasing stress of sample HvMCore1.

To investigate the influence of crack closure more, a breakdown of both P-wave and S-wave speeds for all the tested samples was done. It was chosen to report the speed at 5 MPa, 10 MPa, 40 MPa and 80 MPa, as it was clear from the stress strain analysis that these stress values fell in the middle of the loading phases. Furthermore, the opt for both 5 MPa and 10 MPa was done to showcase the difference 5 MPa makes in the crack closure phase. Tables 4.3 and 4.4 show all the different P- and S-wave speeds at those selected stresses.

Table 4.3: Pressure wave velocities in different stress zones.

Sample ID:	UCS (MPa)	V_p [Max] (m/s)	V_p [80 MPa] (m/s)	V_p [40 MPa] (m/s)	V_p [10 MPa] (m/s)	V_p [5MPa] (m/s)
NSLM1	74.91	6641.96	-	6433.57	6147.10	6045.73
NSLM2	122.41	6532.63	6466.66	6389.71	5672.25	4280.37
NSLM4	115.76	6539.55	6513.87	6379.05	5721.17	5595.50
Average NSLM	119.09	6571.38	6490.27	6400.78	5846.84	5307.20
HvMCore1	125.65	6637.25	6599.59	6546.06	6387.06	6084.09
HvMCore2	119.43	6629.45	6618.63	6505.26	6219.56	4544.53
HvMCore3	138.66	6426.22	6407.81	6287.30	5904.95	4566.79
HvMCore4	106.53	6450.36	6437.40	6363.88	5989.72	4675.74
HvMCore5	133.32	6574.61	6548.68	6457.50	6099.57	5614.25
HvMCore6	150.86	6627.86	6615.18	6580.68	6423.75	6306.11
HvMCore7	113.13	6434.73	6424.84	6256.36	5764.88	4982.42
Average HvM	126.80	6540.07	6521.73	6428.15	6112.78	5253.42
Average Total	***120.07***	***6549.46***	***6514.74***	***6419.94***	***6033.00***	***5269.55***

Table 4.4: Shear wave Velocity in different stress zones.

Sample ID:	UCS (MPa)	V_s [Max] (m/s)	V_s [80 MPa] (m/s)	V_s [40 MPa] (m/s)	V_s [10 MPa] (m/s)	V_s [5MPa] (m/s)
NSLM1	74.91	2498.93	2479.56	2407.52	2358.67	2257.13
NSLM2	122.41	2575.13	2547.14	2536.24	2334.93	2263.19
NSLM4	115.76	2615.07	2550.85	2468.11	2433.04	2418.41
Average NSLM	119.09	2563.04	2525.85	2470.62	2375.55	2312.91
HvMCore1	125.65	2648.42	2542.78	2631.71	2578.48	2555.76
HvMCore2	119.43	2603.10	2577.24	2561.71	2544.47	1870.54
HvMCore3	138.66	2699.43	2485.32	2436.53	2373.01	2338.92
HvMCore4	106.53	2492.15	2499.78	2312.64	1963.44	1596.90
HvMCore5	133.32	2529.99	2530.00	2518.07	2464.32	2226.73
HvMCore6	150.86	2552.97	2551.62	2547.63	2527.76	2519.35
HvMCore7	113.13	2521.92	2417.52	2331.46	2239.30	2034.80
Average HvM	126.80	2578.28	2514.89	2477.11	2384.40	2163.29
Average Total	***120.07***	***2573.71***	***2518.18***	***2475.16***	***2381.74***	***2208.17***

The reason for the large difference between 5 MPa speed, 10 MPa speed and 40 MPa speed may be argued more in the discussion chapter, but it is good to notice how the difference in speeds between samples in the lower stress zones is could be due to the state of the core or RQD (Rock Quality Designation) that is observed during core-logging. The quality of the core was also denoted before the UCS-tests.

Samples with visible cracks and/or a low UCS, like core HvMCore4 or HvMCore7 tend to have lower P-wave speeds. That being said, the speeds measured in these samples cannot be true P-wave speeds, as they indicate that the non-porous sample consists of approximately 30% air. Despite the fact that cracks where visible, it was not apparent that they made up 30% of the rock. It is thus likely that for those tests, the measured P-wave speed is not 'true' but rather the quickest way any wave could reach the sensor and create a noticeable wave-form/amplitude. The S-wave speed, that relies more the absence of cracks for transporting the wave showcases the difference even more. In Appendix D the P-wave speed versus Stress plots for all the samples can be found for more in depth comparison between tests. The variety of stress maxima is observable in those.

As an import part of this research is to translate findings in the lab to in-situ stress knowledge, it is very interesting to find a formula that describes the relation between Stress and P-wave speed. This could subsequently be used in the field. Figure 4.18 shows all the found P-wave speeds per stress increment from the UCS-tests. Visible are the average fit (all data), the lower fit (based on the most cracked sample HvMCore7, UCS = 113 MPa) and the upper fit (based on the strongest sample HvMCore6, UCS = 150 MPa).

A power-curve was chosen for these fits, given the applicability on the aluminium and sandstone samples (Figures 4.12 and 4.11). These fits clearly show that there is a bandwidth in which the P-wave speeds vary. A clear upper boundary is visible which the P-wave speeds do not cross. It was chosen to not introduce this as the upper fit as this is most likely the 'ideal' CHILE response of the rock in terms of P-wave velocity and stress. It is unlikely that this will be encountered in the in-situ tests as we are measuring over much longer distances than 80 mm. Also, the HvMCore7 lower fit shows that a cracked sample does indeed show a much lower P-wave speed, especially in the beginning. After around 80 MPa, the fits do not longer correlate to the sampled speeds, meaning that a different function should be used for the later stages of loading. Whether the fitted curves can be interpreted as 'true' can be argued in the discussion, given the unlikely nature of the speeds in the lower stress domain. Nonetheless, it is interesting to compare these three fits to in-situ situation. This will be done in chapter 5.
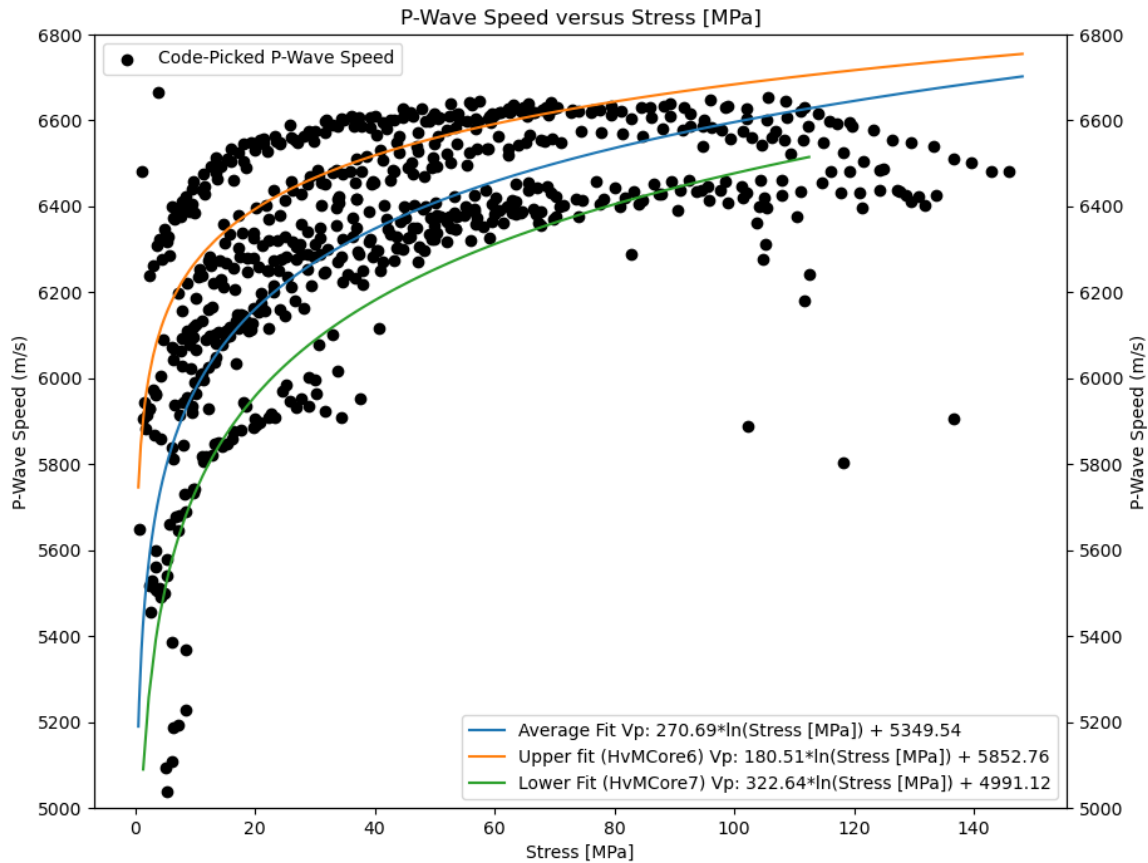
Figure 4.18: P-wave speeds versus stress of all samples of the HvMCores.

The shown fitting formulas are as follows:

$$V_{p-average} = 270.69 \ln \sigma_{c-average} + 5349.54, \qquad \text{m/s} \tag{4.1}$$
$$V_{p-upper} = 180.51 \ln \sigma_{c-upper} + 5852.76, \qquad \text{m/s} \tag{4.2}$$
$$V_{p-lower} = 322.64 \ln \sigma_{c-lower} + 4991.17, \qquad \text{m/s} \tag{4.3}$$

And these can be written into the following form to retrieve confining pressure from P-wave velocity:

$$\sigma_{c-average} = exp(\frac{V_{p-average} - 5349.54}{270.69}), \qquad \text{MPa} \tag{4.4}$$
$$\sigma_{c-upper} = exp(\frac{V_{p-upper} - 5852.76}{180.51}), \qquad \text{MPa} \tag{4.5}$$
$$\sigma_{c-lower} = exp(\frac{V_{p-lower} - 4991.17}{322.64}), \qquad \text{MPa} \tag{4.6}$$

Elastic Properties
For analysis it is useful to denote the elastic parameters of the rock, calculated using the speeds found using the acoustic measurements. These are denoted in Table 4.5. In Chapter 5, a full comparison of all the results will be done, mainly around the found elastic parameters. Interesting to note are the similarities between the acoustically found Poisson's Ratios and Elastic Moduli in two different stress regimes, while these found properties using mechanical tests differ a lot.

Table 4.5: Measured elastic properties of rock through both stress-strain and acoustic measurements.

Parameter	Mechanical - Lab				Acoustics - Lab			
	E [40 MPa]	E [80 MPa]	ν [40 MPa]	ν [80 MPa]	ν_d [80 Mpa]	E_d [80MPa]	ν [40 Mpa]	E_d [40MPa]
Sample ID	(GPa)	(GPa)	-	-	-	(GPa)	-	(GPa)
NSLM1	39.81	-	0.002	-	-	-	0.42	44.40
NSLM2	33.04	47.68	0.35	0.0117	0.41	48.42	0.41	48.86
NSLM4	30.94	46.21	0.29	0.0139	0.41	48.61	0.41	46.45
Average NSLM	31.99	46.95	0.32	0.0128	0.41	47.70	0.41	46.56
HvMCore1	33.50	55.02	0.29	0.21	0.41	48.42	0.40	52.49
HvMCore2	28.09	58.75	0.35	0.024	0.41	49.66	0.41	49.90
HvMCore3	36.85	66.99	0.51	0.28	0.41	46.21	0.41	45.25
HvMCore4	30.96	62.11	0.52	0.259	0.41	46.74	0.42	41.12
HvMCore5	41.98	65.64	0.31	0.0243	0.41	47.91	0.41	48.29
HvMCore6	44.52	67.80	0.33	0.204	0.41	48.74	0.41	49.48
HvMCore7	40.42	64.73	0.26	0.0202	0.42	43.91	0.42	41.66
Average HvM	36.62	63.01	0.37	0.15	0.41	47.35	0.41	46.81

4.2. Field Tests

4.2.1. Flat Jack Test

The final result from the Flat Jack Test is a single stress value, along with a location and a direction of that stress. The found value of in-situ vertical stress in the wall using the flat jack method and calculated using the Tributary Area method (Table 4.6) is found to be 9.8 MPa. A full view of the jack surface and the cut out slot is visible in Figure 4.19. Next to that, the a figure showing the loading and unloading of the flat jack along with the induced strain can be seen in Figure 4.20. Based on elastic theory, elasticity of the rock mass can be calculated aswell.
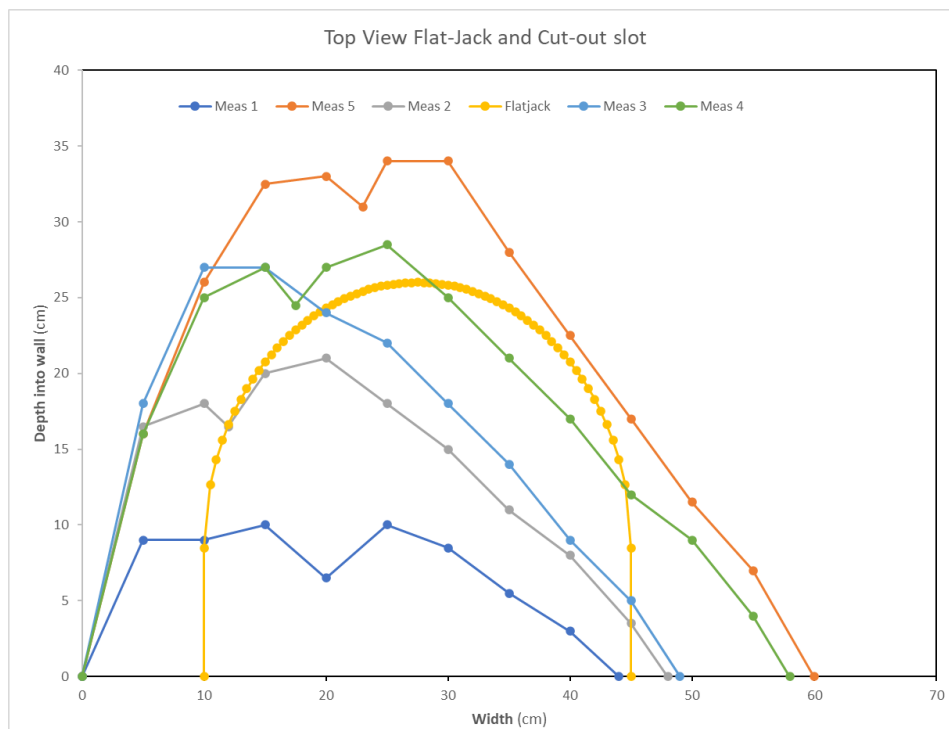
Figure 4.19: Top view crosscut of the flat jack and the flat jack slot in the wall.
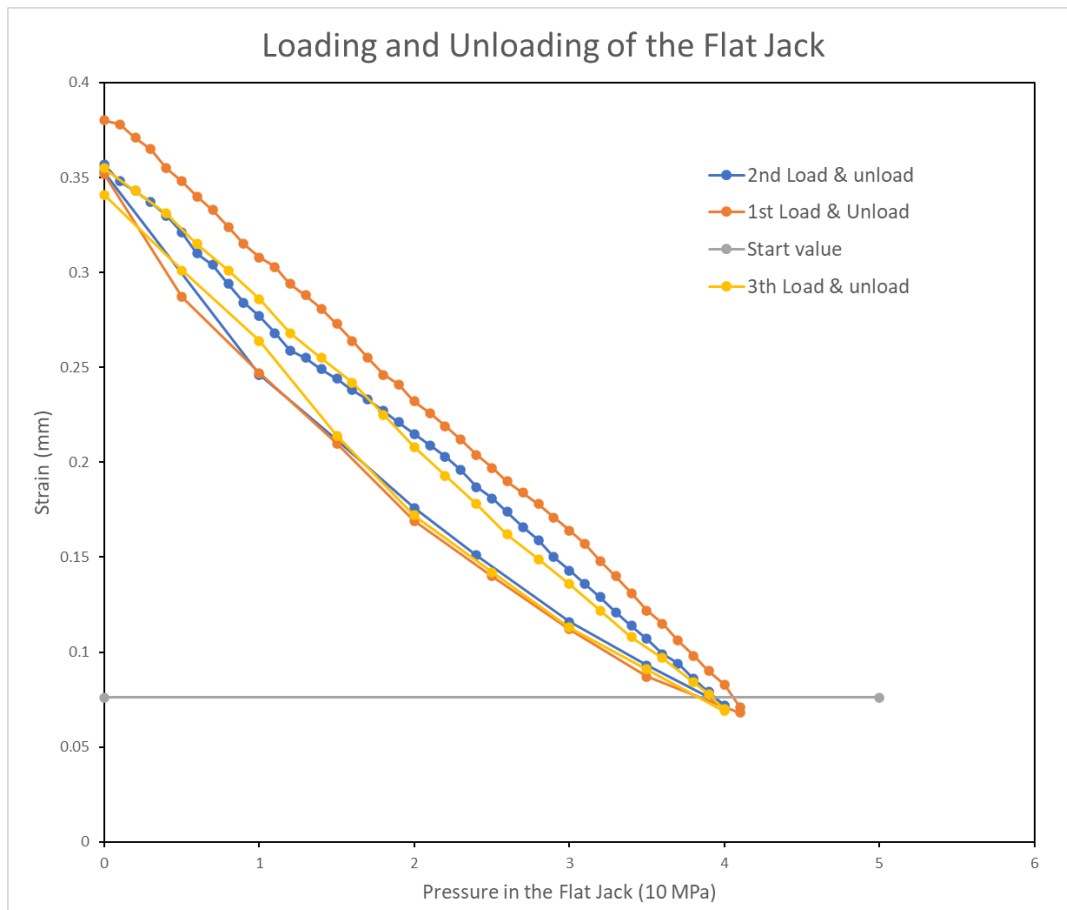
Figure 4.20: Measured strain and pressure during the flat jack test.

As this report aims to compare several different methods, it is important to find properties of the rock that is measured in the data. One of the most dominant properties of rock is its Youngs Modulus. Figure 4.20 shows multiple somewhat straight lines with loading and unloading values for strain and stress. According to ASTM standards, Elastic Moduli can only be taken from samples that have continuous loading or unloading with a constant rate. During the loading this is not satisfied because of the difficulty of pressurizing the hand-pump. During unloading, however, a fairly stable rate could be established to unload the flat jack, giving the surrounding rock equal time intervals to relax in.

Another realization during this process is that the 'relaxation' of the rock mass is actually the stress of the rock mass deforming the rock around the cut-out. By controlling the release of the pressure from the flat jack, the stress from the surrounding rock acts as a hydraulic pressure bench on the sample: the rock between the two measurement points. This means that the unloading of the flat jack actually comes the closest to resembling a stress-strain relationship as seen in the laboratory. The plotting of just the unloading curves results in smoother stress-strain curves that are more coherent with each other.

For comparison, it might also be useful to plot the stress-strain curve in the same way as is done for UCS-tests. By doing that, a remarkable resemblance appears to the first crack closure phase that is known from the UCS-tests, especially if you take into account that 40 MPa in the flat jack, according to the tributary area method, correlates to 9.815 MPa of stress in the surrounding rock mass. 10MPa has been found as the boundary between the crack-closure and the elastic domain. The consequent elasticity measurement was thus chosen to be done in the 30-40 MPa range of the flat jack unloading curves. This gave a Youngs Modulus of 31.7 GPa. Figure 4.21 shows the unloading curves from which the Youngs Modulus has been calculated. Values found with the flat jack method will be compared with previous research and the results from the acoustic velocity measurements in Chapter 5.
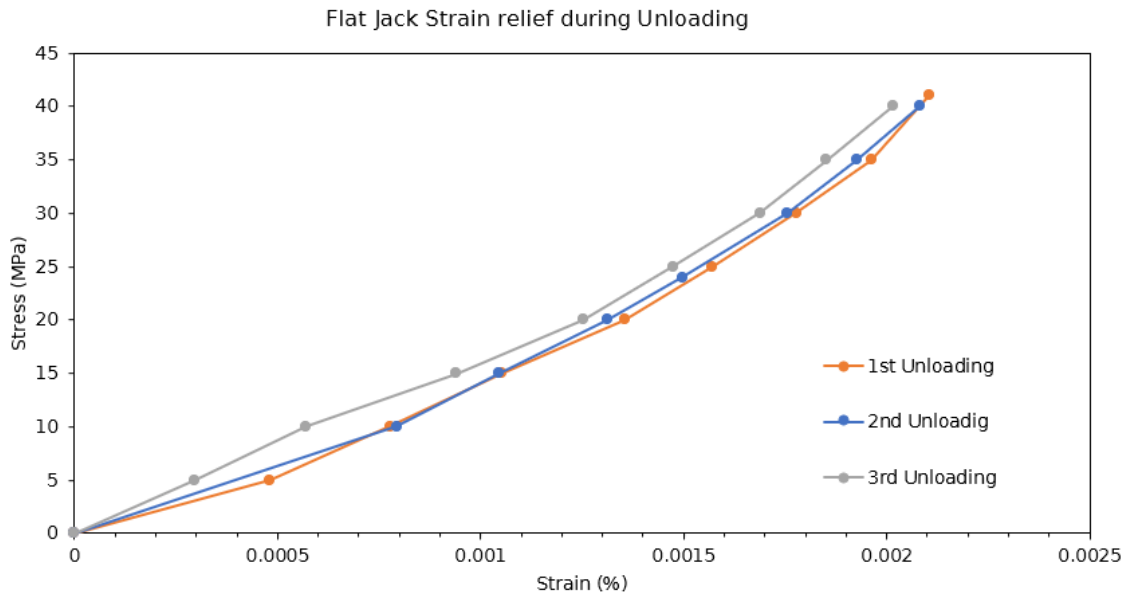
Figure 4.21: Measured stress and strain during the unloading of the flat jack.

Table 4.6: Tributary Area Method as used by Sibelco for analysis of Flat jacks.

Excavation area	0.130	m^2
Flat jack area	0.078	m^2
Unsupported surface	0.052	m^2
Unsupported surface attributed to flat jack	0.021	m^2
Total surface supported by flat jack	0.099	m^2
Extraction ratio/Part carried by flat jack	0.761	
Flat jack Pressure	41.000	MPa
$\sigma_\mathbf{v}$	**9.815**	**MPa**
Equivalent depth	363.508	m
Actual Depth $\pm$	370.000	m
Equivalent $\sigma_\mathbf{v}$	9.800	MPa
Youngs Modulus from Unloading	31.70	GPa

4.2.2. Acoustic Velocity Measurements

The direct results from the acoustic velocity measurements on the pillar at the corner of Myrvang are visualized in Figures 4.22,4.23 and 4.24. As visible from the figures, the Sender has less noise on the wave than the Receiver. Luckily, the maximum amplitudes generated by the blow of the hammer and thus the wave are still distinguishable, making the calculation of the P-wave speeds possible. The speeds of the three blows, along with the average speeds per position and the average speed overall are all visible in Table 4.7.
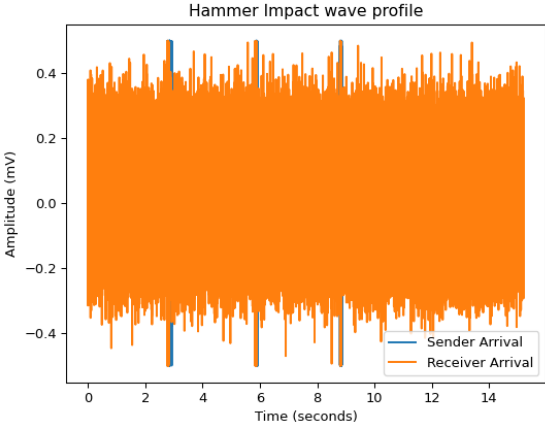
Figure 4.22: Both sender and receiver plotted for hammer blow tomography at position 6.
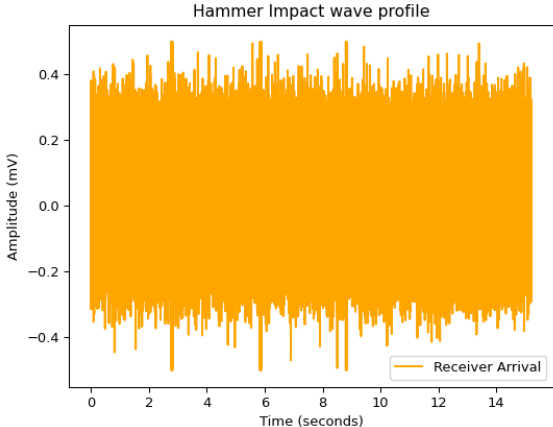
Figure 4.23: Receiver plotted for hammer blow tomography at position 6.
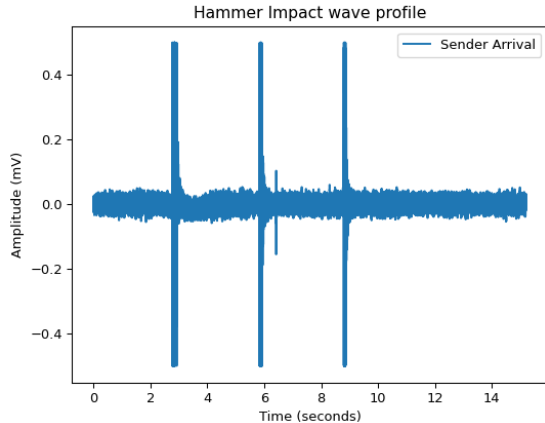
Figure 4.24: Sender plotted for hammer blow tomography at position 6.

Measurements along the wall of the corner of Myrvang have also been done but those had a lot more differing wave arrival times and thus wave speeds. In the Figure 3.20 the locations of all the geophones can be seen from which measurements were done. The geophones through the pillar are named 'POS' 1 to 6, the geophones along the wall of the flat jack are named 'WSP' 1 to 4 and the geophones

on the other wall of the corner of Myrvang are named 'WNP' 1 to 3. The latter measurements were added to see if similar results could be retrieved from both sides of the underground opening. During visual inspection, the 'WNP'-wall was heavily intruded, broken and sheared after the 'WNP3' geophone locations. For this reason, it was chosen not to perform acoustical measurements through that area, giving only 3 geophones.

Table 4.7: Locations and measured speeds between them.

Measurement location	Speed1 (m/s)	Speed2 (m/s)	Speed3 (m/s)	Speed4 (m/s)	Distance (m)	Average Speed (m/s)
Transformer to Tunnel Position 1	6225.98	4911.79	5364.75	6920.33	18.62	5855.71
Transformer to Tunnel Position 2	6789.92	6416.59	6506.02	-	18.67	6570.85
Transformer to Tunnel Position 3	7904.72	6434.72	5474.31	-	18.34	6604.58
Transformer to Tunnel Position 4	6066.83	5030.20	5328.73	-	17.96	5475.26
Transformer to Tunnel Position 5	5600.29	6280.33	7062.21	-	17.58	6314.28
Transformer to Tunnel Position 6	7643.44	6551.52	7122.29	-	18.80	7105.75
Tunnel to Transformer Position 1	4642.32	3902.66	5199.91	-	18.62	4581.63
Tunnel to Transformer Position 2	4456.39	4302.37	5675.47	-	18.67	4811.41
Tunnel to Transformer Position 3	*477.59*	4666.40	4826.04	-	18.34	4746.22
Tunnel to Transformer Position 4	5664.93	5281.71	4947.06	-	17.96	5297.90
Tunnel to Transformer Position 5	6127.15	4925.75	5765.55	-	17.58	5606.15
Tunnel to Transformer Position 6	6124.71	6085.07	6373.85	-	18.80	6194.54
All locations						**5763.69**

The results from these tests were promising, but more research was done after them, also along the wall surface instead of through the pillar. As these tests produced results that were even less corresponding to one another, a little statistical analysis is shown through Histograms 4.25, 4.26, 4.27 and 4.28. Also Table 4.8 shows some insightful statistics.
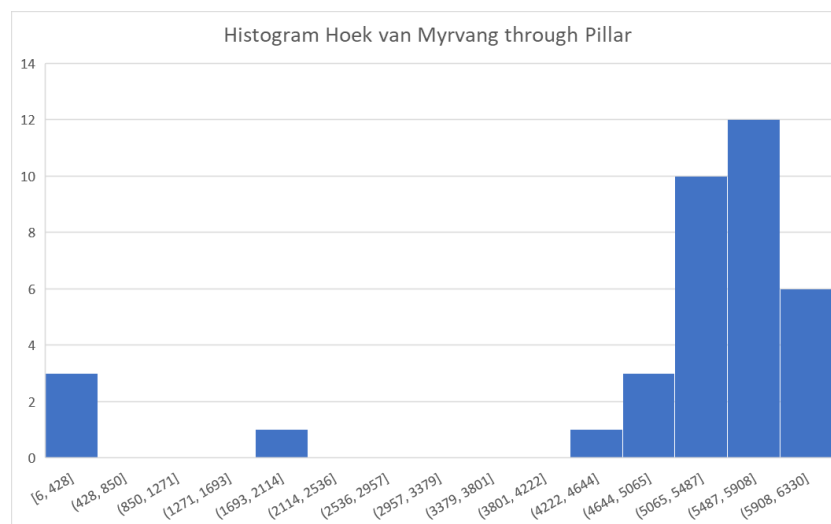
Figure 4.25: Histogram showing the occurrence of P-wave speeds through the pillar at the corner of Myrvang. (POS1-POS6)
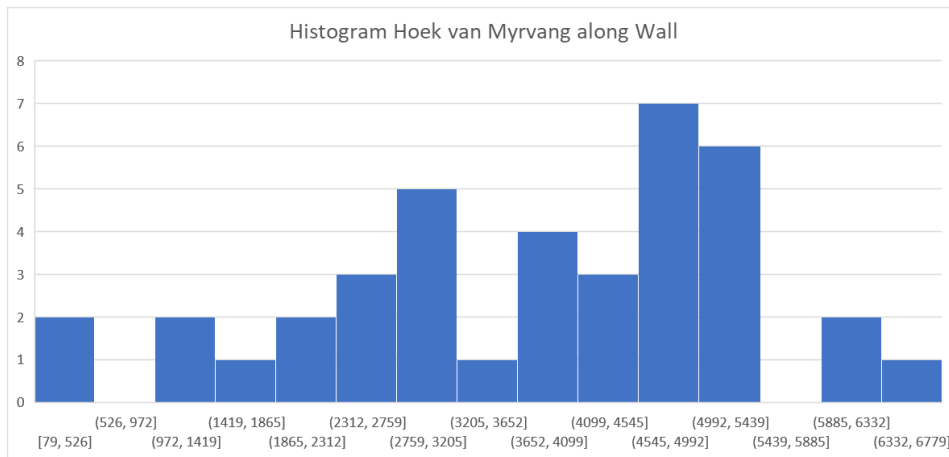
Figure 4.26: Histogram showing the occurrence of P-wave speeds through the flat-jacked wall at the corner of Myrvang.(WSP)
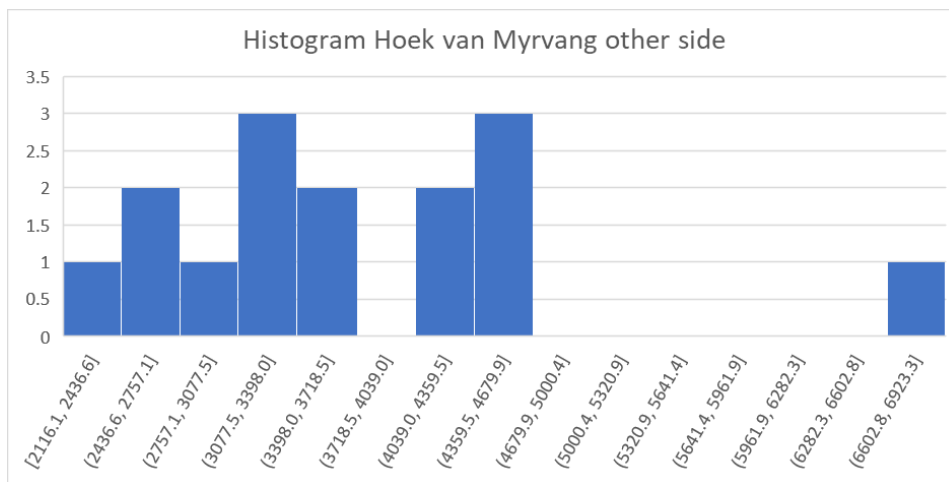
Figure 4.27: Histogram showing the occurrence of P-wave speeds through the wall on the other side of the corner of Myrvang. (WNP)
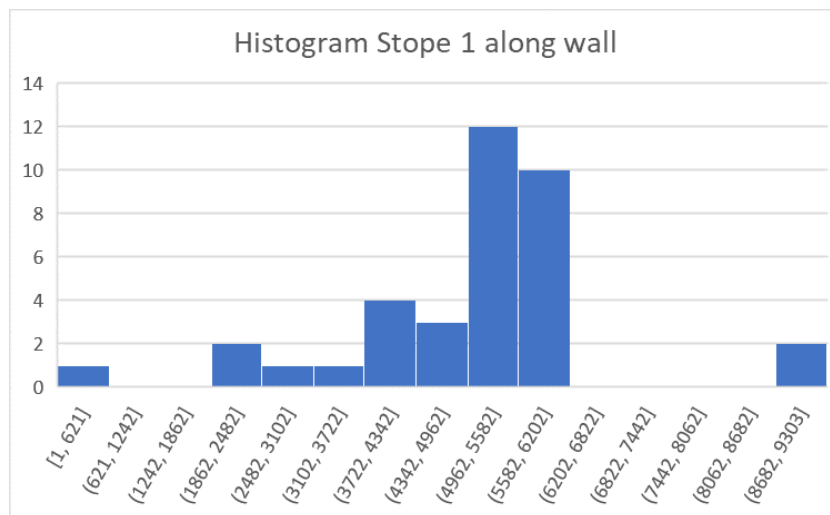
Figure 4.28: Histogram showing the occurrence of P-wave speeds through the flat jacked wall at Stope 1.

To take away from these results is most of all the difference between the test through the pillar at the

Table 4.8: Statistical display of P-wave speeds found during the acoustic velocity measurements after removing impossible upper outliers.

P-wave speeds	HvM Pillar	HvM WSP	Stope 1 Wall	HvM WNP
Average (m/s)	4964.85	3675.50	4809.12	3562.87
Median (m/s)	5524.88	3941.62	5143.44	3735.32
Standard Deviation (m/s)	1663.11	1516.48	719.34	1143.08
Maximum (m/s)	6329.97	6024.13	6092.22	6923.30
95th Percentile (m/s)	6258.47	6024.13	5945.02	5556.26
75th Percentile (m/s)	5754.61	4829.27	5627.68	4387.24

Table 4.9: RMR and Q-value rating input values as retrieved from the field

RMR	Rating:
Strength of intact Rock Material	12
RQD-RMR	20 (high) - 17 (low)
Spacing of Discontinuities	8
Condition of Discontinuities	27
Ground water	15
Q	**Rating:**
RQD (%)	93 (high) - 80 (low)
Joint set number (Jn)	36
Joint roughness number (Jr)	4
Joint alteration number (Ja)	0.75
Joint water reduction factor (Jw)	1
Stress Reduction Factor (SRF)	5

corner of Myrvang and the test through the wall of the same pillar. The test through the wall has a much larger spread with speeds being a lot lower than the usual speed of the nepheline syenite material, between 5500 and 6750 m/s. As a result, the average speed of these measurements vary. Although the measurements vary, the datasets still have some similarities. The standard deviation of both data groups is around 1500 m/s, the maxima lies in the 6000 and the 95th percentile is roughly the same at around 6100 m/s. Given the fact that the same rock mass is measured, this is not strange. The take-away from this is that the wave propagation during the measurement along the wall was more difficult due to multiple reasons.

The data from Stope 1 has a lower standard deviation. It also features two large outliers in the 9000 m/s that cannot be the travel speed through the nepheline syenite. For the histogram it was chosen to leave outliers in, but for the final calculation of maxima and minima they are left out, as they do not represent the measured rock. Overall, the Stope 1 data, which was measured along the wall shares similarities with both corner of Myrvang measurements. It has a larger spread in the "plausible" domain like the HvM-Pillar measurement, but also a reasonable amount of lower speeds like the HvM-wall measurement. Because the stope 1 and the corner of Myrvang are not the same location only the look of the data can be compared, to understand the differing measurement results. It is not possible to compare the datasets on any other aspect.

4.2.3. RMR and Q-value Rating

The RMR and Q-value rating is conducted at the wall in which also flat jack and acoustic measurements were done. To create input variables for the RMR and Q-value rating, joints and joint sets are important. After these joints were found, they were measured on direction and the RMR-rating values and then put into a joint set group. These groups were consequently used to set up the other parameters for the RMR, alongside the RQD, that indicates a range, as RQD can fluctuate over the spacing of the outcrop. Table 4.9 summarizes the input variables for both RMR and Q-value ratings.

After the variables were found, proper calculations could be done to get to a final value. To make results more scientific and comparable to the other methods, multiple RMR and Q calculation formulae

Table 4.10: RMR and Q-rating results

Value	High estimate	Low estimate
RMR89	82	79
RMR89'	82	79
Q	2.7	2.4
Q'	13.7	11.9
GSI	77	74
GSI (Field estimate)	85	85
Youngs Modulus (GPa)	63.1	53.1
RQD	92.5	80.3
RQD (seismic)	81	72.7
RMR according to Q	53	52
RMR according to Q'	68	66

were used, as well as correlations between both numbers and elastic parameters. In the end, the RMR and Q-rating system measure the same rock wall, given different interpretations. Table 4.10 shows the results of the RMR and Q-rating systems.

Standing out from the results is that RMR is fairly stable, the high and low estimate do not differ so much and there is no difference between the adjusted 89 version and the normal 89 version. Next to that, the GSI (Geological Strength Index) from the field estimate is quite close to the GSI calculated by the RMR. The found Youngs Modulus via the RMR is 63.1-53.1 GPa. A larger difference is found in the comparison with the Q-value rating. The RMR-Q comparison gives really different values.To understand it, you must dive into the calculation behind the Q-value rating. As this rating is more heavily influenced by the Joint set number, it is not strange to see them differing. The joint sets observed only appeared in small reoccurring regions along the inspected rock wall. As this rating should be done for the overall rock wall, you assume that a joint set should be everywhere, even when it is not visible. By doing this, however, you might overestimate the real volumetric joint count, as the average volumetric joint count is a lot lower. Therefore, the Q-value rating overestimates the importance of the joint set number and gives a lower final value, once you start comparing them. To give a better idea of the occurrence and dip-directions and angles of the joint sets, stereonets are visible in Figure 4.29. The directions are all measured with a geological compass.

(a) Strereonet of joint set 1 (030/45). Dipping into the tunnel

(b) Stereonet of joint set 2 (015/35).

(c) Stereonet of joint set 3 (005/65).

(d) Stereonet of joint set 4 (220/30).
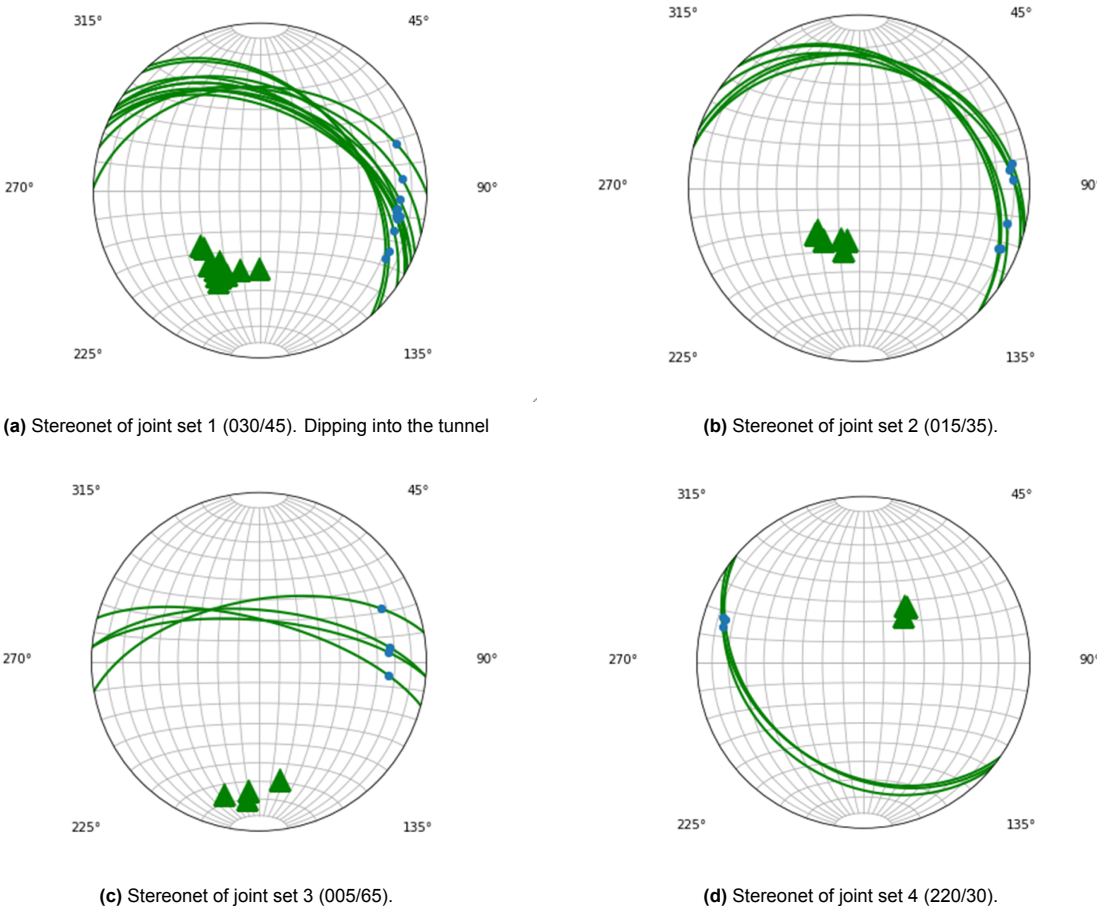
Figure 4.29: Stereonets of the wall at the corner of Myrvang. Random joints are not included.

5

Comparison

The results from the laboratory and field tests are to be compared with each other and by using the methods mentioned in literature. This chapter poses to explain differences and similarities within these comparisons in order to check whether they are correct, make sense and can be used in the future as reference.

5.1. Lab and Literature

Table 5.1 shows the difference in found value if one compares the resulting UCS of the correlation formulas of Rahman and Sarkar (2021) and Yesiloglu-Gultekin et al. (2013), using the P-wave modulus, with the found UCS-value of the NSLM samples. It clearly shows that the correlation formulas estimate the UCS to be higher than the actual found value.

Table 5.1: Comparison of Lab-found UCS values and P-wave velocity using correlation of Rahman and Sarkar and Yesiloglu

Sample ID:	V_p (m/s)	UCS(V_p)(Rahman and Sarkar, 2021)	UCS(V_p)(Yesiloglu-Gultekin et al., 2013)	Actual UCS
NSLM1	6300.00	158.34	150.34	74.91
NSLM2	6600.00	172.71	158.44	122.41
NSLM4	6440.00	164.97	154.12	115.76
Average	6446.67	168.82	154.30	119.09

A possible explanation for this is the dependence of the UCS on the quality of the sample. A minor crack in the sample would lead to a decrease of stress that the sample can take. The P-wave speed, however, does not rely on this, but more on the elastic parameters of the sample. As this relation has no further influence on this research (the exact UCS-value is measured) it is merely a show of the difficulty to express and correlate all rock mechanical parameters with each other. It would be more useful to for instance compare the calculated Youngs Moduli from two different measurement methods with each other and literature. A comparison on the elastic parameters of the sample with correlation formulas found in literature can be seen in Table 5.2.

Table 5.2: Dynamic and Static Youngs Moduli calculated from UCS, Acoustics and correlations.

Sample ID	E (GPa) based on Lab Results			E_s (GPa) correlated using V_p		
	E_s1 from UCS	E_s2 from UCS	E_d\$ from V_p/V_s	King (1983)	Eissa & Kazi (1988)	Eissa & Kazi (1988)
NSLM1	39.81	-	44.40	26.58	32.04	29.86
NSLM2	33.04	47.68	48.42	31.66	35.01	31.73
NSLM4	30.94	46.21	48.61	31.89	35.15	31.82
Average NSLM	*31.99*	*46.95*	*47.70*	*30.75*	*34.48*	*31.40*
HvMCore1	33.50	55.02	48.42	31.65	35.01	31.73
HvMCore2	28.09	58.75	49.66	33.22	35.93	32.30
HvMCore3	36.85	66.99	46.21	28.86	33.37	30.71
HvMCore4	30.96	62.11	46.74	29.53	33.77	30.95
HvMCore5	41.98	65.64	47.91	31.01	34.63	31.50
HvMCore6	44.52	67.80	48.74	32.06	35.25	31.88
HvMCore7	40.42	64.73	43.91	25.96	31.67	29.63
Average HvM	*36.62*	*63.01*	*47.35*	*30.31*	*34.22*	*31.24*

The results of the UCS test show that the samples clearly have two separate elastic stages. The first one gave a slightly lower Young's Modulus value and the second stage resulted in a slightly higher value. The Young's Modulus found in the second stage shows great resemblance to the Young's Modulus found using the acoustic speeds. Therefore, the found values using UCS and the Acoustics of the Young's Modulus can be interpreted as dynamic elastic moduli.

Within Rock Mechanics, however, static moduli are normally used. In order to convert the found dynamic moduli back to static moduli, correlation formulas by King (1983) and Eissa and Kazi (1988) are used. It is noteworthy that the static moduli resulting from this conversion are very similar to the elastic modulus of the first stage of loading (Table 5.2). These results do indicate that the samples showed a dynamic elastic response to the applied pressure and that the Young's Modulus, both static and dynamic, can be an important factor to check the correlation between mechanical and acoustic results of rock mechanical testing.

5.2. Lab and Field

5.2.1. Acoustics

The first and most important comparison done in this research is the comparison between mechanical test results and the acoustical test results. In the lab, some relations have been found between the two different material properties. It is then thus interesting to take a look at how these relations are applicable in the lab. Table 5.3 shows the application of these relations based on relations (4.1, 4.2, 4.3, 4.4, 4.5, 4.6) on the field data. The input data in these formula are the 50th-percentile (median) as the lower-fit, 75th percentile as the average-fit and 95th percentile as the upper-fit speeds as specified in Table 4.8. The pressure input is the found value in the flat-jack test. As a result, it is clearly observed that only the HvM-pillar acoustic measurements give resembling values. The measurements along the wall gave lower speeds in the statistics. For HvM-wall this can be because of the large distribution of measured values. For the Stope 1 measurements, which were less distributed, this can be due to the fact that extension was observed during the cutting of the slot of a flat-jack by R. Schmitz in 2019.

Table 5.3: Measured and calculated P-wave speeds and stresses at various locations using different fitting formulas.

		σ_c [MPa]	V_p [m/s]
HvM-Pillar			
	95th percentile	9.8	6258.47
Measured	75th percentile	9.8	5754.61
	50th percentile	9.8	5524.88
	Upper-fit	9.46	6264.75
Calculated	Average-fit	4.47	5967.36
	Lower-fit	5.23	5727.56
HvM-Wall			
	95th percentile	9.8	6024.13
Measured	75th percentile	9.8	4829.27
	50th percentile	9.8	3941.62
	Upper-fit	2.58	6264.75
Calculated	Average-fit	0.15	5967.36
	Lower-fit	0.039	5727.56
Stope 1			
	95th percentile	*The stress was*	6092.22
Measured	75th percentile	*not measured*	5627.68
	50th percentile	*but extension observed*	5143.44
	Upper-fit	3.79	
Calculated	Average-fit	2.79	
	Lower-fit	1.60	

A possible take-off from the found values in the mechanical and acoustic field tests is the understanding

that a perfect CHILE rock mass does not exist. Therefore, a lot of wave attenuation happen during an acoustic test. One can only cherry pick results from the measurements done to better interpret such a rock mass. Assuming that a rock mass has a path in which the wave can travel most efficiently, the travel speed through that path will be the maximal speed through the homogeneous media. This should coincide with the highest possible speed through a rock mass at a certain stress. In combination with the understanding that the lab-found upper-fit resembles the P-wave speed in CHILE nepheline-syenite, a different view on the comparison exists. Looking just at the upper-fit values in Table 5.3 it becomes clear that this coincides reasonably well with the found stress with the flat jack test. Following from this knowledge, one can argue that with more measurements, a better statistical analysis of the P-wave speeds can be done to make a more precise relation between measured P-wave speed and the resulting inferred stress. Also, this is a great example of the difficulty of dealing with a low-stress regime in an underground opening. As we know from the laboratory relationship between stress and P-wave velocity there is a sharp exponential increase in P-wave velocity in the first loading stages of the rock (until about 15 to 20 MPa). After this, cracks have potentially closed and the rock behaves more homogeneous. As these pressures are not reached in a large part of the Stjernøya mine, relating stress with P-wave velocity is extremely difficult. It should become more distinct with higher (confining) pressure.

5.3. P-wave Speeds

Given that continuous, homogeneous , isotropic and linear-elastic (CHILE) nepheline syenite would have a P-wave speed that is the maximum of the found in the laboratory tests, any value lower than that maximum measures speed through CHILE nepheline syenite, as well as some discontinuous, inhomogeneous, anisotropic, non-elastic (DIANE) nepheline syenite. Once the nepheline syenite becomes more DIANE, the speed is expected to become lower.

This can be observed in the comparison between P-wave speed and UCS-test visible in Figure 5.2 and P-wave amplitude and UCS-test in Figure 5.1, along with an explanation of the rise and fall of the P-wave velocity according to the loading stages specified in Chapter 3. These figure show the stress and P-wave evolution of sample HvMCore1. This sample behaved the most elastic in both the stress-strain curve and the acoustical representation, making it very suitable for a comparison.
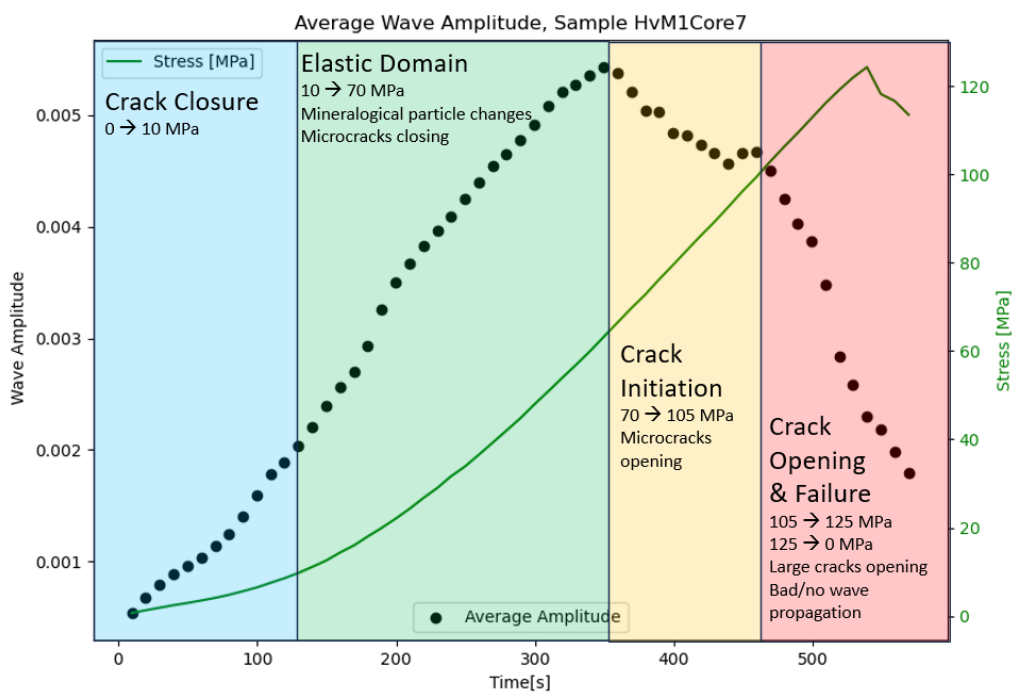
Figure 5.1: Average amplitude against stress on sample HvMCore1 with explanation.
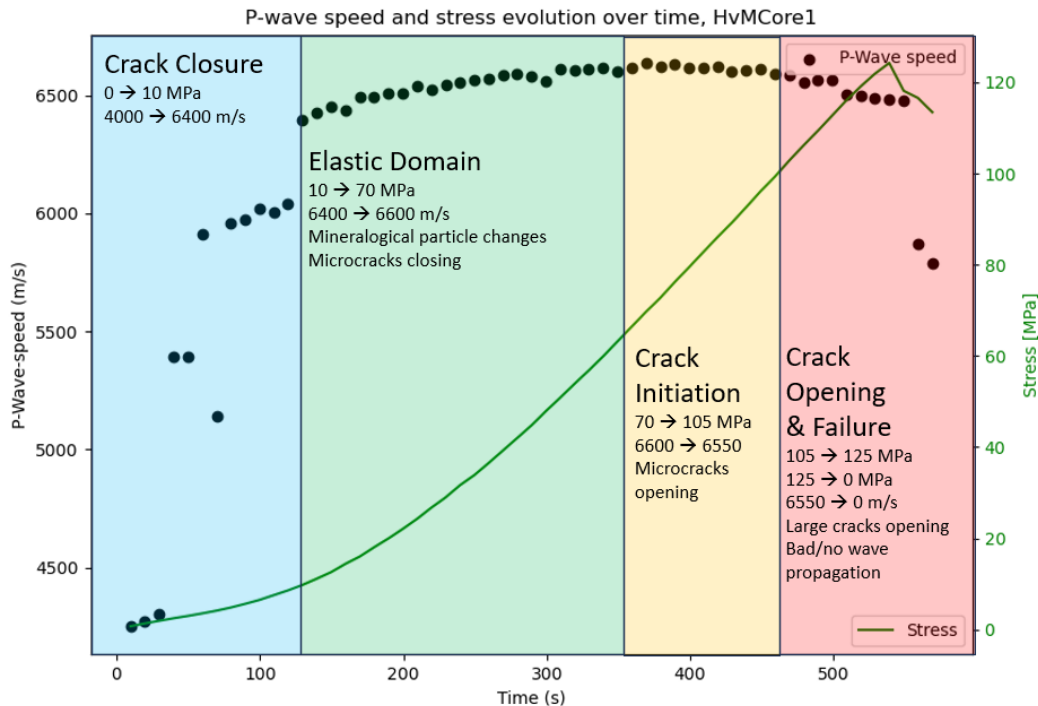
Figure 5.2: P-wave speed against stress on sample HvMCore1 with explanation.

The apparent jumps in P-wave speeds in the crack closing phase in Figure 5.2 could be closing cracks. It must however be noted that sample HvMCore1 did not show any apparent visual cracks before loading and that a speed of 4000 m/s coincides with a nepheline syenite that is made up out of some 40 percent air. That is unlikely. Especially when these jumps are not observed in the Figure portraying amplitude against stress (Figure 5.1). The possible explanation for these low values is thus most likely the inability of both the wave-picking script and the hand-picking method (given Figure 4.10c) to observe any wave signal in the low stress phases. This signal attenuation can be caused by micro crack closure, but by looking at the average wave amplitude, this closure process goes much slower than the jumps portrayed in Figure 5.2. The only logical explanation for those jumps can thus be picking bias.

Luckily, in the field, the wave signal is much clearer and observable due to the nature of the source (a hammer). Nonetheless, also in the field values lower than 5500 m/s are regularly observed, especially when measuring along the wall. The reason for these slow speeds can be that the measurement is measuring something else than nepheline syenite, like attenuating large cracks filled with air. This means that When comparing the speeds with speeds found in the lab, the only logical thing to be said is that when a speed lower than 6000 m/s is found, one is most likely in either the Crack closure or Crack opening phase, which are on the other sides of the stress curve. Once speeds are measured that are higher than these zones, a clear correlation between stress and P-wave speed can potentially be made.

5.3.1. Mechanical Stress and Strain
Next to a comparison on the acoustical methods, a comparison between the two mechanical tests in this research, UCS in the lab and flat jack in-situ, can also be interesting. As strain relief methods, like the flat jack, can generally not be performed in the lab, it is more useful to see how a strain relief method in-situ can be analysed as a strain-induced method. During a UCS-test, strain is induced on a rock sample by applying pressure to it. This pressure, or stress, makes the sample change shape. When cutting a slot into the wall, the rock mass surrounding it also applies pressure on the rock nearby the slot, changing the shape of that rock. By applying pressure to undo that deformation of shape with a flat jack, it is found how much pressure the nearby rock mass applied to deform the rock around the slot.
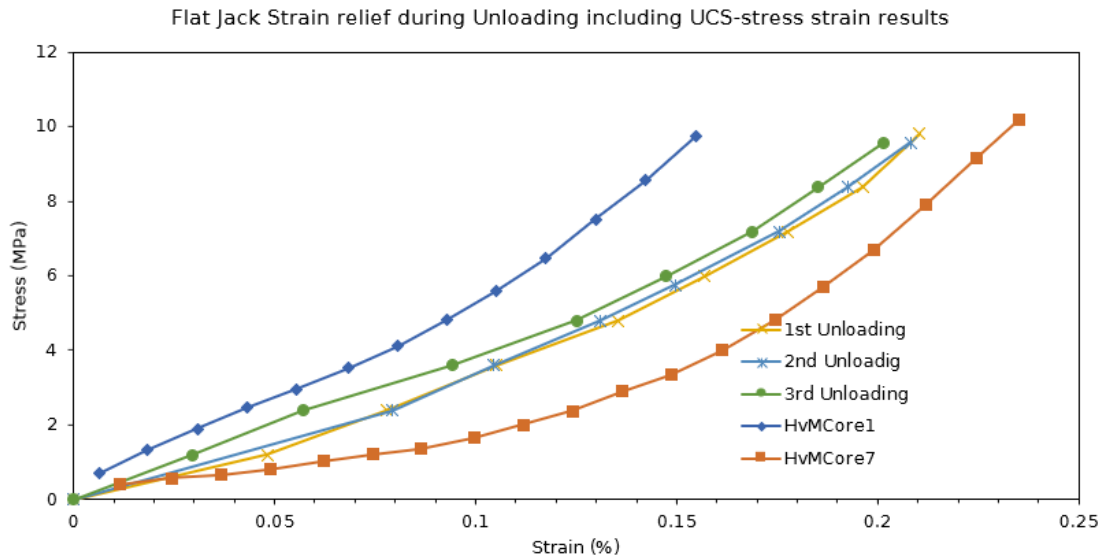
Figure 5.3: Measured stress and strain during the unloading of the flat jack and HvMCore1-7 with adjusted stress and strain.

By analogy, it can thus be inferred that the rock mass is the hydraulic press pressing on the rock nearby the slot, the sample. The loading of the flat jack can than be acting as the unloading of the rock sample. Following this analogy, one can plot together the initial loading stages of both a sample (80 mm) in a UCS-test up to the adjusted cancellation pressure of the flat jack and that of the rock sample above the slot in between the laser and the connection point of the measuring plate (125 mm). As can be observed in Figure 5.3, the paths show resemblance, but they are not the same. The almost perfect HvMCore1 reaches 10 MPa whilst enduring only 0.15% axial strain, whereas the visibly broken HvMCore7 reaches 10 MPa with 0.23 % axial strain. The unloading of the flat jack is somewhere in between those two, following a somewhat similar path. This plot shows that the rock mass in the field behaves mechanically similar to the lab, when performing a flat jack test and a UCS test.

5.3.2. Comparison of tests

The tests performed in this research have a lot of advantages for the geotechnical team in Stjernøya. Added to the fact that they are available in the mine and can be performed on request in multitude by a small group of engineers, the performing of one flat-jack test can be done in approximately two shifts and extensive acoustic velocity measurements in one area can be done in two hours. In comparison to the overcoring test and the hydraulic fracturing test, this is a huge difference. The cost of performing those tests is very high. Additionally the influence of logistics on the possibility of performing the tests is also high, which could mean that if a test is urgently required, it can be performed a week later at the shortest notice.

Next to that, the overcoring and hydraulic fracturing tests require knowledge of at least one in-situ stress tensor. Usually, this tensor is taken to be the vertical stress tensor, dependent on the weight of the overburden. This, however, is a difficult thing in the Stjernøya mine, given the altering topography of the fjord and the mining operation above. All in all, multiple things speak against the use of overcoring and hydraulic fracturing in Stjernøya and in favor of the flat jack test in combination with acoustic measurements. Those two methods are cost and time effective and give immediate results without the necessity of knowing or assuming the stress regime. Next to that, the acoustical method is the only non-invasive method to measure stresses, which can be very suitable to investigate heavily broken areas in the underground mine.

BEFORE EXCAVATION for planning		Geotechnical Category		
Consequences class (CC)	Examples. Typical rock constructions	Ground Uncertainty		
		low	medium	High
CC1 Low	- Simple foundations on rock - Low – moderately high rock cuttings - Tunnels of small size (< 4 m span)	GC1	GC1 / GC2	GC2
CC2 Medium	- Complicated foundations on rock - High to very high rock cuttings - Large tunnels (4 to 15 m span) - Environmental requirements	GC1 / GC2	GC2	GC2 / GC3
CC3 High	- Undersea tunnels, all sizes - Unlined pressure tunnels, all sizes - Strict environmental requirements - Large caverns or very large tunnels (span > 15m) - Tunnels with limited rock overburden	GC2	GC2 / GC3	GC3

Consequences classes (in accordance with EN 1990):
CC1: **Low** consequences for loss of human life, or economic; social or environmental consequences are **small or negligible**
CC2: **Medium** consequences for loss of human life; or economic; social or environmental consequences are **considerable**
CC3: **High** consequences for loss of human life, or economic; social or environmental consequences are **very high**

Classes of Geological and Ground Uncertainty (before excavation):
Low: Clear and simple geology and ground conditions. Ground parameters can be easily found. Experience from construction in similar ground conditions.
Medium: Clear geology and ground conditions. Methods exist both to assess ground conditions and for dimensioning. Experience from construction in similar ground conditions can be documented.
High: Unclear geology and/or ground conditions with potential for problematic tunnel excavation. There are limited possibilities to assess the ground conditions before excavation starts

Figure 5.4: Eurocode 7 categories and risks (Stille and Palmström, 2018).

5.3.3. Eurocode 7

Even though the flat jack tests and acoustical investigative method are quicker to be performed than their non-available counterparts, there still is a large difference between them in time and information they give. To accurately choose the right measurement tool for the geotechnical project, one should take into account the Eurocode 7 Category (Figure 5.4). For a Category 1 project, the acoustical investigative method could provide enough data to confirm the stable and low-risk nature of the rock mass. Possibly helped by a Rock Mass Rating and a three dimensional stress model, this would suffice that category.

A Category 2 project needs a least some certainty regarding stress tensors. This can only be (quickly) achieved with one, or multiple, flat jack test(s). Elastic knowledge of the rock from laboratory work will help generate more trust in the data. Also, a Rock Mass Rating can provide information on the possible necessity of additional structural stability construction works, as well as helping in confirming results from the stress test.

For a Category 3 project, a multitude of both flat jack tests and acoustical investigative methods could provide large enough information about the rock mass in question. Laboratory work is then necessary to aid the acoustics as well as providing elastic properties of the rock. If the Category 3 project in Stjernøya is performed, it might be helpful to also call in a rock mechanical consultancy company or contractor to perform a different stress test if not enough trust is given to the results found by the tests performed with the 'hand-held' equipment.

5.4. The Corner of Myrvang

The main area of research in the Stjernøya mine has been the corner where A. Myrvang did a overcoring test in the 1970s. The findings this overcoring test, which was performed ad 38 cm depth into the rock wall, can be found in Table 4.1. Most interestingly, the vertical pressure was found to be 9.7 MPa. This coincides really well with the vertical pressure (9.81 MPa) found with the flat jack between 0 and 45 cm

Table 5.4: Results from geotechnical research on the corner of Myrvang in the Stjern{\o}ya mine.

Parameter	Description	Value	Note
Stjernøya Overall			
UCS	MPa	117.5	Johansson (2001)
P-wave Speed	m/s	5369	Johansson (2001)
Elastic Modulus (high)	GPa	65.6	Johansson (2001)
Elastic Modulus (low)	GPa	26	Dahle (2007)
Elastic Modulus (average)	GPa	45.8	
Poissons Ratio	-	0.24	Dahle (2007)
Lab - Samples from Corner of Myrvang			
UCS	MPa	125.1	Average
P-wave Speed	m/s	6549	Averaged Maximum
Elastic Modulus (high)	GPa	63.01	Average Second Stage
Elastic Modulus (low)	GPa	36.62	Average First Stage
Elastic Modulus (average)	GPa	49.82	
Elastic Modulus (acoustics)	GPa	47.35	From P/S-wave modulus
Poissons Ratio (high)	-	0.15	Average Second Stage
Poissons Ratio (low)	-	0.37	Average First Stage
Corner of Myrvang			
σ_v	MPa	**9.81**	Flat Jack
σ_v	MPa	**9.80**	Overburden stress
σ_v	MPa	**9.7**	Overcoring test (Myrvang, 1973)
P-wave Speed	m/s	6258	95th Percentile (HvM-Pillar)
P-wave Speed	m/s	5755	75th Percentile (HvM-Pillar)
P-wave Speed	m/s	5525	50th Percentile (HvM-Pillar)
RMR89	-	82	(Q = 2.7 and GSI = 77)
RQD (high estimate)	%	92.5	from RMR89
RQD (low estimate)	%	80.3	from RMR89
RQD	%	81	from seismic velocity
Elastic Modulus	GPa	33.7	inferred from Flat Jack Pressure (low-stress domain)
Elastic Modulus	GPa	17.57	ASTM-method, low because of wrong procedure.
Elastic Modulus	GPa	63.1	inferred from RMR89 results

into the wall. It is logical that this value is found, as it coincides with the pressure the overburden (370 metres) should apply on the rock. Also, because the corner of Myrvang is in a relatively undisturbed area of the mine, its pressure profile should not have significantly changed over the years. These results further speak in favour of the result found with the flat jack measurement and the result of the overcoring test by Myrvang. Next to that, acoustic measurements through the pillar also find velocities that could further confirm the stress regime. Finally, the RMR and Q classification of the outcrop indicate a good rock mass quality. Comparing the found elastic moduli with the flat jack tests and in the lab with the ones inferred by the RMR further confirms the understandable and predictable behaviour of the pillar at the corner of Myrvang. A list of the final rock mechanical parameters of all the tests done on the area, along with generally accepted values in the Stjernøya mine can be seen in the Table 5.4 and (partially) visualised in Figure 5.5. Please note the differences between the different P-wave measurements. Also, the topography stress refers to the stress caused by the overburden, calculated using the difference between topography and measurement point in the vertical direction.
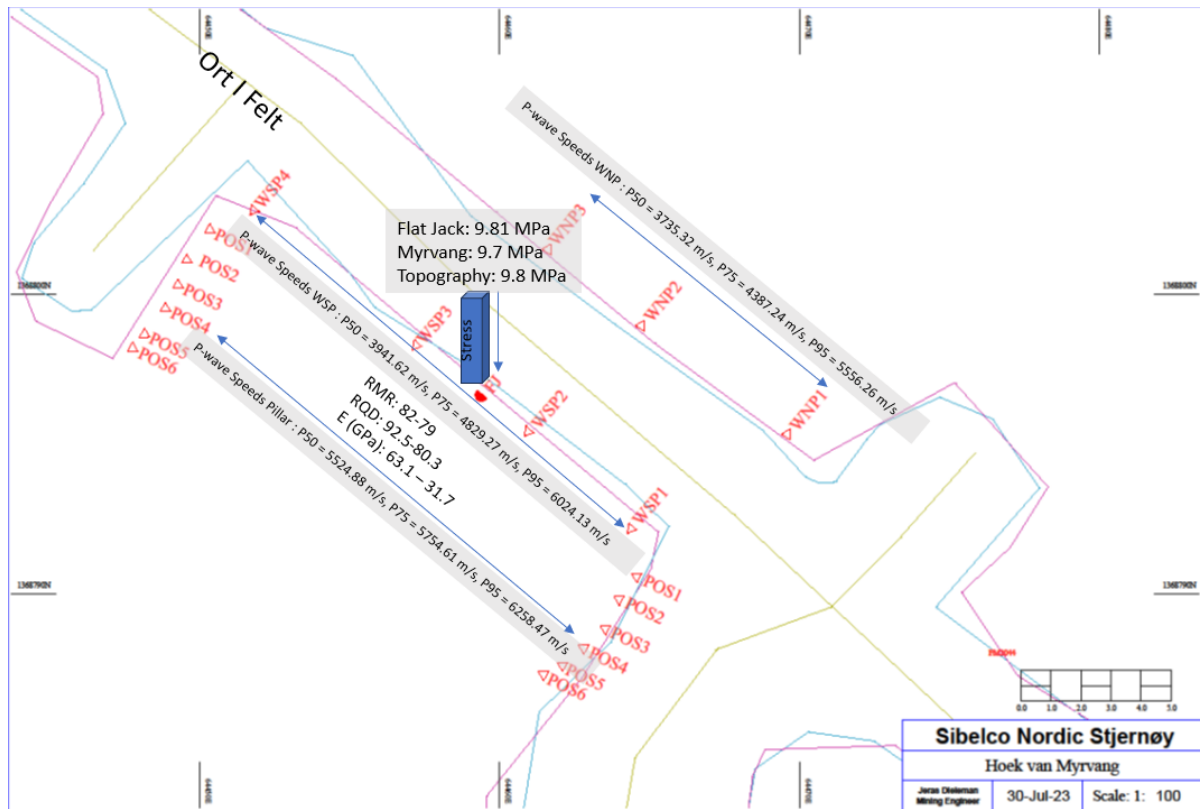
Figure 5.5: Results of the corner of Myrvang plotted in the map.

For visualisation purposes, a bar chart of the different Elastic moduli is visible in Figure 5.6. It is apparent that the laboratory results from the samples retrieved from the corner of Myrvang show great resemblance to the values found in literature. Also, the elastic modulus calculated using elastic theory (Formulae 3.3,3.11,3.5,3.10) is found to be almost exactly the same as the average elastic modulus found in the UCS-test. When comparing the found elastic moduli with the field tests, the RMR-classification gives a similar high peak at around 65 GPa. The elastic modulus inferred from the loading pressure-strain curves of the flat jack gives a similar elastic modulus to the low-stress domain elastic modulus found using the UCS-tests and literature. Sadly, the elastic modulus found using the ASTM-proposed method of finding the elastic modulus using the flat jack test cannot be correctly interpreted, due to the fact that only one measuring point is used in measuring strain.
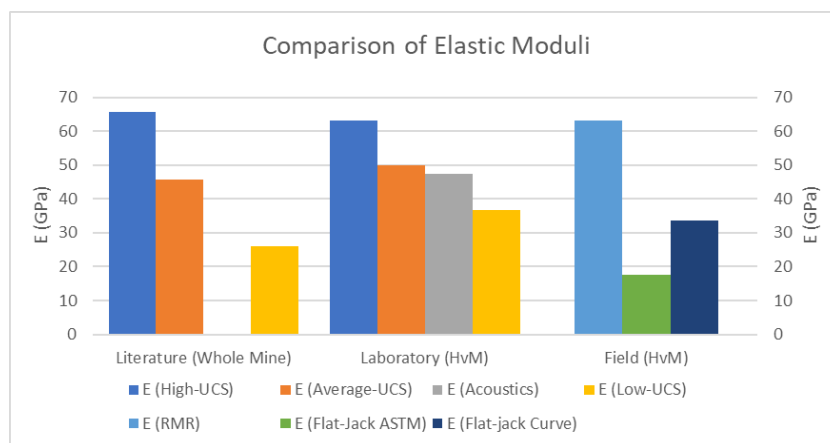
Figure 5.6: Comparison of elastic moduli for the different tests. (UCS refers to UCS-test)

<div align="right">

6

</div>

<div align="right">

Discussion

</div>

The following discussion will refer to several stages in this research. It will summarize them and their results. Also, it will indicate where the workings were influenced by several factors. Some of these factors were chosen for, as they were necessary for the research to happen or for the research to stay within the scope. Other factors that had an influence on results were uncontrollable factors, which you can expect during experimental (field) work. This discussion thus poses to explain the limitations of the research and potential areas to explore further in the future.

6.1. Summary

This research aimed at creating more knowledge about several stress measuring techniques in the near-surface low-stress hard rock mine of Stjernøya. Consequently, a more precise strategy could then be created for varying rock mechanical researches in the mine. To do this, a multitude of rock mechanical and acoustic tests were conducted either in the lab or in the field. The results from the lab are clear, a proper understanding of the samples retrieved from the field research area is achieved. The found laboratory values coincide with findings in previous researches on the nepheline syenite in the mine of interest. Additionally, a clear logarithmic relation is found between the increase in stress and the increase in P-wave speed, given a CHILE sample.

The application of this relation in the field proved to be more difficult. A lot of acoustic measurements were done on the location, next to a single flat jack test, in order to measure the vertical stress along the wall. The acoustic tests through the pillar at the location gave plausible velocities, whereas the measurements along the wall gave a large spread of results that were harder to interpret and combine with the relation into a stress reading.

The final results, however, do give a distinct result where the multiple tests agree on the state of the rock. Stress found in literature add up with the stress found using the flat jack test and with the stress applied by the overburden. Next to that, seismic velocities could be used to assume a stress-level in the rock. Confirmation of tests comes by comparing their elastic moduli, that show two distinct stages, along with an average. Finally, empirical and visual measurements done using a rock rating classification like RMR or RQD confirmed the state of the rock and also inferred rock mechanical parameters that agreed with test measurements. By combining all the tests, a thorough understanding of the nepheline syenite and the state of the corner of Myrvang was created, along with a confirmation that all the measurement techniques could be used to generate useful, consistent and trustworthy information about the rock.

6.2. Implications

The difficulty of this research appeared to be in the application and later combination of different stress measurements, given their respective efficiency and accuracy, in relation to a challenging geology and environment. A geotechnical engineer on site would like to know certain rock mechanical parameters,

given the Eurocode 7 (STANDARD, 2004) geotechnical category. The combination of the rock mechanical parameters, including stress, gives a level of geotechnical knowledge, befitting a Eurocode 7 category. Based on the trust in the measurement technique and the generated results of the measurement technique, this level of geotechnical knowledge is created. This research gives multiple possibilities for a geotechnical engineer to create this geotechnical knowledge with a high level of trust, worthy of multiple categories within the Eurocode 7.

Next to that, the research also opens up multiple paths into further research on the measurement techniques and the nepheline syenite. Significant statements can be made about the stress response of the nepheline syenite during laboratory stress and acoustic tests. Furthermore, the confirmation and broadening of knowledge about the rock is valuable for the mining engineers in the Sibelco team. Additionally, the research confirms rock-mechanical difficulties that can be encountered in a low-stress underground opening.

6.3. Limitations

This research was conducted on one reasonably undisturbed area of the mine. An acoustic experiment was briefly tested at one other area within the underground complex, but a multitude of tests spread throughout the mine fell outside of the scope of the thesis. Also does this research not give a clear solution for finding the σ_1, σ_2 and σ_3 in and around the underground opening. For engineering, this is also not necessary, as an approximation of the reigning stress field already gives a lot of information. Three different flat jack tests could create the Cauchy tensors, but some literature (He and Hatzor, 2015) states that a minimum of six tests is required. Directly retrieving stress values from P-wave velocity is also difficult, as this research does not specify which stress tensor that gives. In the end, a 2D or 3D numerical stress model could help the retrieval of the 3 principle stresses. If it is found that a rock mass, like the pillar at the corner of Myrvang, behaves consistent with the general rock mechanical rules of the underground complex, the retrieval of the stress from the model could suffice.

6.3.1. Laboratory tests

The most straightforward test conducted in this research is the UCS test. It is well known and well documented in the ASTM D4729-19 (2019). After adhering to the guidelines as specified in the standard, the results from the UCS-tests are understandable and clear. More testing could create a larger sampling group with even more certainty, but as the results from this research are very consistent with previous research on the Norwegian nepheline syenite (Johansson, 2001), this is not deemed necessary. What could be interesting is studying the fracture planes of the broken samples in a CT-scan, to measure their orientations. This could give valuable information for modelling the failure of the rock in-situ. Also, reviewing the samples after the so-called 'spalling-event' (Figure 6.1) is not done in this research but might be interesting in the future. As specified in the introduction, spalling is a failure mode that is observed at multiple locations in the mine, but not yet understood.
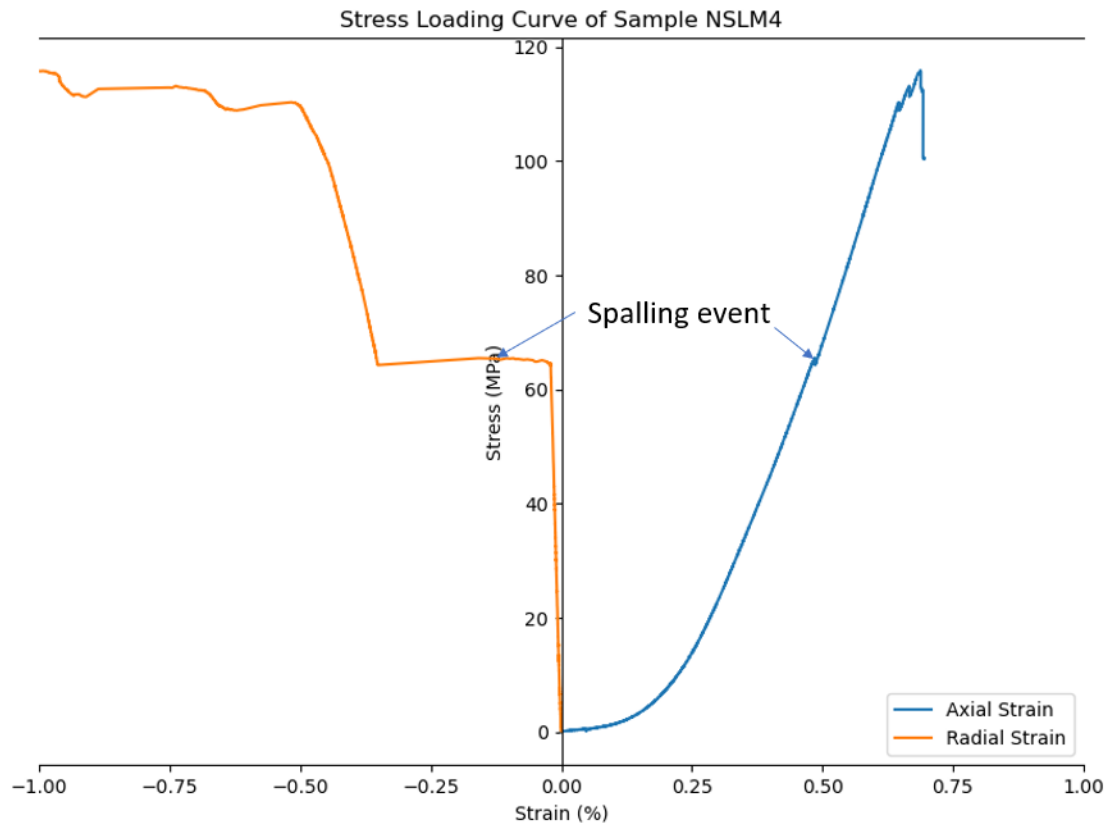
Figure 6.1: "Spalling event" occurring at around 1/2 the UCS of sample NSLM4.

One other limiting factor on the laboratory UCS-test is the sample geometry. Due to in-situ sampling with a handheld drill of no more than 15 cm, the samples were cut in small, sometimes broken cores. This lead to the decision to use samples with 80 mm in length and 40 mm in diameter. Despite this being on the edge of the boundaries set by various standards on UCS-testing, they did adhere to the regulations and the 80x40 samples gave very similar results to the 70x30 samples from earlier research.

The acoustic-wave generation and acquisition in the laboratory is done with great precision that cannot be achieved in the field. Nonetheless, the maximum possible voltage or power that can be created by the amplifier is 1V. In the lower stress domain this sometimes lead to very bad propagation of the wave. In both the P-wave and S-wave amplitudes this problem can be seen. During the analysis this became a problem, as wave onsets were very hard to classify.

It can be discussed that a hard boundary had to be set and that all the wave onsets had to be hand-picked, but due to the size of the dataset and the bias of a sole observer it was chosen to let the computer code do this task. In the end, the results from the computer code seemed correct for homogeneous samples. Visibly cracked samples had a much larger difficulty in propagation when the first 20 MegaPascals were applied to them. This is visible in Figure 6.2. In the cracked HvMCore7 sample especially undulating noise, offset and poor wave-onset made proper picking difficult. Because of the maximum voltage available it cannot be contributed fully to the cracks in the sample, as explained by Figures 5.1 and 5.2. Lower amplitudes could mean that the P-wave onsets are just not measurable in the lower-stress regime. To increase the amplitude and make the generated wave more visible, future tests could be done using a 1 Kilo Hertz wave instead of a 1 Mega Hertz wave.
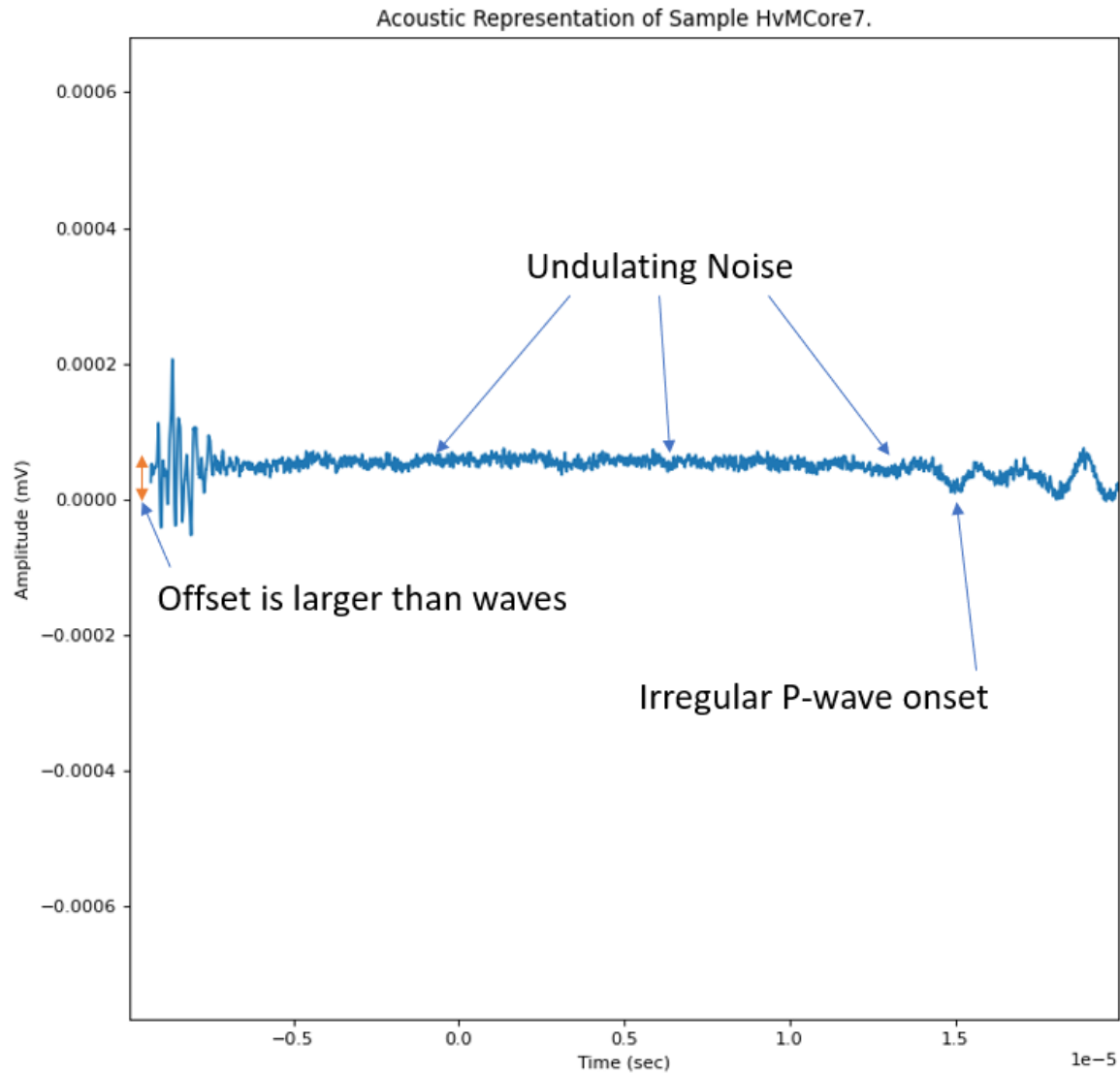
Figure 6.2: Problems encountered during the picking of P-wave arrival times.

Another problem with the laboratory acoustics is the fitting of the stress-relation curves. Because of the visual observed similarity with a power-curve it was chosen to take an exponential approach to the fitting process. The exponential fits only hold until a certain stress-level (+-70 MPa, Figure 4.18). In some cases, however, a quadratic function produces a fit with a greater correlation coefficient. Only at the edges of the dataset, the low and high stresses, the quadratic function does not hold properly. Whether one is better than the other can be argued and statistically researched in future investigations, but for this research, as it focuses on low stress domains, it was chosen to take the power function as the main relation, because of its better fit in lower stress domains.

Finally, the laboratory tests are merely a show of the heterogeneity of the samples and thus the rock in the Stjernøya mine. Despite the samples being from the same borehole, they show variety in UCS, Elasticity, Poisson's ratio and P/S-wave speeds. The differences observed in, for instance, maximum P-wave speed might be entirely due to mineral composition. The stress history of the sample (Kaiser-effect, Mulder (2019)) and the closeness to the underground opening could also have influenced the heterogeneity of the sample set.

6.3.2. Field tests

Flat Jack test

In the field, not everything can be as precisely controlled as in the laboratory. At the start of conducting measurements, the rock mass is not as well defined as a cut-out sample in the lab and therefore it is always a question what you are actually measuring. Especially with the flat jack test this is of importance. During testing there is only so much you can control. For starters, the measurement device used is a laser attached to a 2 metre wide bar attached onto the wall at 2 rock bolts. The first assumption made is that during deformation because of the opening of a slot, no movement is caused at the attachment points of the bar. Mestdag (2022) argues that deformation happens during measurement, but there is no measurement done to back up this argument and also in other literature there is no evidence found that deformation in the rock mass occurs further than 0.5 metres parallel to the slot. This research did not aim at proving or disproving the hypothesis by Mestdag (2022).

Also control over the slot proved to be really difficult. As you are diamond-cutting into very hard and somewhat stressed rock, cutting is difficult. The cutting mechanism works, but an ideal flat-jack shaped slot is not realised. This could limit the accuracy of the final pressures and strains found. To mitigate the problems caused by this irregular cut slot, the tributary area method is used. Although this method is proven to work in a large room and pillar mine, it is uncertain whether the method still holds in such a small and confined rock mass. Nonetheless, the application of a certain geometric method adheres to the (withdrawn) standard mentioned in ASTM D4729-08 (2017). Next to that, the found results using the tributary area method coincide with other findings, which speaks in favor of the method. Room for improvement is possible in the slot creation with more precision and symmetry.

After insertion, the flat jack is powered up by a hydraulic press that is hand-operated using a analogue manometer. As the operator needs to forcefully operate the flat jack, next to taking measurements and safeguarding the test, there is a lot of room for error. It should be noted that no errors were found during the test, but a mechanical or automatic pump could generate a safer process along with more accurate readings and a steady loading rate. For not just this particular reason it was chosen to utilize the more easily controlled pressure release for the elastic calculations. The loading/unloading cycles are difficult to get correct in the first try and thus multiple loading cycles are done using the flat jack. It can be argued that the cyclic loading of the rock surrounding the flat jack could break the rock, but the gathered data does not indicate this. Also, the lab tested samples do not show any fatigue in the low stress (0-40 MPa) domain after repetitive loading. In this case it could be argued that because the install process takes so long compared to the actual measurement, more tests are always justified for more accurate data and a better understanding of the rock in-situ.

Another act that might improve the attainable data from the flat jack method is the creation of multiple strain measuring points. This can help in understanding the rock mass, as well as in finding a more accurate elastic modulus using the ASTM-method.

Field Acoustics

This research stated that the nepheline syenite measured using the acoustic investigative method is not CHILE. It is not Continuous, Homogeneous, Isotropic and Linear Elastic. This lies at the heart of the limitations of the field acoustic measurements. Because of the heterogeneity of the rock mass, measurements could all be a true representation of the wave propagation through the rock mass. It is because of this principle that there are a lot of uncertainties and thus limitations associated with the results from the field acoustic measurements.

For starters, the data generated is extremely dense due to the high capabilities of the geophones to pick up any vibration in the rock. The blow of the hammer still stands out, but some measurements featured strange bursts of amplitude that could not be easily explained. Some sort of damping could prevent this, but for longer tests, geophones might not pick up the wave altogether. Nonetheless, the current geophones do work, but generate data that is very hard to understand without misinterpreting and/or filter the data wihtout modifying it. It is understood from this research that the filtering process could remove datapoints that set-off the hammer-blow waveform by just the slightest, making it hard to find an arrival time.

For this reason, it could be interesting to also test different geophones that are being used by, for instance, the TU Delft in field measurements. It would be interesting if the same dense data is generated by those or if they are modified better to pick up sound waves and filter out noise. Better geophones does mean more elaborate data and could allow for wave-form analysis and given a large enough group of geophones, possibly even seismic tomography. Using this seismic tomography, a visual interpretation could be made of the structures in the rock mass of interest. This research did not include this, but for future research this could be extremely valuable information for a geotechnical engineer.

Recurring monitoring could be possible using the acoustic investigative method. As the rock bolts are already installed, it would be very interesting to repeat the test using the rock-bolts after a couple of weeks, months or years. The changes observed in P-wave could possibly be an indication of the changing stress regime in the rock mass. As a monitoring tool, the acoustic investigative method shows great promise and has been done within Sibelco (Schmitz, 2020), but more future research, on for instance the Corner of Myrvang in 6 months time, could give valuable answers.

It would also be possible to do a cross-borehole measurement, like performed by (Barton et al., 1994). This would give better information about stress states in the rock mass, in contrary to the altered stress state observed around and because of the underground opening. A cross-borehole test, however, is not possible with the current equipment available at Stjernøya. Therefore, it is a recommendation for future research.

Another point of discussion concerning the acoustic field tests is the subject of measurement. It was chosen to measure both through the pillar and along the wall of that pillar in the corner of Myrvang. The results varied a lot. Not only did the measurement through the pillar statistically gave higher P-wave speeds, the data was also a lot more homogeneous than that of the measurement along the wall. It must be noted that those two tests were done on different days and that during the test along the wall measurement difficulties were encountered with the set up. Nonetheless, a similar wall-measurement along the barrier pillar in underground mine 2 of the Stjernøya complex gave a much more homogeneous result. This raises the question whether the results along the wall at the corner of Myrvang are (partially) correct or the measurement was just not executed properly due to operator or equipment malfunction.

In the end, the acoustic field test is limited by the choices made for this research. The array-like difference between the geophone locations was chosen to be around 5 metres along the wall, but not measured prior to taking the geophone readings. Measurements spaced further away or closer together could generate better data, but this effect was not investigated during this research. Also the blow of the Estwing geological hammer was not constantly performed by even the same geotechnical engineer, which could give difference in data measured. Next to that, the location of the blow varied based on the capability of the rock surrounding the geophone. To prevent hammering a loose slab and creating instant reflective waves, a solid block was chosen to hammer on, which was not always directly next to the geophone. Future research could investigate the possibility of installing a rock bolt right next to the rock bolt of the geophone, which reassures a smooth transition of the hammer blow and its wave into the rock. This would also make it possible to not hammer inbetween two geophones when measuring along a wall surface.

Rock Mass Rating and Q-value Rating

Measurements done for the Rock Mass Rating (and Q-value) are biased by the performer of the measurements. It is a visual/haptic method so it is prone to interpretation bias. Despite this, the rating systems can give good additional information of the rock mass. The proceedings of the rating like Elastic Modulus, P-wave Velocity and RQD are very good to compare with similar data generated by other measurements. The final scores of the Rock Mass Rating and especially the Q-value rating are very limited in giving proper information about only the rock, as they take into account non-rock parameters like SRF (stress reduction factor) based on the type of underground opening and the risk associated with that opening. This heavily influences the final score. Also, the water reduction factor or the near-surface blasting influence factors are not defining of the rock and the stresses in it. The Q-value rating

also uses an arbitrary logarithmic scale to defining stability of the rock mass. This makes it hard to interpret as a single extra joint set could create a very large jump in Q-value rating. The rating systems are, overall, too general and not specific enough for this rock type. That being said, it cannot be denied that there is use for them in checking found variables, doing a quick survey of an area of interest and finding different rock parameters like the friction angle and cohesion, which are important inputs for the geotechnical model.

6.4. Recommendations

Following this research, geotechnical engineers in Stjernøya should have a better understanding on what tests to perform in which situation. More investigations can be done on every test done. In the lab, the spalling-event, as well as fracture planes can be investigated further. Also, acoustical tests with different frequencies than 1 MHz could be done, to see whether wave propagation through the sample improves in the lower stress domain. In the field, flat jack tests could be done with better cut out slots and with more control of the hydraulic pumping and releasing. Research on the applicability of the tributary area method could benefit the flat jack findings. It would also be interesting to perform a different test, like overcoring or hydraulic fracturing on the corner of Myrvang to further check the values found and calibrate the acoustical investigative method. This acoustical investigative method could also be redone with different standard geophones on a larger array and with different spacings or using a cross-borehole technique. The repetition of the same tests could indicate the usefulness of the acoustic investigative method as a monitoring tool. Finally, specific modelling of the stresses using a 2D or 3D numerical model would be recommended to confirm the found results and further the trust in the hand-held measurement methods used in the Stjernøya underground complex.

7
Conclusion

In this research, a full rock mechanical investigation was launched in both the laboratory and in the field. Based on the similarities found in this research between the laboratory results of the tests and the results in the field, it was deemed probable that the measurement procedures in the lab could partially be recreated in the field. By allowing this, stress measurements in the field could be done using two different methods; the mechanical flat jack method and the acoustical investigative method using P-wave velocity. Following are statements resulting from this research;

In the lab, it was established that there exists a relation between stress and P-wave velocity. Despite the heterogeneous nature of the rock, it was found probable that a similar relation should exist in the field. The flat jack test and the acoustic investigative method should then be done on the same rock mass to establish this relation in the field also.

A set up of a flat jack test is difficult and requires scientific precision. Nonetheless, if the tools are available, like on Stjernøya, the set up can be done in less than a day with two skilled geotechnical engineers. The time and cost to do a flat jack test is a lot lower than that of its mechanical counterparts, like overcoring or hydraulic fracturing. Next to that, it can be done almost anywhere in any direction where there is a straight undisturbed surface.

As a result the flat jack test produced one accurate stress tensor measured from up to 50 cm into the wall, that coincided with other (older and empirical) stress-tensors. Additionally, the flat jack test provides information on induced strains to generate the elastic modulus. Next to that, the flat jack test can identify local extensional instead of compression forces. In terms of Eurocode 7, a trio of flat jack tests would be sufficient for a Category 2 project. In combination with an acoustical and laboratory research it could also suffice a Category 3 project.

The acoustical investigative method gives accurate P-wave speeds, provided that well working sensors are available. A statistical analysis of the results using a reference stress relation could potentially give an indication of the stress regime. This research, however, did not find that measuring stress using acoustical investigative methods would always work. This research confirmed that there exists a relation between stress and P-wave speed, but it is questionable whether you are measuring the stress response of the rock in the field instead of for instance Rock Quality. As lab results show, a low acoustic velocity can only be observed in rock with low stress or in (almost) failed rock masses.

One of the takeaways from the acoustical investigative method is that the tests can be done very quickly and almost anywhere where there exists a surface of interest in an area of which the rock properties (elasticity and acoustic velocities) are known. Additionally, it was observed that cross-pillar measurements are more accurate than cross-wall measurements. Because it only gives an indication on the overall acting stress on the field ($\sigma_{1,2,3}$), P-wave measurements should only be used as a sole source of information for a Eurocode 7 Category 1 project. In Category 2 or 3 projects it can be very helpful in generating additional data on the quality of the rock and as a quick way to check found stress values.

Rock Mass Rating and/or Q-value rating should not be seen as a real stress measurement tool but rather as a complementary test to confirm or benefit found results in the different tests. They can also help the geotechnical engineer in looking more thoroughly at the rock in an efficient way. In any Eurocode 7 Category, the final step in the geotechnical investigation could be the application of the Rock Mass Rating or Q-value rating.

The difficulty in Stjernøya with measuring stress is due to a low in-situ stress. Despite it being beneficial for the stability of mine-openings, this research found that a low in-situ stress makes it more difficult to calibrate mechanical stress tests, due to the unknown principal stress direction and size. Next to that, acoustic P-wave speed measurements are being done in a very low stress regime, in and around the first phase of the loading phase (Crack Closure). This makes it hard to interpret the found acoustic velocities as it could be that the cracks in the rock mass are being measured instead of the velocity that is induced by the stress.

To conclude, combining flat jack testing (or any other mechanical testing method that gives a stress tensor and elastic response) and acoustic velocity measurements, in both the laboratory and the field, a profound knowledge of a rock mass and the stresses in it can be generated, which is to be benefited by a visual rock mass rating. All the measurements can be done with 'hand-held' measurements and in a relative short period of time, given logistical constraints. Additionally, implementing that knowledge into a 2D or 3D numerical stress model should suffice the highest Category of geotechnical projects.

Bibliography

A. Argilaga, F. C. (September 2017). Numerical modelling of the stress state evolution of sibelco stjernoy mine. *Sibelco*. Université de Liège.

Alexander, L. (1960). Field and laboratory tests in rock mechanics. In *Proceedings of the Third Australian-New Zealand Conference on Soil Mechanics and Foundation Engineering*, pages 161–168.

ASTM D4729-08 (2017). Standard Test Method for In Situ Stress and Modulus of Deformation Using Flatjack Method (Withdrawn 2017). Standard, ASTM International, West Conshohocken, Pennsylvania, US.

ASTM D4729-19 (2019). Standard test method for in situ stress and modulus of deformation using the flat jack method. Standard, ASTM International, West Conshohocken, Pennsylvania, US.

ASTM D5878-19 (2019). Standard guides for using rock-mass classification systems for engineering purposes. Standard, ASTM International, West Conshohocken, Pennsylvania, US.

ASTM D7012-14e1 (2017). Standard Test Methods for Compressive Strength and Elastic Moduli of Intact Rock Core Specimens under Varying States of Stress and Temperatures. Standard, ASTM International, West Conshohocken, Pennsylvania, US.

Barton, N. (2002). Some new q-value correlations to assist in site characterisation and tunnel design. *International Journal of Rock Mechanics and Mining Sciences*, 39(2):185–216.

Barton, N. (2006). *Rock quality, seismic velocity, attenuation and anisotropy*. CRC press.

Barton, N., Chryssanthakis, P., Tunbridge, L., Kristiansen, J., Løset, F., Bhasin, R., Westerdahl, H., and Vik, G. (1994). Predicted and measured performance of the 62 m span norwegian olympic ice hockey cavern at gjøvik. In *International Journal of Rock Mechanics and Mining Sciences & Geomechanics Abstracts*, volume 31, pages 617–641. Elsevier.

Barton, N., Lien, R., and Lunde, J. (1974). Engineering classification of rock masses for the design of tunnel support. *Rock mechanics*, 6:189–236.

Bieniawski, Z. (1978). Determining rock mass deformability: experience from case histories. *International Journal of Rock Mechanics and Mining Sciences and Geomechanics Abstracts*, 15(5):237–247.

Bieniawski, Z. (1993). 22 - classification of rock masses for engineering: The rmr system and future trends. In HUDSON, J. A., editor, *Rock Testing and Site Characterization*, pages 553–573. Pergamon, Oxford.

Bieniawski, Z. T. (1989). *Engineering rock mass classifications: a complete manual for engineers and geologists in mining, civil, and petroleum engineering*. John Wiley & Sons.

Bruland, T. (1980). Lillebukt alkaline complex: Mafic dykes and alteration zones in nabberen nepheline syenite. *Cand. real thesis UiB, 163pp*.

Bryhni, I. (1962). Structural analysis of the grøneheia area, eikefjord, western norway. *Norsk. geol. Tidsskr.*, 42:331.

Cauchy, A.-L. (1827). Exercices de mathématiques.

Çelik, S. B. (2017). The effect of cubic specimen size on uniaxial compressive strength of carbonate rocks from western turkey. *Arabian Journal of Geosciences*, 10:1–15.

Chen, Y., Zuo, J., Guo, B., and Guo, W. (2020). Effect of cyclic loading on mechanical and ultrasonic properties of granite from maluanshan tunnel. *Bulletin of Engineering Geology and the Environment*, 79:299–311.

Dahle, H. (May 2007). Numerisk modellering av pilartykkelse mellom eksistrerende gruva og fremtidig dagbrudd, stjernoy. *Tech. Rep.*

Deere, D. U. (1964). Technical description of rock cores for engineering purpose. *Rock Mechanics and Enginee-ring Geology,*, 1(1):17–22.

Dodds, D. (1969). Flatjack tests. *Report to the Army Corps of Engineers*.

Dong, L., Pei, Z., Xie, X., Zhang, Y., and Yan, X. (2022). Early identification of abnormal regions in rock-mass using traveltime tomography. *Engineering*.

Eissa, E. and Kazi, A. (1988). Relation between static and dynamic young's moduli of rocks. *International Journal of Rock Mechanics and Mining & Geomechanics Abstracts*, 25(6).

Friedel, M., Jackson, M., Scott, D., Williams, T., and Olson, M. (1995). 3-d tomographic imaging of anomalous conditions in a deep silver mine. *Journal of applied geophysics*, 34(1):1–21.

Gautneb, H., Ihlen, P., and Boyd, R. (2009). Review of the geology and the distribution of phosphorus in the lillebukt alkaline complex, and adjacent areas, stjernøy northern norway. *Trondheim: Geological Survey of Norway (2009.060)*.

Geis, H. (August 1979). Nepheline syenite on stjernoy, northern norway. *Economic Geology*, 74(5):1286–1295.

Goodman, R. E. (1991). *Introduction to rock mechanics*. John Wiley & Sons.

Hauquin, T., Deck, O., and Gunzburger, Y. (2016). Average vertical stress on irregular elastic pillars estimated by a function of the relative extraction ratio. *International Journal of Rock Mechanics and Mining Sciences*, 83:122–134.

He, B.-G. and Hatzor, Y. H. (2015). An analytical solution for recovering the complete in-situ stress tensor from flat jack tests. *International Journal of Rock Mechanics and Mining Sciences*, 78:118–126.

Heidbach, O., Rajabi, M., Reiter, K., and Ziegler, M. (2016). *World Stress Map Database Release 2016. V. 1.1. GFZ Data Services.* `https://doi.org/10.5880/WSM.2016.001` [Accessed: April - 2023].

Heier, K. (1961). Layered gabbro, hornblendite, carbonatite and nepheline syenite on stjernØy, north norway. *Norsk Geologiik Tidsskrift*, 41:109–155.

Hemmati Nourani, M., Taheri Moghadder, M., and Safari, M. (2017). Classification and assessment of rock mass parameters in choghart iron mine using p-wave velocity. *Journal of Rock Mechanics and Geotechnical Engineering*, 9(2):318–328.

Hoek, E. (2000). *Practical Rock Engineering*.

Johansson, A. (March 2001). Todimensionaler bergspenningsmalinger pa niva 320, stjernoy. *Tech. Rep.*

Kaiser, P., Diederichs, M., Martin, C., Sharp, J., and Steiner, W. (2000). Underground works in hard rock tunnelling and mining. In *ISRM international symposium*. OnePetro.

Khodabin, M. and Hosseinitoudeshki, V. (2014). Confidence interval in kirsch equations. *International Journal of Applied Mathematics Research*, 3(4):375.

King, M. S. (1983). Static and dynamic elastic properties of igneous and metamorphic rocks from the canadian shield.

Kirsch, C. (1898). Die theorie der elastizitat und die bedurfnisse der festigkeitslehre. *Zeitschrift des Vereines Deutscher Ingenieure*, 42:797–807.

Leeman, E. (1964). The measurement of stress in rock: Part i: The principles of rock stress measurements. *Journal of the Southern African Institute of Mining and Metallurgy*, 65(2):45–81.

Li, H., Chen, G., and Zhou, W. (2006). Measurements of plutonic rock elastic properties utilizing ultrasonic waves. In *Golden Rocks 2006, The 41st US Symposium on Rock Mechanics (USRMS)*. OnePetro.

Liu, J., Dai, G., and Gong, W. (2021). Joint frequency in the rock mass rating 2014 classification system based on field p-wave propagation velocity tests: a new rating method. *Geotechnical and Geological Engineering*, 39:4697–4708.

Mestdag, J. (September 2022). Étude de l'essai au vérin plat dans la mine de syénite néphélinique de stjernøy. *Master Thesis*. Université de Liège.

Momeni, A., Karakus, M., Khanlari, G., and Heidari, M. (2015). Effects of cyclic loading on the mechanical properties of a granite. *International Journal of Rock Mechanics and Mining Sciences*, 77:89–96.

Mulder, L. (2019). Experimental analysis of passive acoustic emission, in particular the kaiser effect, under dynamic stress conditions. exploring the implications for in-situ failure monitoring in underground mines. *Master Thesis*.

Myrvang, A. (1973). vedrörende begtrykksmalinger ved norsk nefelin, stjernöy. *Tech. Rep.*

Myrvang, A. (2007). Bergmekaniske data i forbindelse med gruvedrifte pa stjernoy. *Tech. Rep.*

Newman, A. (2018). *Seismology*. `http://geophysics.eas.gatech.edu/classes/Geophysics/misc/Seismology.html` [Accessed: April - 2023].

Oostman, H. (February 2023). Spalling in the lillebukt nepheline mine. *Internal Sibelco-TU Delft cooperation*.

Panek, L. A. and Stock, J. A. (1964). *Development of a rock stress monitoring station based on the flat slot method of measuring existing rock stress*, volume 6537. US Department of the Interior, Bureau of Mines.

Pedersen, R., Dunning, G., and Robins, B. (1989). U-pb ages of nepheline syenite pegmatites from the seiland magmatic province, n. norway. In *The Caledonides geology of Scandinavia. Conference dedicated to the Memory of Dr Sven Foyn*, pages 3–8.

Rahman, T. and Sarkar, K. (2021). Lithological control on the estimation of uniaxial compressive strength by the p-wave velocity using supervised and unsupervised learning. *Rock Mechanics and Rock Engineering*, 54:3175–3191.

Ramsay, D. M. and Sturt, B. A. (1970). The emplacement and metamorphism of a syn-orogenic dike swarm from stjernoey, northwest norway. *American Journal of Science*, 268(3):264–286.

Reginiussen, H., Ravna, E. K., and Berglund, K. (1995). Mafic dykes from øksfjord, seiland igneous province, northern norway: geochemistry and palaeotectonic significance. *Geological Magazine*, 132(6):667–681.

Robins, B. and Gardner, P. (1975). The magmatic evolution of the seiland province, and caledonian plate boundaries in northern norway. *Earth and Planetary Science Letters*, 26(2):167–178.

Schmitz, R. (2018). Geotechnical handbook sibelco. *Tech. Rep.*

Schmitz, R. and Hack, R. (2022). Sibelco stjernoy mine, advise related to the observed spalling. *Tech. Rep.*

Schmitz, R. M. (2020). Geotechnical risk management of slopes in quarries, mines and dredging operations of sibelco: geotechnical monitoring. *North of England Institute of Mining and Mechanical Engineers*, pages 7–13.

Schmitz, R. M. and Bertges, M. (2020). Improved methodology in flat jack testing in hard rock mines. *North of England Institute of Mining and Mechanical Engineers*.

Sheorey, P. (1994). A theory for in situ stresses in isotropic and transverseley isotropic rock. *International Journal of Rock Mechanics and Mining Sciences and Geomechanics Abstracts*, 31(1):23–34.

STANDARD, B. (2004). Eurocode 7: Geotechnical design—.

Stephansson, O. (1987). Fennoscandian rock stress data base-frsdb.

Stille, H. and Palmström, A. (2018). Practical use of the concept of geotechnical categories in rock engineering. *Tunnelling and Underground Space Technology*, 79:1–11.

Sturt, B., Pringle, I., and Roberts, D. (1975). Caledonian nappe sequence of finnmark, northern norway, and the timing of orogenic deformation and metamorphism. *Geological Society of America Bulletin*, 86(5):710–718.

Thill, R. E., Jessop, J. A., and Friedel, M. J. (1989). Crosshole seismics: Applications in mining. In *The 30th US Symposium on Rock Mechanics (USRMS)*. OnePetro.

Tincelin, M. (1953). Measurement of earth pressure in the iron-ore mines of eastern france. Technical report, US Geological Survey.

Ulusay, R., Hudson, J., et al. (2007). Suggested methods prepared by the commission on testing methods. *International Society for Rock Mechanics*, page 628.

van Tooren, M. (2022). Spalling syeniet stjernoy, noorwegen. *Tech. Rep.*

Yesiloglu-Gultekin, N., Gokceoglu, C., and Sezer, E. A. (2013). Prediction of uniaxial compressive strength of granitic rocks by various nonlinear tools and comparison of their performances. *International Journal of Rock Mechanics and Mining Sciences*, 62:113–122.

Young, T. (1845). *A Course of Lectures on Natural Philosophy and the Mechanical Arts (Miscellaneous Papers, Reprinted with Corrections).*, volume 1. Taylor and Walton.

Zang, A. and Stephansson, O. (2009). *Stress field of the Earth's crust*. Springer Science & Business Media.

Zang, A., Stephansson, O., Stenberg, L., Plenkers, K., Specht, S., Milkereit, C., Schill, E., Kwiatek, G., Dresen, G., Zimmermann, G., et al. (2017). Hydraulic fracture monitoring in hard rock at 410 m depth with an advanced fluid-injection protocol and extensive sensor array. *Geophysical Journal International*, 208(2):790–813.

Zhang, L., Zhang, Z., Zhang, R., Gao, M., and Xie, J. (2021). The ultrasonic p-wave velocity-stress relationship and energy evolution of sandstone under uniaxial loading-unloading conditions. *Advances in Materials Science and Engineering*, 2021:1–11.

A
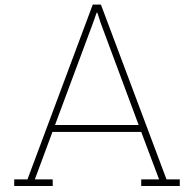
Lillebukt Geological Map
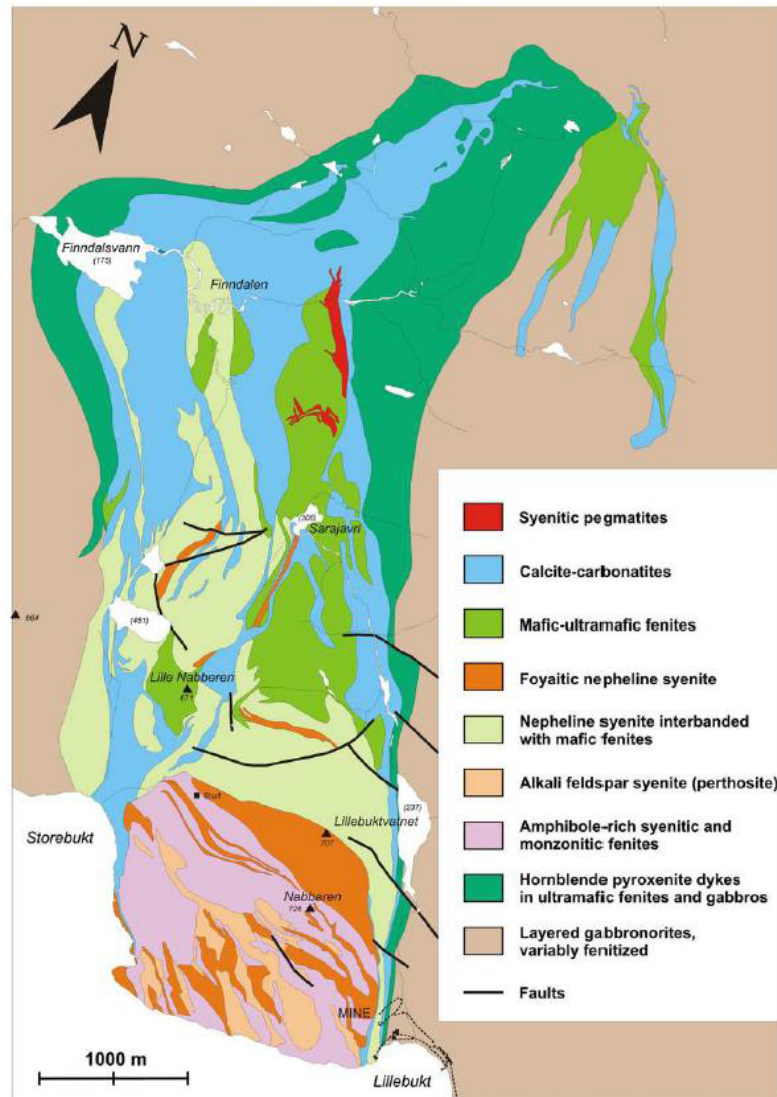
Figure A.1: Geological map of the Lillebukt Complex (Bruland, 1980)

B

Rock Mass Rating

Table 2: RMR classification guide for excavation and support in rock tunnels (Bieniawski, 1989).
Shape: horseshoe; Width: 10 m; Vertical stress: below 25 MPa; Excavation by drill & blast

Rock mass class	Excavation	Support		
		Rock bolts (20 mm diam., fully bonded)	Shotcrete	Steel sets
1. Very good rock RMR: 81-100	Full face: 3 m advance	Generally no support required except for occasional spot bolting		
2. Good rock RMR: 61-80	Full face: 1.0-1.5 m advance; Complete support 20 m from face	Locally bolts in crown, 3 m long, spaced 2.5 m with occasional wire mesh	50 mm in crown where required	None
3. Fair rock RMR: 41-60	Top heading and bench: 1.5-3 m advance in top heading; Commence support after each blast; Commence support 10 m from face	Systematic bolts 4 m long, spaced 1.5-2 m in crown and walls with wire mesh in crown	50-100 mm in crown, and 30 mm in sides	None
4. Poor rock RMR: 21-40	Top heading and bench: 1.0-1.5 m advance in top heading; Install support concurrently with excavation - 10 m from face	Systematic bolts 4-5 m long, spaced 1-1.5 m in crown and walls with wire mesh	100-150 mm in crown and 100 mm in sides	Light ribs spaced 1.5 m where required
5. Very poor rock RMR < 21	Multiple drifts: 0.5-1.5 m advance in top heading; Install support concurrently with excavation; shotcrete as soon as possible after blasting	Systematic bolts 5-6 m long, spaced 1-1.5 m in crown and walls with wire mesh. Bolt invert	150-200 mm in crown, 150 mm in sides, and 50 mm on face	Medium to heavy ribs spaced 0.75 m with steel lagging and forepoling if required. Close invert

Figure B.1: The RMR-rating results as specified by Bieniawski (1993)

Table 1: RMR classification of rock masses (Bieniawski, 1989).

A. CLASSIFICATION PARAMETERS AND THEIR RATINGS

	PARAMETER		Range of values // ratings						
1	Strength of intact rock material	Point-load strength index	> 10 MPa	4 - 10 MPa	2 - 4 MPa	1 - 2 MPa	For this low range uniaxial compr. strength is preferred		
		Uniaxial compressive strength	> 250 MPa	100 - 250 MPa	50 - 100 MPa	25 - 50 MPa	5 - 25 MPa	1 - 5 MPa	< 1 MPa
		RATING	15	12	7	4	2	1	0
2	Drill core quality RQD		90 - 100%	75 - 90%	50 - 75%	25 - 50%	< 25%		
	RATING		20	17	13	8	5		
3	Spacing of discontinuities		> 2 m	0.6 - 2 m	200 - 600 mm	60 - 200 mm	< 60 mm		
	RATING		20	15	10	8	5		
4	Condition of discontinuities	Length, persistence	< 1 m	1 - 3 m	3 - 10 m	10 - 20 m	> 20 m		
		Rating	6	4	2	1	0		
		Separation	none	< 0.1 mm	0.1 - 1 mm	1 - 5 mm	> 5 mm		
		Rating	6	5	4	1	0		
		Roughness	very rough	rough	slightly rough	smooth	slickensided		
		Rating	6	5	3	1	0		
		Infilling (gouge)	none	Hard filling		Soft filling			
			-	< 5 mm	> 5 mm	< 5 mm	> 5 mm		
		Rating	6	4	2	2	0		
		Weathering	unweathered	slightly w.	moderately w.	highly w.	decomposed		
		Rating	6	5	3	1	0		
5	Ground water	Inflow per 10 m tunnel length	none	< 10 litres/min	10 - 25 litres/min	25 - 125 litres/min	> 125 litres /min		
		$p_w / \sigma 1$	0	0 - 0.1	0.1 - 0.2	0.2 - 0.5	> 0.5		
		General conditions	completely dry	damp	wet	dripping	flowing		
		RATING	15	10	7	4	0		

p_w = joint water pressure; $\sigma 1$ = major principal stress

B. RATING ADJUSTMENT FOR DISCONTINUITY ORIENTATIONS

		Very favourable	Favourable	Fair	Unfavourable	Very unfavourable
RATINGS	Tunnels	0	-2	-5	-10	-12
	Foundations	0	-2	-7	-15	-25
	Slopes	0	-5	-25	-50	-60

C. ROCK MASS CLASSES DETERMINED FROM TOTAL RATINGS

Rating	100 - 81	80 - 61	60 - 41	40 - 21	< 20
Class No.	I	II	III	IV	V
Description	VERY GOOD	GOOD	FAIR	POOR	VERY POOR

D. MEANING OF ROCK MASS CLASSES

Class No.	I	II	III	IV	V
Average stand-up time	10 years for 15 m span	6 months for 8 m span	1 week for 5 m span	10 hours for 2.5 m span	30 minutes for 1 m span
Cohesion of the rock mass	> 400 kPa	300 - 400 kPa	200 - 300 kPa	100 - 200 kPa	< 100 kPa
Friction angle of the rock mass	< 45°	35 - 45°	25 - 35°	15 - 25°	< 15°

Figure B.2: The RMR-rating sheet as specified by Bieniawski (1993)

C

Q-rating System

Barton et al. (1974)
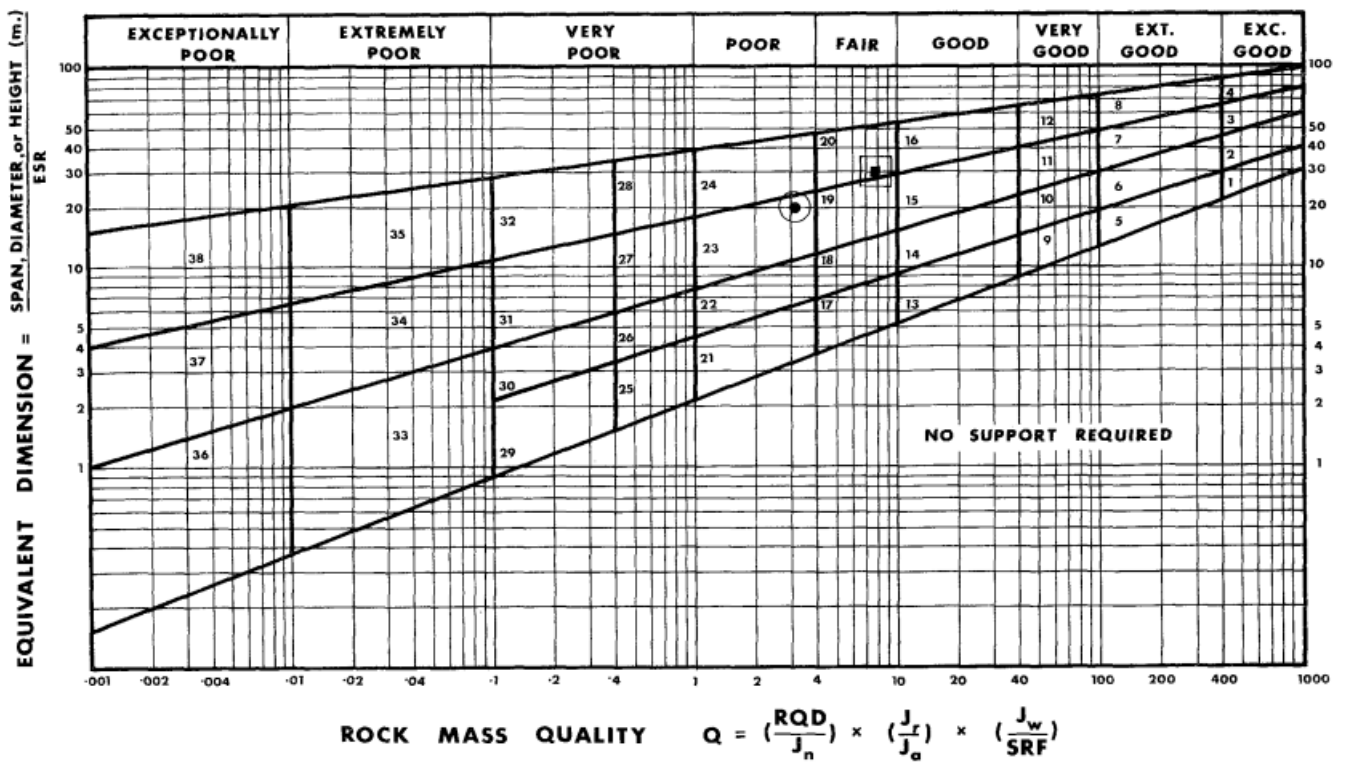
Figure C.1: The Q-rating results as specified by Barton et al. (1974)

Table 1. Description and ratings for the input parameters of the Q-system (simplified from Grimstad and Barton, 1993).

RQD *(Rock Quality Designation)*

Very poor	RQD = 0 - 25%
Poor	25 - 50
Fair	50 - 75
Good	75 - 90
Excellent	90 - 100

Notes:
(i) Where RQD is reported or measured as < 10 (including 0),
  a nominal value of 10 is used to evaluate Q
(ii) RQD intervals of 5, i.e. 100, 95, 90, etc.
  are sufficiently accurate

Jn *(joint set number)*

Massive, no or few joints	Jn = 0.5 - 1
One joint set	2
One joint set plus random joints	3
Two joint sets	4
Two joint sets plus random joints	6
Three joint sets	9
Three joint sets plus random joints	12
Four or more joint sets, heavily jointed, "sugar-cube", etc.	15
Crushed rock, earthlike	20

Notes: (i) For tunnel intersections, use (3.0 x Jn); (ii) For portals, use (2.0 x Jn)

Jr *(joint roughness number)*

a) Rock-wall contact, b) rock-wall contact before 10 cm shear		c) No rock-wall contact when sheared	
Discontinuous joints	Jr = 4	Zone containing clay minerals thick enough to prevent rock-wall contact	Jr = 1.0
Rough or irregular, undulating	3		
Smooth, undulating	2	Sandy, gravelly or crushed zone thick enough to prevent rock-wall contact	1.0
Slickensided, undulating	1.5		
Rough or irregular, planar	1.5	*Notes:*	
Smooth, planar	1.0	*i) Add 1.0 if the mean spacing of the relevant joint set is greater than 3 m*	
Slickensided, planar	0.5	*ii) Jr = 0.5 can be used for planar, slickensided joints having lineations,*	

Note : i) Descriptions refer to small scale features,
  and intermediate scale features, in that order
  provided the lineations are oriented for minimum strength

Ja *(joint alteration number)*

	JOINT WALL CHARACTER		Condition	Wall contact
Contact between joint walls	CLEAN JOINTS	Healed or welded joints:	filling of quartz, epidote, etc.	Ja = 0.75
		Fresh joint walls:	no coating or filling, except from staining (rust)	1
		Slightly altered joint walls:	non-softening mineral coatings, clay-free particles, etc.	2
	COATING OR THIN FILLING	Friction materials:	sand, silt, calcite, etc. (non-softening)	3
		Cohesive materials:	clay, chlorite, talc, etc. (softening)	4

	FILLING OF:	Type	Some wall contact Thin filling (< 5 mm)	No wall contact Thick filling
Some or no wall contact	Friction materials	sand, silt calcite, etc. (non-softening)	Ja = 4	Ja = 8
	Hard cohesive materials	compacted filling of clay, chlorite, talc, etc.	6	5 - 10
	Soft cohesive materials	medium to low overconsolidated clay, chlorite, talc.	8	12
	Swelling clay materials	filling material exhibits swelling properties	8 - 12	13 - 20

Jw *(joint water reduction factor)*

Dry excavations or minor inflow, i.e. < 5 l/min locally	$p_w < 1$ kg/cm^2	Jw = 1
Medium inflow or pressure, occasional outwash of joint fillings	1 - 2.5	0.66
Large inflow or high pressure in competent rock with unfilled joints	2.5 - 10	0.5
Large inflow or high pressure, considerable outwash of joint fillings	2.5 - 10	0.3
Exceptionally high inflow or water pressure at blasting, decaying with time	> 10	0.2 - 0.1
Exceptionally high inflow or water pressure continuing without noticeable decay	> 10	0.1 - 0.05

Note: (i) The last four factors are crude estimates. Increase Jw if drainage measures are installed
  (ii) Special problems caused by ice formation are not considered

SRF *(Stress Reduction Factor)*

	Multiple weakness zones with clay or chemically disintegrated rock, very loose surrounding rock (any depth)	SRF = 10
Weakness zones intersecting excavation	Single weakness zones containing clay or chemically disintegrated rock (depth of excavation < 50 m)	5
	Single weakness zones containing clay or chemically disintegrated rock (depth of excavation > 50 m)	2.5
	Multiple shear zones in competent rock (clay-free), loose surrounding rock (any depth)	7.5
	Single shear zones in competent rock (clay-free), loose surrounding rock (depth of excavation < 50 m)	5
	Single shear zones in competent rock (clay-free), loose surrounding rock (depth of excavation > 50 m)	2.5
	Loose, open joints, heavily jointed or "sugar-cube", etc. (any depth)	5

Note: (i) Reduce these SRF values by 25 - 50% if the relevant shear zones only influence, but do not intersect the excavation.

		σ_c / σ_1	σ_θ / σ_c	SRF
Competent rock, rock stress problems	Low stress, near surface, open joints	> 200	< 0.01	2.5
	Medium stress, favourable stress condition	200 - 10	0.01 - 0.3	1
	High stress, very tight structure. Usually favourable to stability, may be except for walls	10 - 5	0.3 - 0.4	0.5 - 2
	Moderate slabbing after > 1 hour in massive rock	5 - 3	0.5 - 0.65	5 - 50
	Slabbing and rock burst after a few minutes in massive rock	3 - 2	0.65 - 1	50 - 200
	Heavy rock burst (strain burst) and immediate dynamic deformation in massive rock	< 2	> 1	200 - 400

Notes: (ii) For strongly anisotropic stress field (if measured): when 5 < σ_1/σ_3 <10, reduce σ_c to 0.75 σ_c. When σ_1/σ_3 > 10, reduce σ_c to 0.5σ_c
(iii) Few case records available where depth of crown below surface is less than span width. Suggest SRF increase from 2.5 to 5 for low stress cases

			σ_θ / σ_c	SRF
Squeezing rock	Plastic flow of incompetent rock under the influence of high pressure	Mild squeezing rock pressure	1 - 5	5 - 10
		Heavy squeezing rock pressure	> 5	10 - 20
Swelling rock	Chemical swelling activity depending on presence of water	Mild swelling rock pressure		5 - 10
		Heavy swelling rock pressure		10 - 15

Figure C.2: The Q-rating sheet as specified by Barton et al. (1974)

D

UCS-Test Results
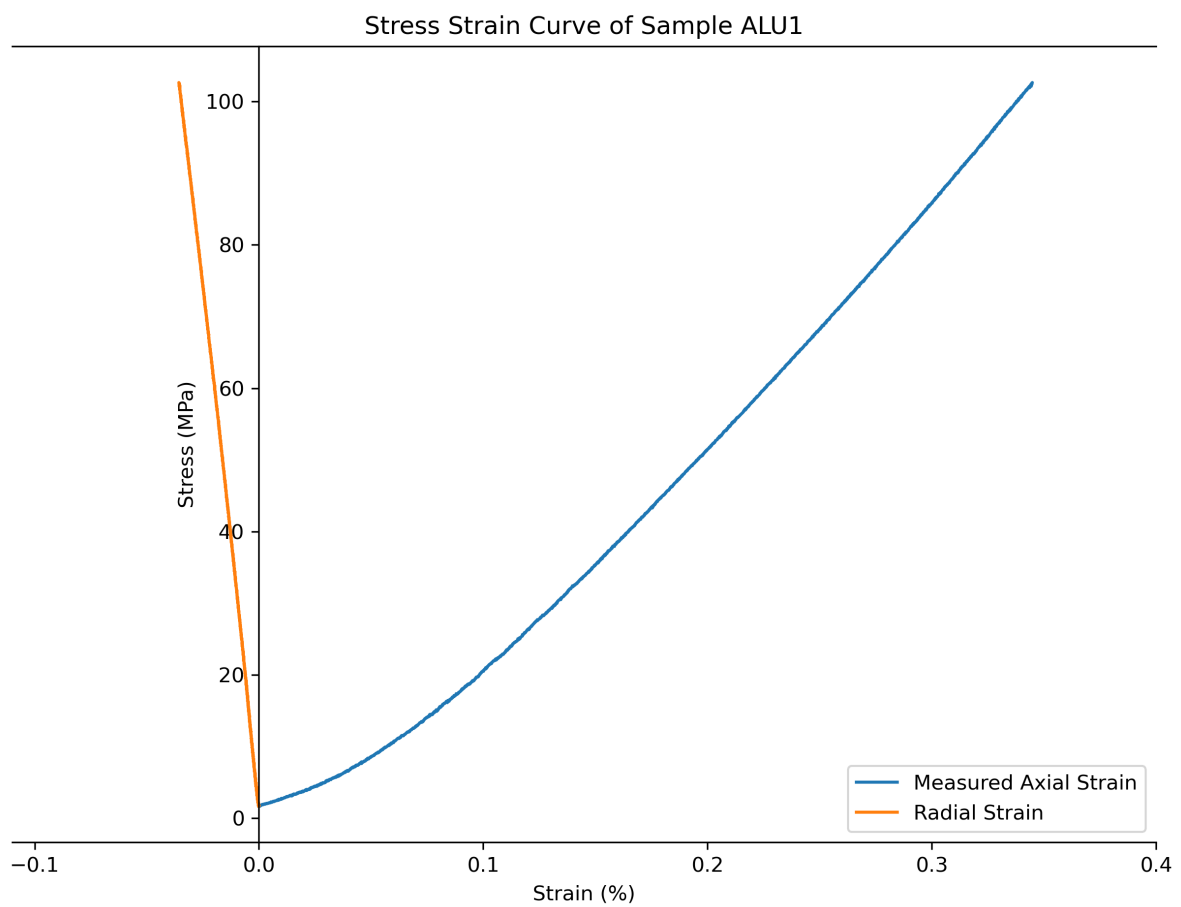
Figure D.1: Stress-strain curve from nepheline-syenite sample ALU1.
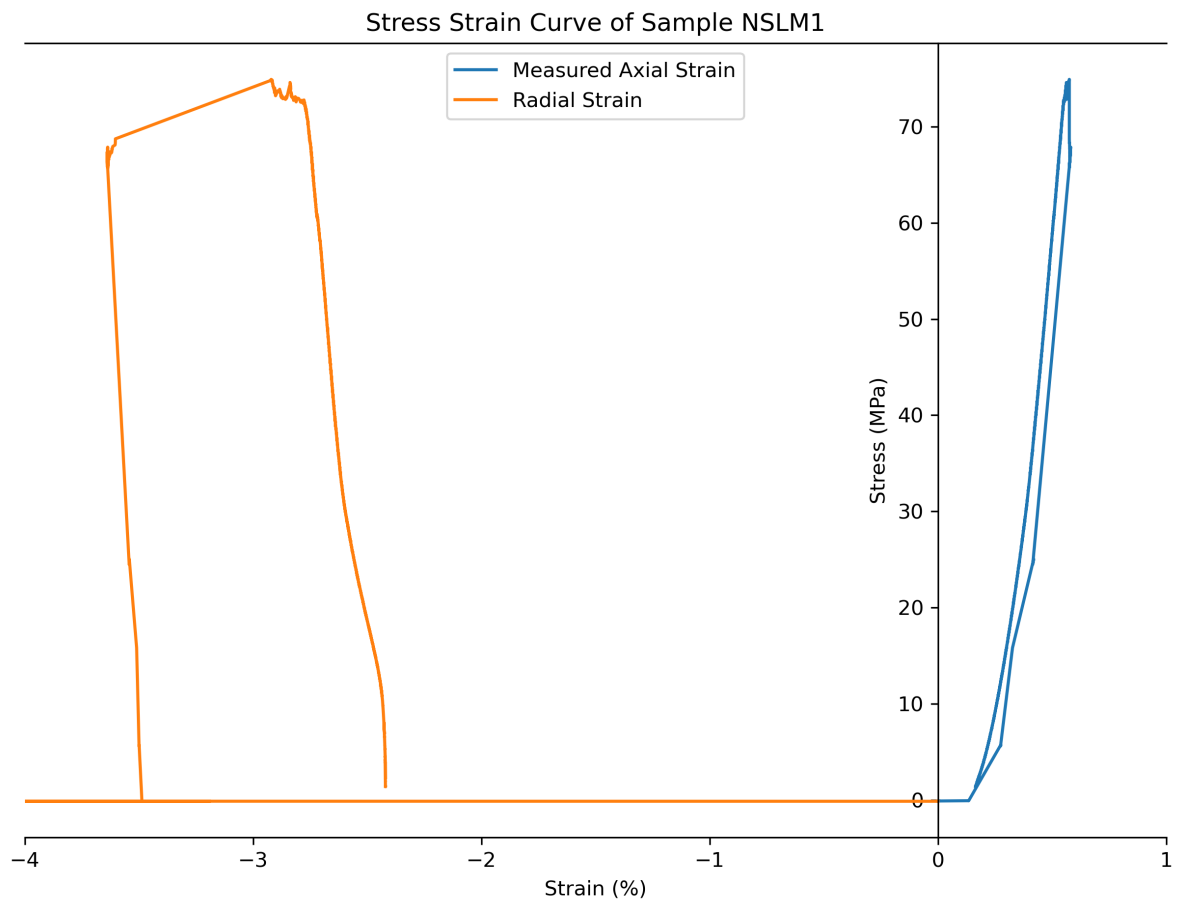
Figure D.2: Stress-strain curve from nepheline-syenite sample NSLM1.
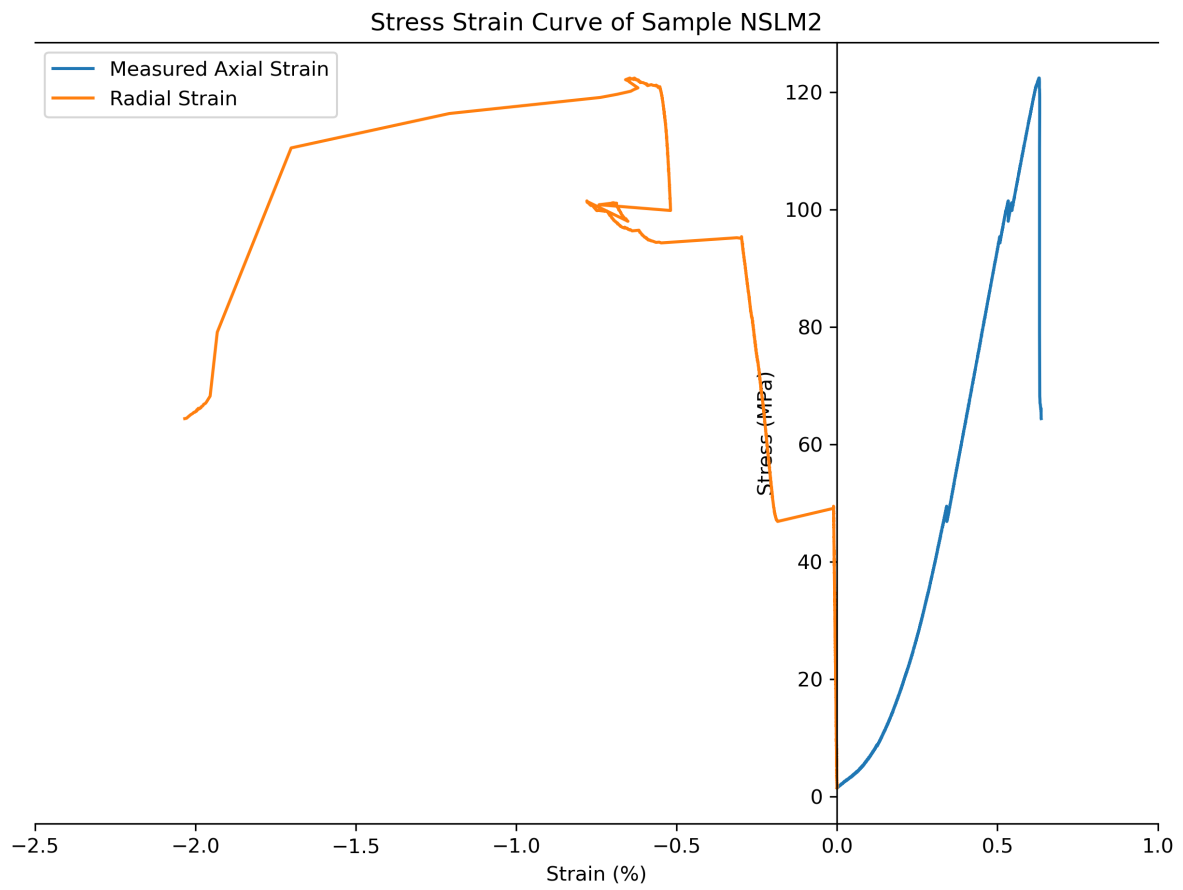
Figure D.3: Stress-strain curve from nepheline-syenite sample NSLM2.

Stress Strain Curve of Sample NSLM4
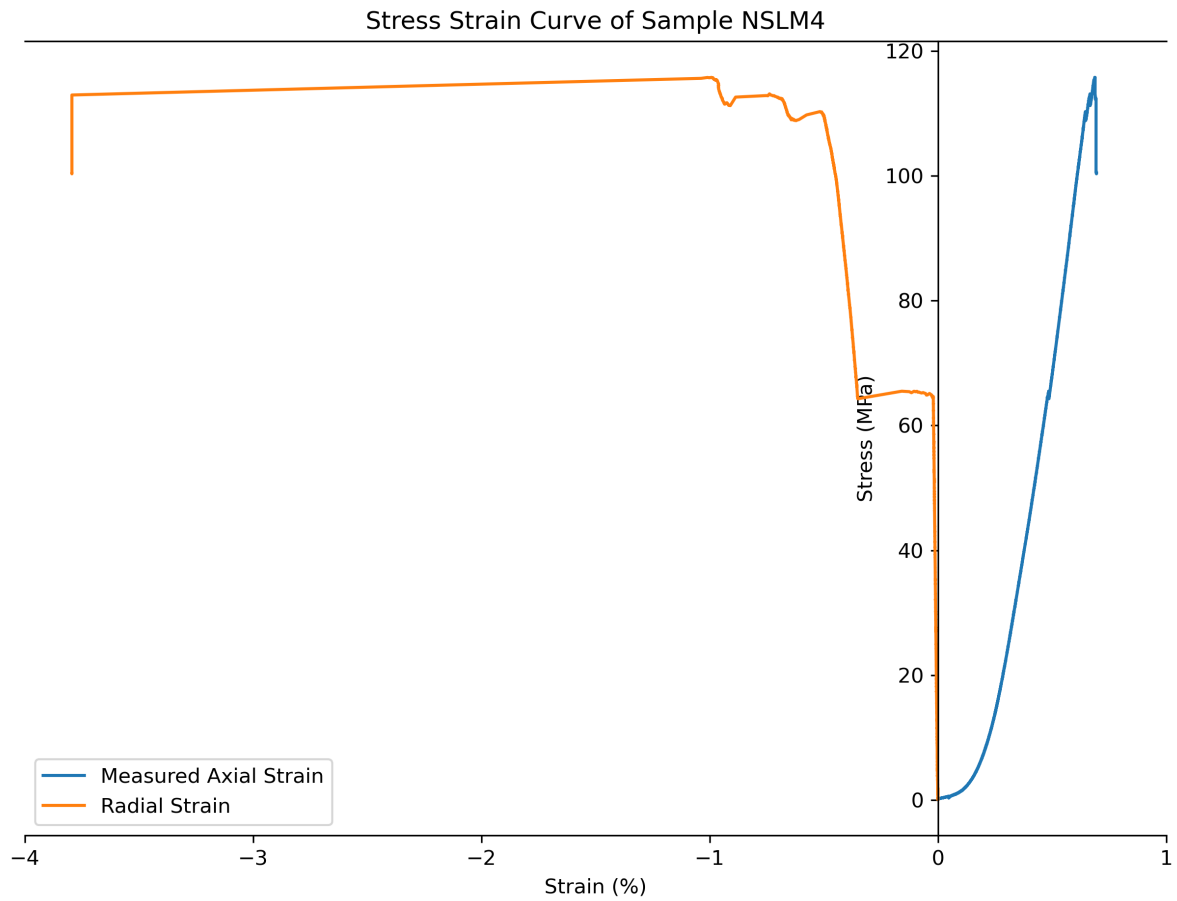
Figure D.4: Stress-strain curve from nepheline-syenite sample NSLM4.

Arrival time per timed loop
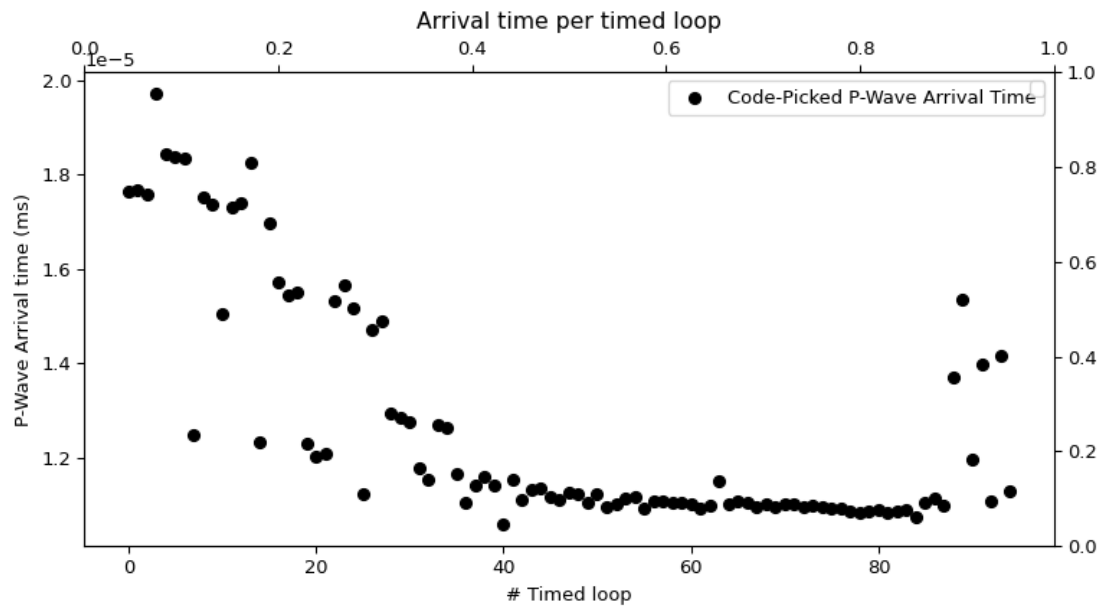
Figure D.5: Code picked Arrival times of sample NSLM4.
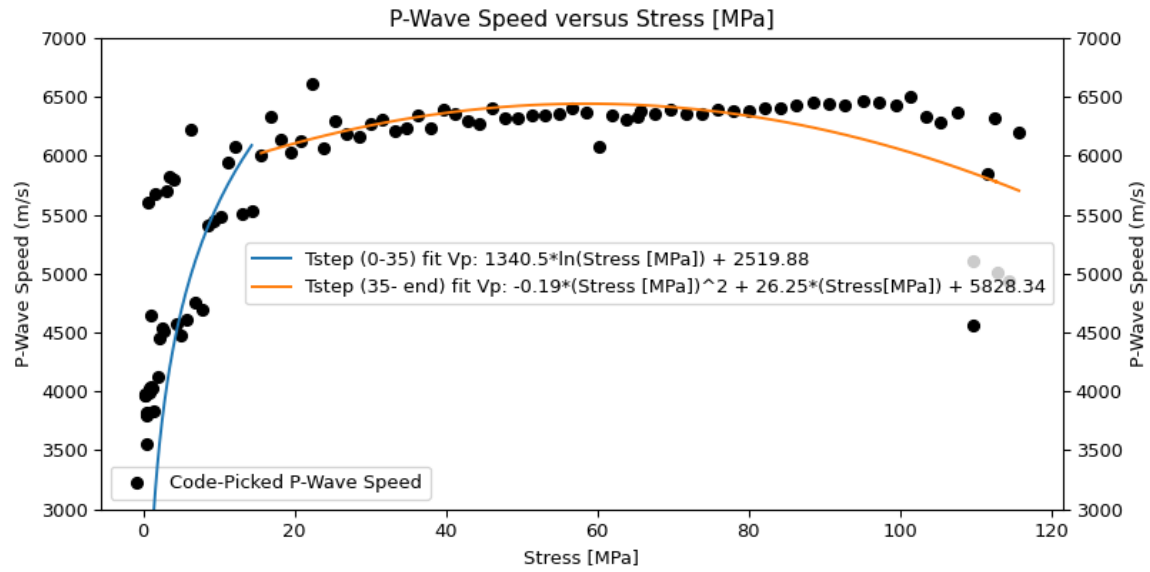
Figure D.6: Code Picked P-wave speed and fitted P-wave speed of sample NSLM4.
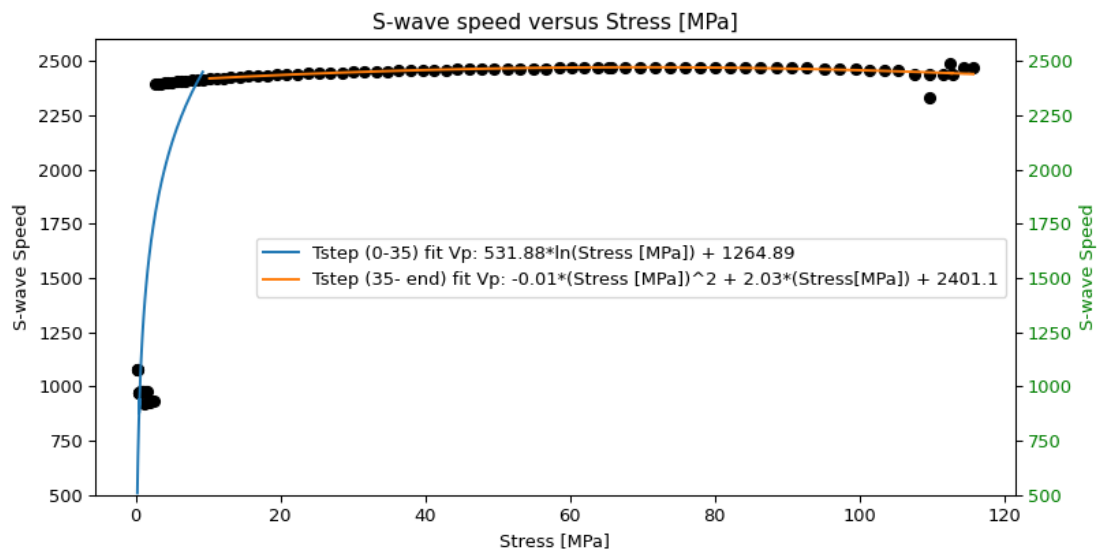
Figure D.7: Code Picked S-wave speed and fitted S-wave speed of sample NSLM4.
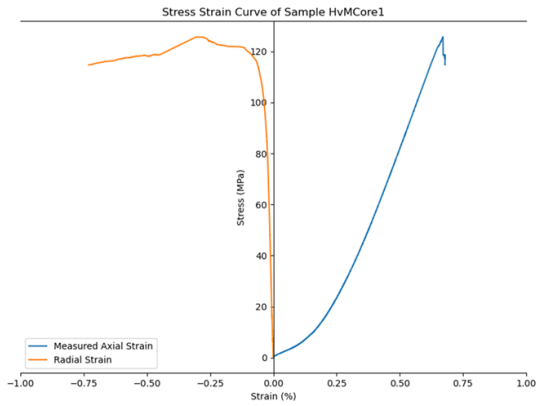
(a) Stress-Strain Curve of Sample HvMCore1
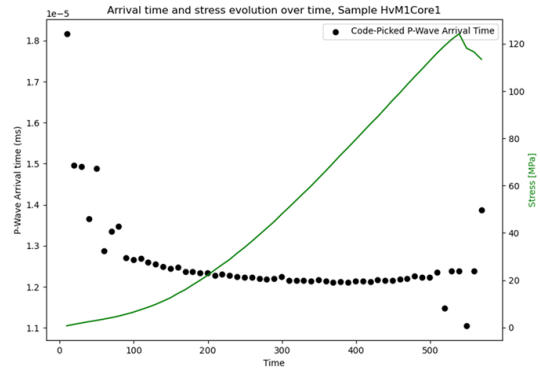
(b) Stress-Arrival time Curve of Sample HvMCore1
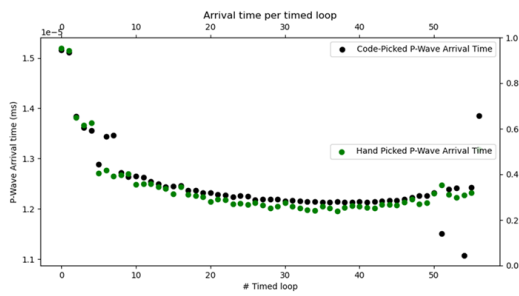
(c) Code-Pick vs. Hand-Pick of P-wave arrival time of Sample HvMCore1
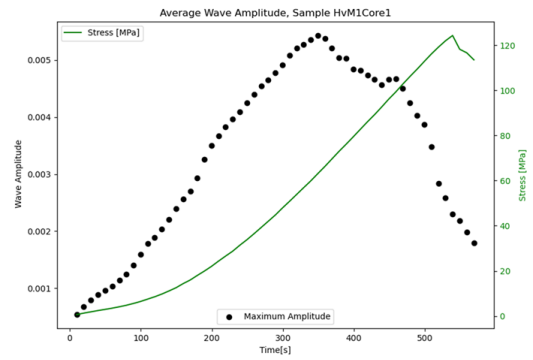
(d) Average Wave Amplitude growth of Sample HvMCore1
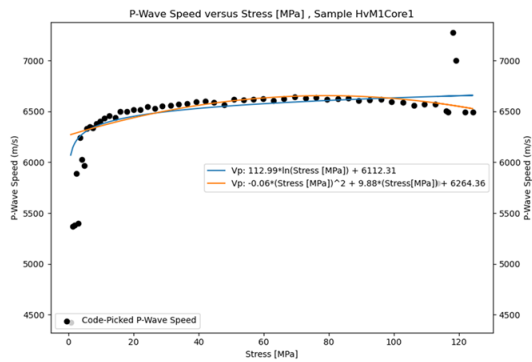
(e) P-wave Speed versus Stress of Sample HvMCore1 + fit
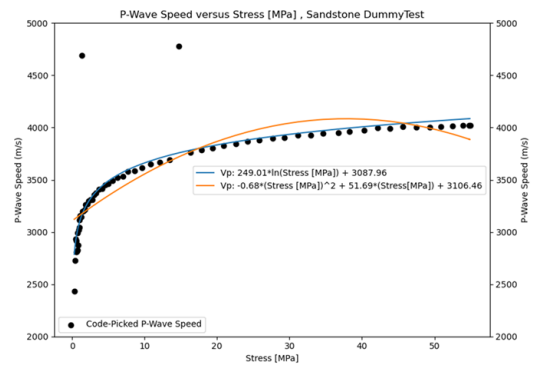
(f) Sandstone dummy sample P-wave speed + fit

Figure D.8: Analysis of UCS test + acoustics on sample HvMCore1.
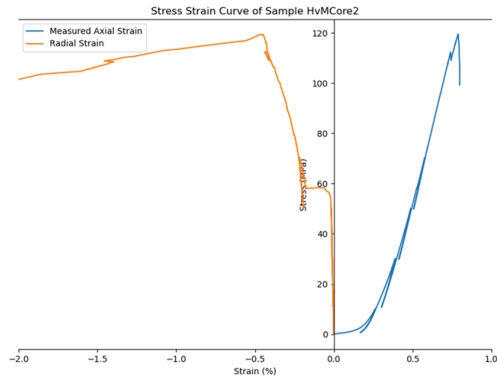
(a) Stress-Strain Curve of Sample HvMCore2
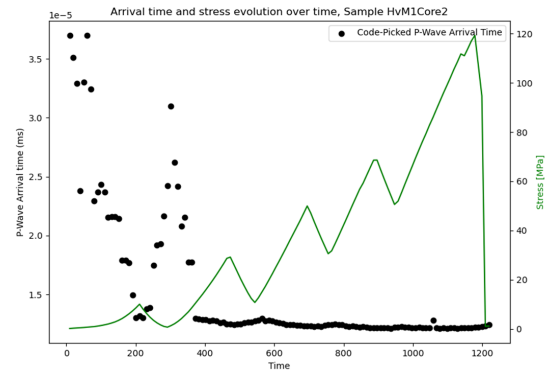
(b) Stress-Arrival time Curve of Sample HvMCore2
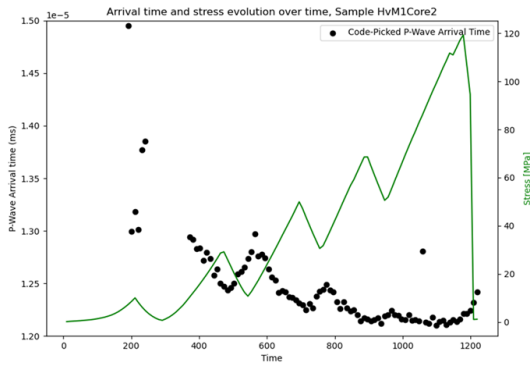
(c) Close-up of P-wave arrival time of Sample HvMCore2
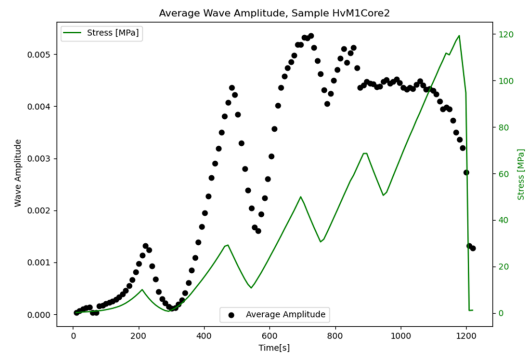
(d) Average Wave Amplitude growth of Sample HvMCore2
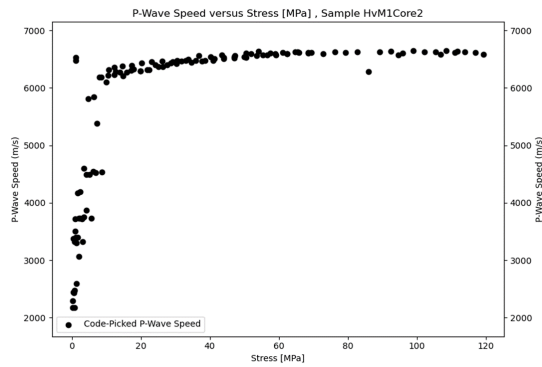
(e) P-wave Speed versus Stress of Sample HvMCore2
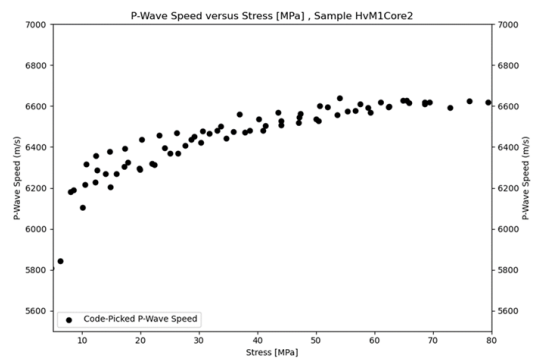
(f) Close up of P-wave speed of sample HvMCore2

Figure D.9: Analysis of UCS test + acoustics on sample HvMCore2.
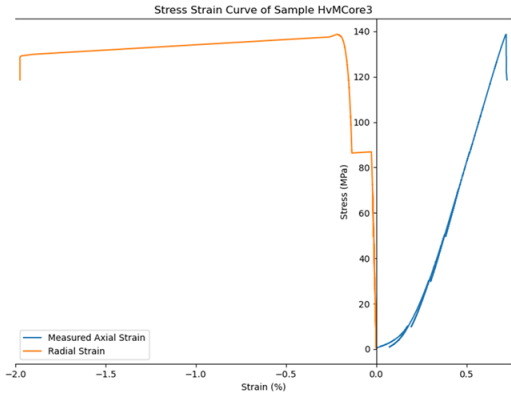
(a) Stress-Strain Curve of Sample HvMCore3
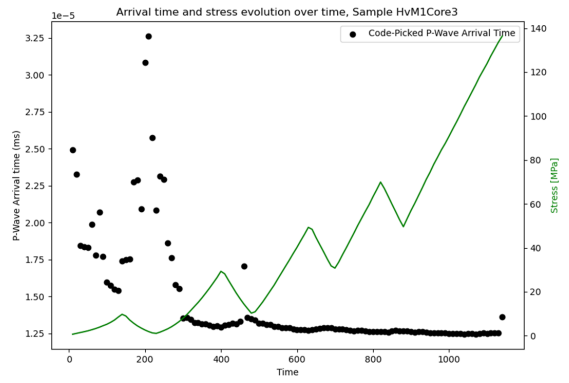
(b) Stress-Arrival time Curve of Sample HvMCore3
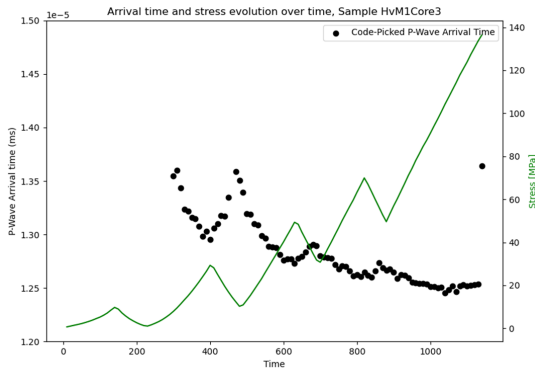
(c) Close-up of P-wave arrival time of Sample HvMCore3
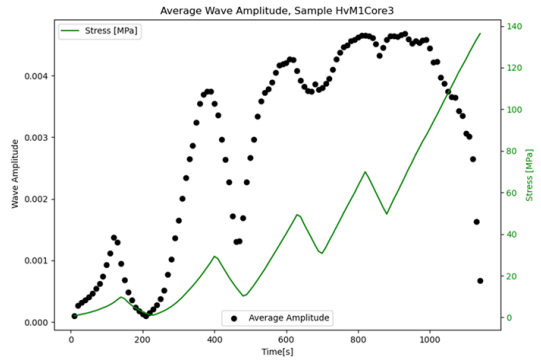
(d) Average Wave Amplitude growth of Sample HvMCore3
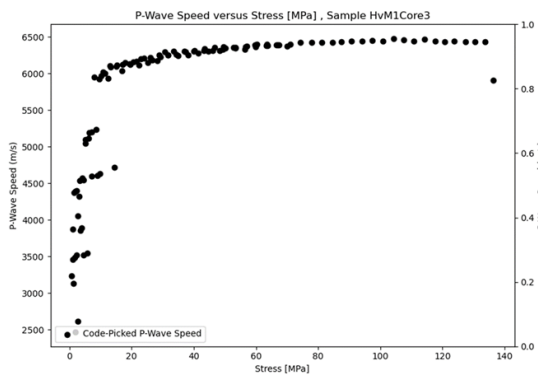
(e) P-wave Speed versus Stress of Sample HvMCore3
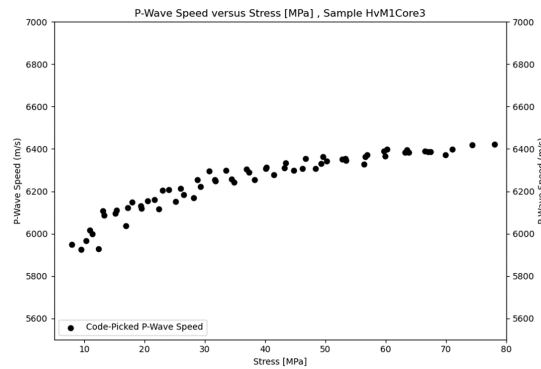
(f) Close up of P-wave speed of sample HvMCore3

Figure D.10: Analysis of UCS test + acoustics on sample HvMCore3.
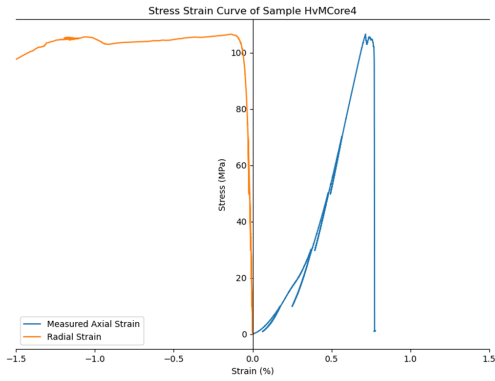
(a) Stress-Strain Curve of Sample HvMCore4
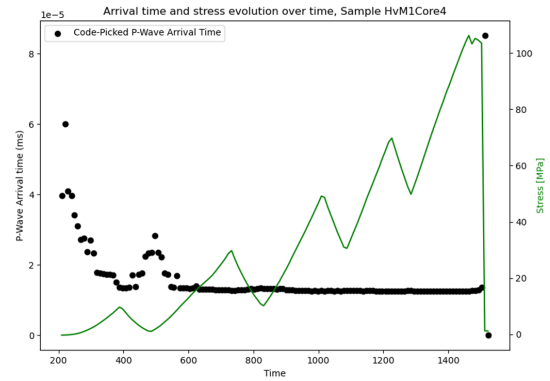
(b) Stress-Arrival time Curve of Sample HvMCore4
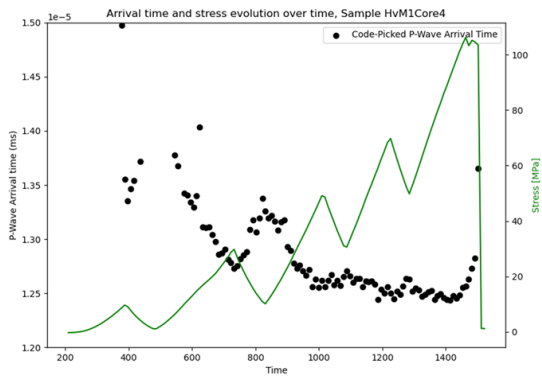
(c) Close-up of P-wave arrival time of Sample HvMCore4
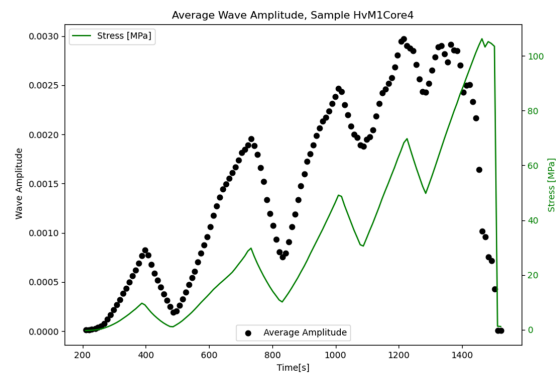
(d) Average Wave Amplitude growth of Sample HvMCore4
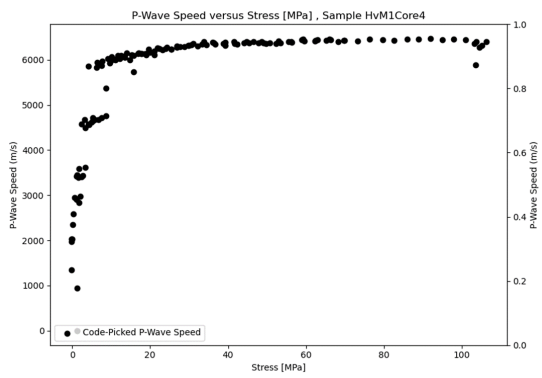
(e) P-wave Speed versus Stress of Sample HvMCore4
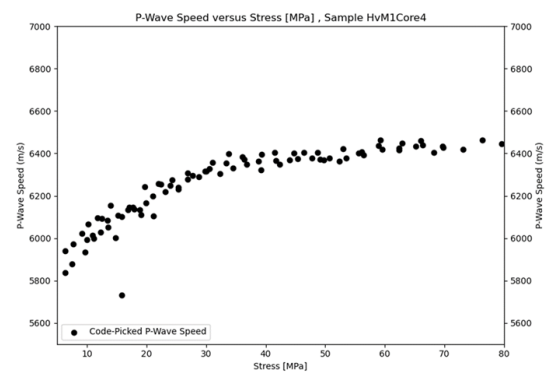
(f) Close up of P-wave speed of sample HvMCore4

Figure D.11: Analysis of UCS test + acoustics on sample HvMCore4.
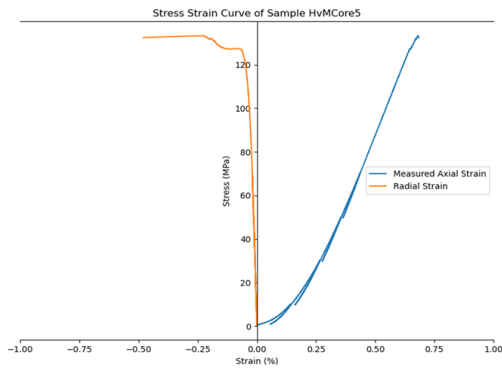
(a) Stress-Strain Curve of Sample HvMCore5
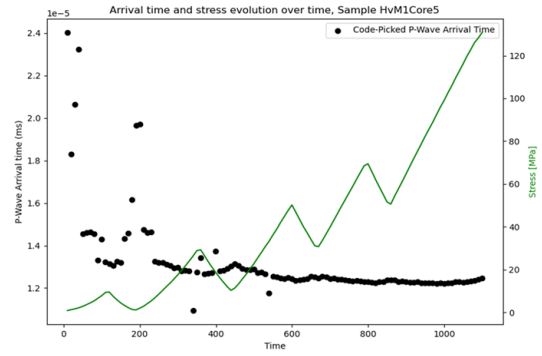
(b) Stress-Arrival time Curve of Sample HvMCore5
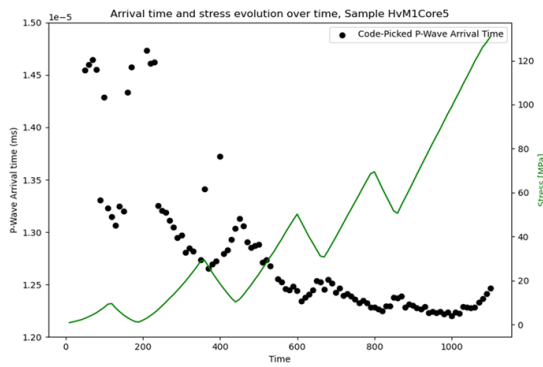
(c) Close-up of P-wave arrival time of Sample HvMCore5
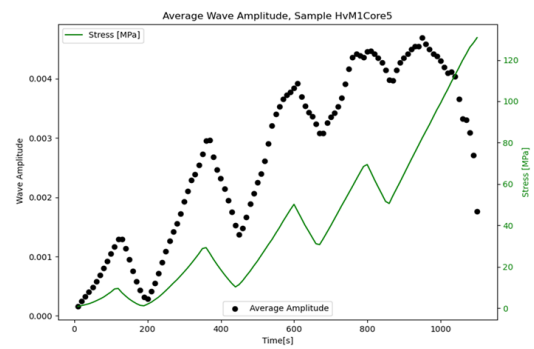
(d) Average Wave Amplitude growth of Sample HvMCore5
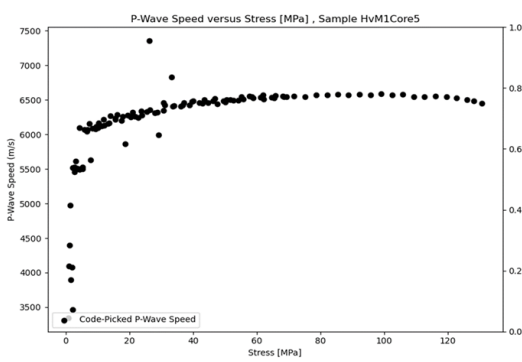
(e) P-wave Speed versus Stress of Sample HvMCore5
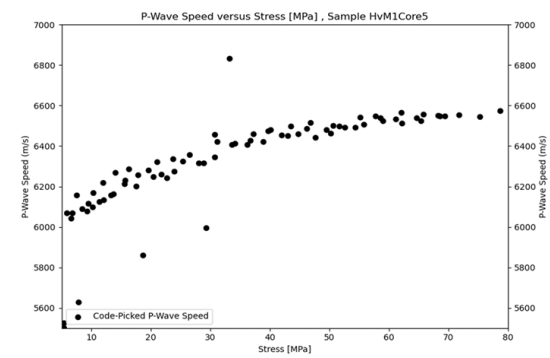
(f) Close up of P-wave speed of sample HvMCore5

Figure D.12: Analysis of UCS test + acoustics on sample HvMCore5.
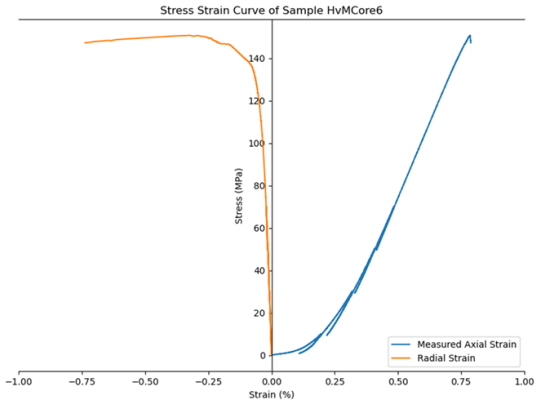
(a) Stress-Strain Curve of Sample HvMCore6
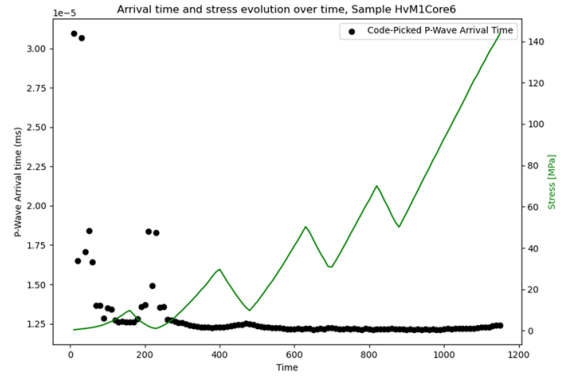
(b) Stress-Arrival time Curve of Sample HvMCore6
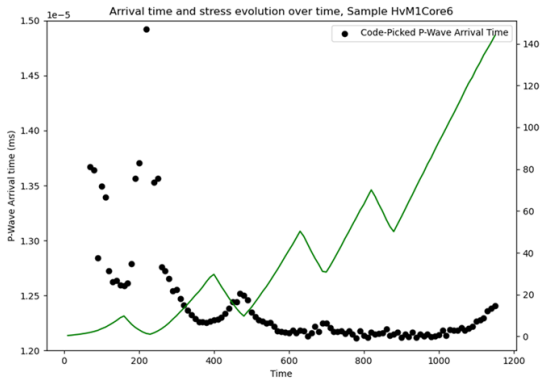
(c) Close-up of P-wave arrival time of Sample HvMCore6
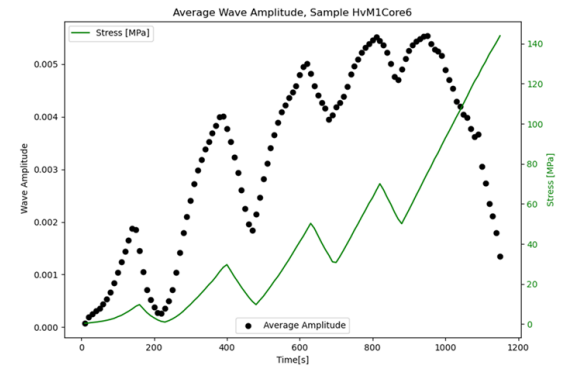
(d) Average Wave Amplitude growth of Sample HvMCore6
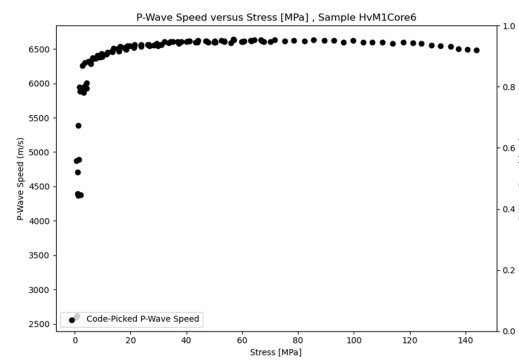
(e) P-wave Speed versus Stress of Sample HvMCore6
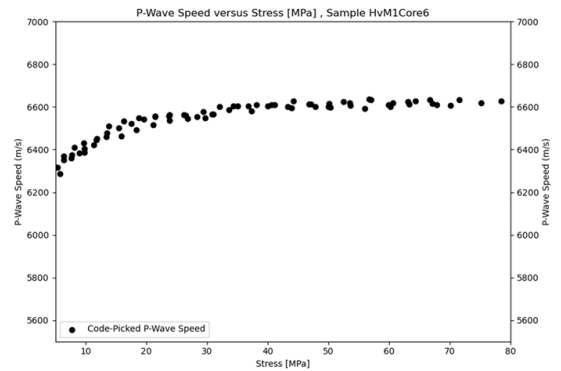
(f) Close up of P-wave speed of sample HvMCore6

Figure D.13: Analysis of UCS test + acoustics on sample HvMCore6.
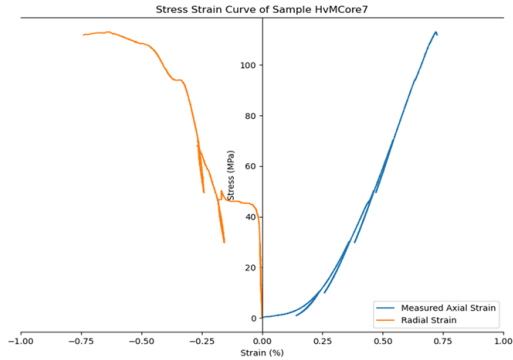
(a) Stress-Strain Curve of Sample HvMCore7
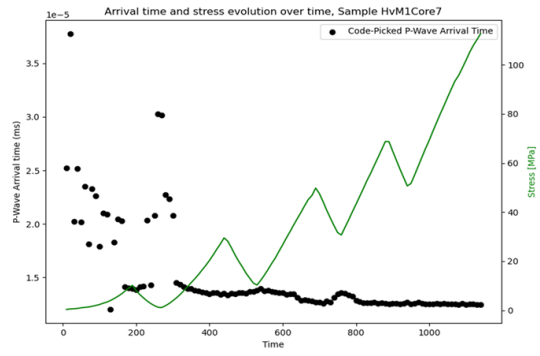
(b) Stress-Arrival time Curve of Sample HvMCore7
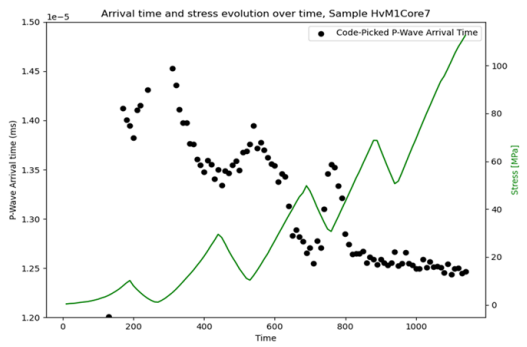
(c) Close-up of P-wave arrival time of Sample HvMCore7
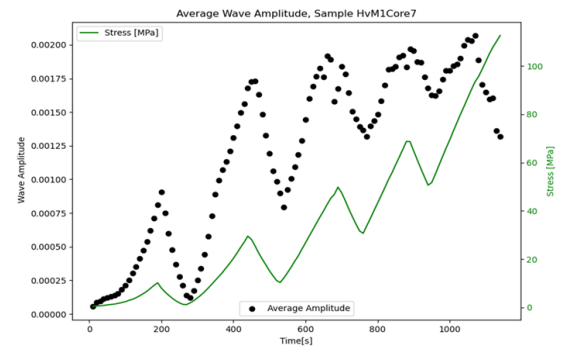
(d) Average Wave Amplitude growth of Sample HvMCore7
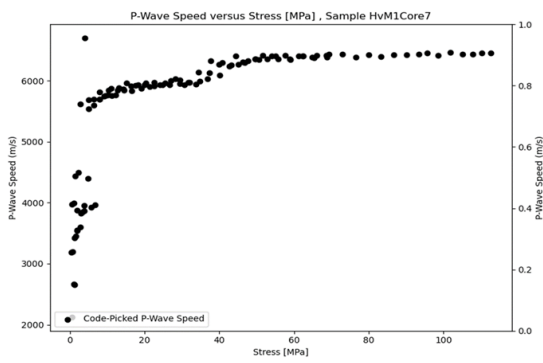
(e) P-wave Speed versus Stress of Sample HvMCore7
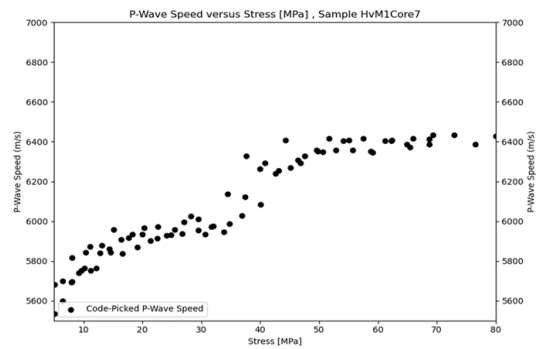
(f) Close up of P-wave speed of sample HvMCore7

Figure D.14: Analysis of UCS test + acoustics on sample HvMCore7.